Recognition of Nucleic Acid Mismatches by Luminescent Ruthenium Complexes

Thesis by

Hang Song

In Partial Fulfillment of the Requirements

for the Degree of

Doctor of Philosophy in Chemistry

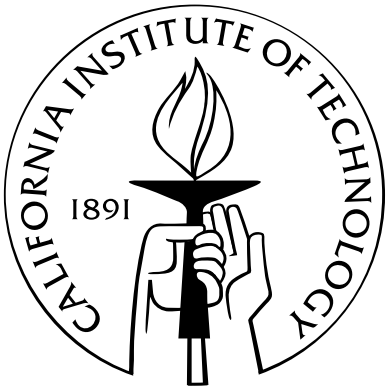

California Institute of Technology

Pasadena, California

2012

(Defended October 27, 2011)

Acknowledgements

My foremost acknowledgement goes to my graduate advisor, Professor Jacqueline K. Barton, for your enthusiasm, wisdom and vision in the complex worlds of science and life. Thank you for your support, guidance, and confidence in me throughout my time here. It has been a truly delightful and humbling journey along the rocky path of scientific discovery, and I am grateful that you have been there with me to help me see the gems in the piles of gravel.

I would like to thank my thesis committee, Professors Harry Gray, Doug Rees, and Shu-ou Shan. Your guidance has made me a better scientist, and your generous support throughout the years has opened many doors for me.

I would also like to acknowledge Maureen Renta for her sage advice and for keeping us all out of trouble.

My mentors in the laboratory, Brian Zeglis and Mi Hee Lim, deserve special thanks for taking me under their wings. Thank you for your patience and help; your humor, creativity and scientific intuition will always be an inspiration.

Pam Sontz and Natalie Muren, you have been there with me every step of the way, and I am grateful for your love and friendship. We will always be the invincible trio!

Many members of the Barton group, past and present, have helped me tremendously throughout my journey. A big thank you to Russ Ernst, for being a big brother to me and for good laughs; Cindy Puckett, for being a big sister to me and for your wittiness; Paul Lee, for heading the baking committee and for various other gastronomical adventures; Joey Genereux, for your knowledge and insight in (almost) everything in the world; Christine Romano, for showing me the world of microbiology and for organizing group camping trips; Amie Boal, for your grace and generosity; Marisa Buzzeo, for your optimism and for looking after Brian and Paul; Curtis Schneider, for your invaluable advice on chemistry in the hood and chemistry at home with brewing supplies; Wendy Mercer, for your advice on life and your fearless attitude; Eric Olmon, for sharing your gifts of art, music, and spectroscopy;

Catrina Pheeney, for being an amazing bay mate and desk neighbor; Tim Mui, for keeping the HPLC running and for all the insider deals; Katie Schaefer, for cakes, treats and stories; Alexis Komor, for your passion and for being such a fast learner; Anna Arnold, for keeping us safe at all times; Mike Grodick, for your determination and positive energy; Anna McConnell, for your enthusiasm and advice; Mike Smeaton, for showing me tricks in cell work; Ariel Furst, for your courage and faith; Alyson Weidmann, for cheering up the corner; Helen Segal, for letting me use my initials; and Elizabeth Dervan, for a memorable summer of research and fun.

I would especially like to express my gratitude for Jens Kaiser, whose guidance and expertise in crystallography led me to solve the beautiful crystal structures presented in this work. I will always remember the day we found the crystal that diffracted to 0.92 Å—my twenty-seventh birthday.

I would also like to thank members of the CCE, Biology divisions, and the Safety Office, without whom my research would have been impossible. Scott Virgil, Julie Hoy, Shelley Diamond, Pavle Nikolovski, Bill Dempsey, Tom Dunn, Agnes Tong, Steve Baldwin, Mona Shahgholi, Dave VanderVelde, Steve Gould, Joe Drew, Leah Santat, Ted Weintrob, Nathan Dalleska, Nicole Ford, Alec Durrell, Justin Chartron, and Haick Issaian: thank you for always being there to help.

I must also express my appreciation for my mentors outside of the department, Jean Huang, Elizabeth Tricomi, and Xiaolan Zhang, for your nuggets of wisdom and for being wonderful role models.

My life away from the laboratory has been colorful, thanks to my dear friends. Caglar Tanrikulu, Ozgun Konca, Muruvvet Buyukboyaci, Selim Hanay, Omer Durak, Ercan Gurses, Aycan Yurtsever, Bahar Bingol, Necmiye Ozay, Cevat Ustun, Murat Acar, and Samet Oymak, thank you for good company and good times.

The transformative power of graduate school does not stop at the door of the laboratory—I have also picked up a brown belt in karate. Thank you, Sensei Ian Ferguson and the Caltech Karate Club, for bringing the art of karate-do into my life.

Finally, I would like to thank my family for their unconditional love, support and encouragement. Bàba, māma, naǐnai, xièxie nǐmén! This thesis is dedicated to you. And to my fiancé and best friend, Ersen Bilgin.

Abstract

Deficiencies in DNA mismatch repair (MMR) have been implicated in the development of several forms of cancers, and MMR-deficient cells tend to be resistant to commonly employed cancer therapeutics such as cisplatin. Mismatch-targeting metalloinsertors developed in our laboratory have shown great promise as therapeutic and diagnostic agents for MMR-deficient cancers. In this work, we examine fundamental aspects of binding interactions of octahedral rhodium and ruthenium complexes to DNA mismatches, and strive to develop a luminescent sensor for mismatches inside cells.

We first demonstrate that the mismatch binding affinity of rhodium metalloinsertors directly correlates with their antiproliferative effect against MMR-deficient colorectal carcinoma cells. Smaller ancillary ligands on the rhodium center facilitate binding to mismatches via metalloinsertion from the narrow minor groove of DNA. Complexes with higher mismatch binding affinity in turn selectively inhibit the growth of MMR-deficient cells compared to MMR-proficient ones. This correlation suggests that DNA mismatches are indeed the biological target of rhodium metalloinsertors inside cells.

Besides rhodium metalloinsertors, luminescent ruthenium complexes are found to bind DNA mismatches as well. Mismatch binding is accompanied by enhanced luminescence intensity. We determined two crystal structures of Δ-Ru(bpy)$_2$dppz^{2+} bound to oligonucleotide duplexes. For an oligonucleotide containing AA mismatches, the atomic-resolution structure revealed that the ruthenium complex binds to DNA mismatches also through metalloinsertion: the complex inserts a planar ligand into the mismatched site from the minor groove, ejecting the mismatched bases out of the helix. Several binding geometries of the complex intercalated between well-matched DNA were also observed.

To improve the mismatch selectivity of luminescent ruthenium complexes, we tethered the complexes to organic dye molecules in an effort to amplify mismatch-associated luminescence signal through resonance energy transfer. We also modified the structure

of the inserting ligand in an attempt to improve the binding affinity to mismatches over well-matched DNA. Coupling mismatch binding to luminescence response has proved most challenging in these endeavors.

Finally, we venture into the realm of RNA. Unlike their nonspecific binding to DNA, ruthenium complexes bind poorly to well-matched RNA but quite avidly to RNA mismatches. As a result, mismatched RNA produces a higher luminescence signal from bound ruthenium. We subsequently applied the ruthenium complex to image RNA mismatches inside live HeLa cells using fluorescence microscopy.

Contents

Chapter 1

Role of Ancillary Ligands in DNA Mismatch Recognition and Cellular Antiproliferation by Rhodium Metalloinsertors

Adapted from Russell J. Ernst, Hang Song, and Jacqueline K. Barton, *Journal of the American Chemical Society*, **2009**, *131* (6), 2359–2366. R. J. E. synthesized $Rh(DIP)_2chrysi^{3+}$ and performed all cellular proliferation assays.

1.1 Introduction

The integrity of genetic information is ensured by the correct base pairing between the two strands of DNA: adenine (A) always pairs with thymine (T), and guanine (G) with cytosine (C) (Figure 1.1). This strict base-pairing scheme allows the sequence of a complementary strand to be determined solely from that of the template strand, which forms the basis for DNA replication. Errors in DNA replication will cause DNA base mismatches, which, left unrepaired, will become mutations in subsequent rounds of replication.[1,2] Healthy cells rely on their mismatch repair (MMR) pathway to maintain a genome that is virtually free of mismatches (1 in a billion base pairs per cell division).[3,4] The MMR pathway corrects single base errors and insertion/deletion loops that arise during DNA synthesis, increasing the fidelity of DNA replication by a factor of 50–1000.[1] If uncorrected, mismatches are converted to mutations in subsequent cycles of DNA replication, and cells with MMR deficiencies, not surprisingly, exhibit elevated mutation rates.[5–7] Germline mutations in hMLH1 or hMSH2, essential genes for MMR in humans, dramatically increase the risk of developing hereditary nonpolyposis colon cancer (HNPCC), the most common type of inherited colon cancer.[8,9] HNPCC is marked by early onset and the presence of cancers in several other tissue types.[9] Roughly 15% of sporadic colorectal cancer cases have also been linked to MMR deficiency.[10] Epigenetic silencing of the MMR genes has been identified as the cause of MMR deficiency in these cases.[11] In addition to colorectal cancer, mismatch repair deficiencies have been found in approximately 16% of solid tumors of all tissue types.[6,12]

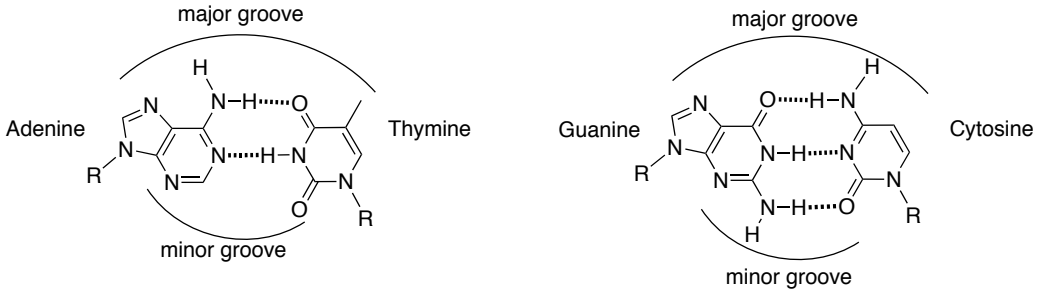

Figure 1.1. Base pairing in DNA.

Importantly, MMR deficiency confers resistance or tolerance to many of the anticancer agents currently in clinical use.[13,14]Alkylation by the commonly used chemotherapeutic agents N-methyl-N-nitrosourea (MNU) and N-methyl-N'-nitro-N-nitrosoguanidine (MNNG)

at the O6 position of guanine nucleotides triggers an apoptotic response after recognition of O6-meG:C and O6-meG:T base pairs by the MMR pathway, while MMR-deficient cells tolerate this DNA methylation.[13–15] Failure to recognize DNA adducts is also involved in the resistance of MMR-deficient cells to the platinum compounds cisplatin and carboplatin.[13–16] The incorporation of antimetabolites such as 5-fluorouracil and 6-thioguanine into DNA triggers cell cycle arrest and apoptosis through the MMR pathway, and consequently MMR-deficient cells are resistant to these agents as well.[17,18] Other studies have shown low-level resistance to the type I topoisomerase poisons camptothecin and topotecan in hMLH1-deficient lines and to the type II topoisomerase poisons doxorubicin, epirubicin, and mitoxantrone in hMLH1- or hMSH2-deficient lines.[19] It has also been hypothesized that treatment regimens with agents such as cisplatin might enrich tumors for MMR-deficient cells,[20] and it has been shown that a substantial portion of secondary, or therapy-related, leukemias show signs of MMR deficiency.[20,21] Collectively, these results show the broad involvement of MMR in mediating drug response, the effects of MMR deficiency on this response, and the need to develop therapeutic agents that specifically target MMR-deficient cells, perhaps through broad recognition of DNA mismatches.

DNA mismatch recognition is commonly achieved through oligonucleotide- or enzyme-based methods. Oligonucleotide-based detection schemes rely on differential hybridization between fully complementary and mismatched duplexes.[22–27] Enzyme-based methods typically employ mismatch recognition enzymes such as *E. coli* MutS.[28] Small molecule-based detection schemes are relatively less common. Saito and Nakatani groups have demonstrated the use of naphthyridine dimers to recognize several mismatches by hydrogen bonding to the bases.[29–31] Teulade-Fichou and co-workers reported a luminescent bisanthracene derivative that discriminates between well-matched and mismatched DNA.[32] In the field of inorganic small molecules, our laboratory has developed metal complexes that recognize over 80% of all base mismatches, and the therapeutic effect of these metal complexes are being investigated.[33]

The successful design of this new class of metal complexes to recognize mismatches was predicated on a careful examination of the structure and dynamics of mismatches. Mismatches are similar to Watson-Crick base pairs in terms of their hydrogen bonded structures, and do not distort the double helical structure of duplex DNA (Figure 1.2).[34–37] However, compared with Watson-Crick base pairs, mismatches are thermodynamically less stable, a

trait reflected by the fact that melting temperatures decrease notably for oligonucleotides containing mismatches (though not always for G-containing mismatches).[38,39] Mismatches also show increased dynamic motion and longer base-pair opening lifetimes, as observed in NMR.[38,40–42] These characteristics of mismatched bases led our laboratory to devise recognition strategies that enabled the synthesis of metal complexes which bind mismatches with high affinity and specificity.

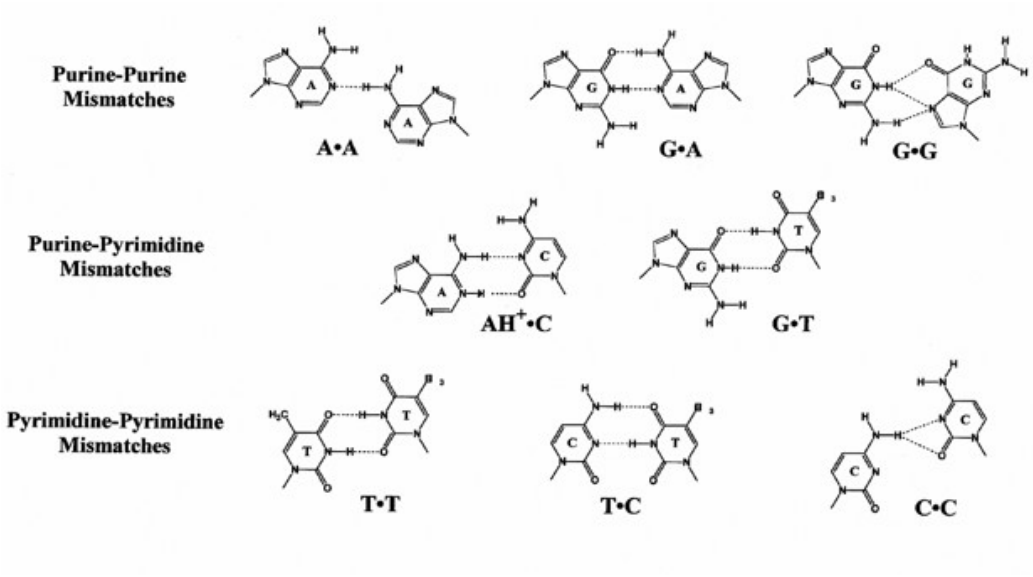

Figure 1.2. Chemical structures of base mismatches.

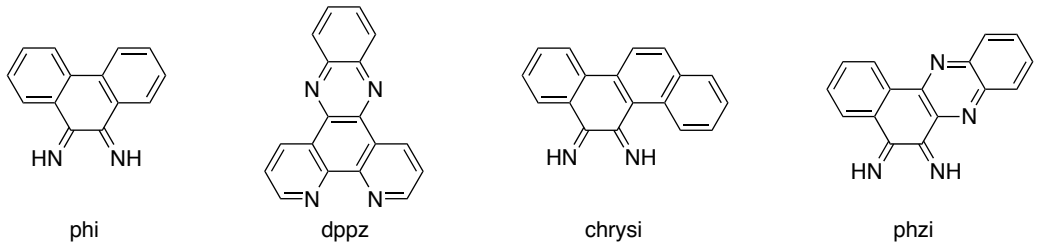

Figure 1.3. Chemical structures of intercalating and inserting ligands.

The most important trait of the new class of mismatch-recognizing metal complex is a sterically expansive ligand, either chrysi (chrysene-5,6-quinone diimine) or phzi (benzo-[*a*]-phenazin-5,6-quinone diimine, Figure 1.3) that confers this mismatch specificity. Chrysi or phzi, at 11.3 Å in width, does not fit into a well-matched DNA π-stack. For comparison, smaller ligands such as phi (9,10-phenanthrenequinone diimine) or dppz (dipyrido[3,2-*a*:2',3'-*c*]phenazine), also shown in Figure 1.3, fit easily between the DNA backbone, allowing

resultant metal complexes to intercalate between almost any two neighboring base pairs. Thus, although incapable of intercalation between well-matched base pairs, chrysi or phzi is able to insert into the π-stack at destabilized mismatch sites via the minor groove, ejecting the pair of mismatched bases out of the helix. This insertion mode of binding via the minor groove was fully elucidated by the crystal structure determination of $Rh(bpy)_2chrysi^{3+}$ bound to AC mismatches in a 12-mer duplex (Figure 1.4).[43] Later crystal structures revealed identical structural features of $Rh(bpy)_2chrysi^{3+}$ insertion at an AA mismatch.[44] Further, NMR studies also support the minor-groove insertion of the chrysi ligand and ejection of mismatched bases in solution.[45] Interestingly, this insertion mode of binding was first proposed almost half a century ago by Lerman,[46] but had never been confirmed experimentally with small organic or inorganic molecules until the discovery of metalloinsertors. In total, $Rh(bpy)_2chrysi^{3+}$ has been shown to bind specifically to a single mismatch in a 2725bp linearized plasmid heteroduplex, and recognize over 80% of mismatch sites in all the possible single base pair flanking sequence contexts.[47] Similar to $Rh(L)_2(phi)^{3+}$ complexes, $Rh(L)_2chrysi^{3+}$ or $Rh(L)_2phzi^{3+}$ photocleaves the DNA backbone when irradiated between 300 and 400 nm. They also show extremely enantiospecific binding, the Δ-enantiomer (Figure 1.5) being much more effective at binding to B-form DNA.[48]

The *in vivo* effects of $Rh(bpy)_2chrysi^{3+}$and $Rh(bpy)_2phzi^{3+}$ have been characterized in the isogenic cell lines HCT116N and HCT116O.[49] The HCT116 cell line is a colorectal carcinoma line deficient in the hMLH1 gene. Two derivative cell lines, HCT116N and HCT116O, have been made through transfection of human chromosome 3 (ch3) and human chromosome 2 (ch2), respectively. The presence of a functional copy of ch3 restores MMR proficiency in the HCT116N line, while the HCT116O line transfected with ch2 remains MMR deficient.[50] The mismatch recognition compounds were shown to selectively inhibit the proliferation of the repair-deficient HCT116O line.[49]

Recent work within our laboratory on luminescent ruthenium complexes has also shown that these tris(chelate) complexes are taken up inside cells through passive diffusion facilitated by the membrane potential.[51,52] Variations in ancillary ligands have dramatic effects on cellular uptake, with increased lipophilicity facilitating uptake. Uptake can also be increased through functionalization with a nuclear localizing peptide.[53]

In this chapter, we examine the effects of ancillary ligand variation in the $Rh(L)_2chrysi^{3+}$ family (Figure 1.6) on the ability of these complexes to target DNA mismatches *in vitro* and

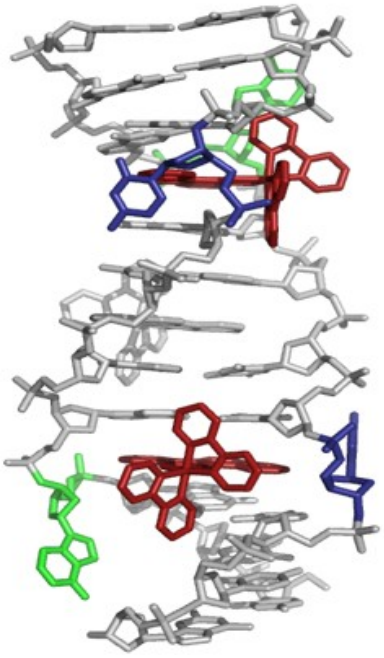

Figure 1.4. Crystal structure showing the insertion of $Rh(bpy)_2chrysi^{3+}$ (red) via the minor groove at two AC mismatch sites in a 12-mer duplex. The mismatched bases are ejected (adenosine is colored green and cytosine colored blue).

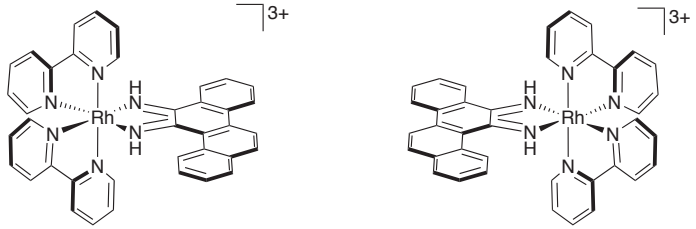

Figure 1.5. Λ- (left) and Δ- (right) isomers of $Rh(bpy)_2chrysi^{3+}$.

in vivo. Importantly, we establish that the differential inhibition of cellular proliferation in MMR-deficient cells is correlated with mismatch binding affinity.

1.2 Experimental protocols

1.2.1 Materials

$RhCl_3$ was purchased from Pressure Chemical (Pittsburgh, PA). $[Rh(NH_3)_5Cl]Cl_2$ was obtained from Strem Chemical (Newburyport, MA). Isoquinoline, 2,2'-dipyridylamine (HDPA), 4,7-diphenyl-1,10-phenanthroline (DIP), and Sephadex ion-exchange resin were obtained from Sigma-Aldrich (St. Louis, MO). Sep-Pak C18 solid-phase extraction cartridges were

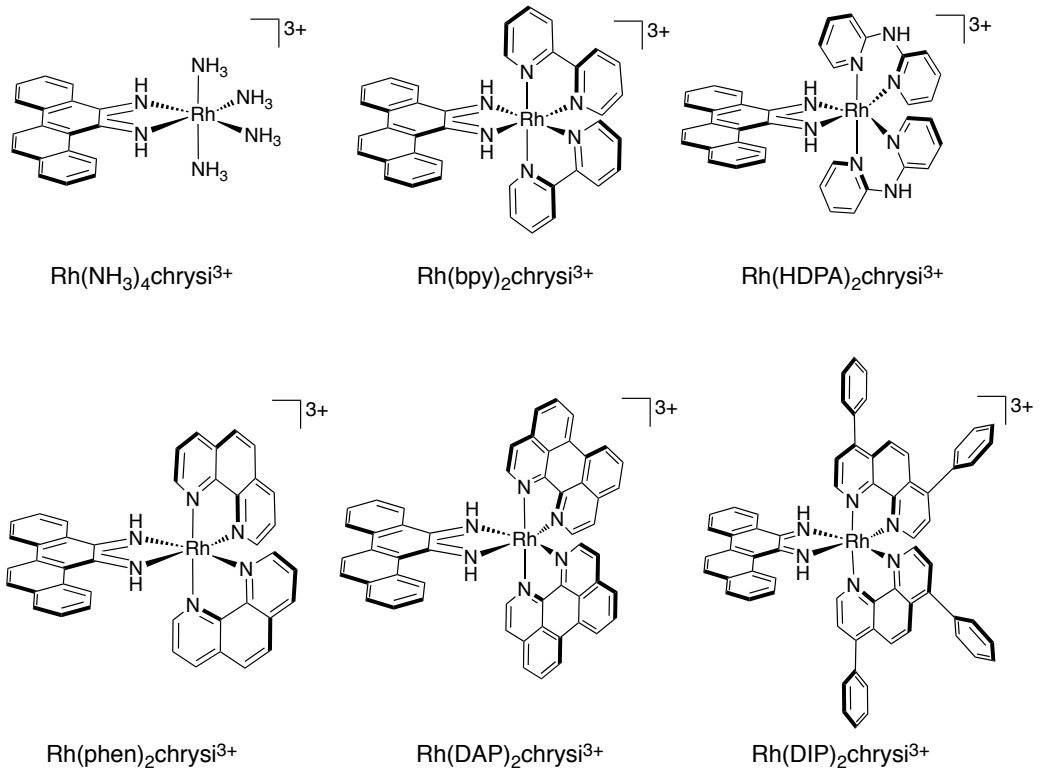

Figure 1.6. Chemical structures of $[Rh(L_2)(chrysi)]^{3+}$ complexes surveyed in this study.

purchased from Waters Chemical Co. (Milford, MA). Phosphoramidites were purchased from Glen Research (Sterling, VA). Media and supplements were purchased from Invitrogen (Carlsbad, CA). BrdU, antibodies, buffers, and peroxidase substrate were purchased in kit format from Roche Molecular Biochemicals (Mannheim, Germany). All commercial materials were used as received.

1.2.2 DNA synthesis, purification, and quantification

Oligonucleotides were synthesized on an AB 3400 DNA synthesizer using standard phosphoramidite chemistry. DNA was synthesized with a 5'-dimethoxy trityl (DMT) protecting group. The oligonucleotides were cleaved from the beads by reaction with concentrated ammonium hydroxide at 60 °C overnight. The resulting free oligonucleotides was purified by HPLC using a C18 reverse-phase column (Varian, Inc.) on a Hewlett-Packard 1100 HPLC. The DMT group was removed by reaction with 80% acetic acid for 15 min at room temperature. The DMT-free oligonucleotides were precipitated with absolute ethanol and purified again by HPLC. Positive identification of the oligonucleotides and their purity were con-

firmed by MALDI-TOF mass spectrometry. Quantification was performed on a Beckman DU 7400 spectrophotometer using the extinction coefficients at 260 nm (ϵ_{260}) estimated for single stranded DNA.

1.2.3 Rhodium complex synthesis

The compound 1,12-diazaperylene (DAP) was synthesized according to literature procedures.[54] Chrysene-5,6-dione, $Rh(bpy)_2chrysi^{3+}$ and $Rh(phen)_2chrysi^{3+}$ were laboratory stocks synthesized according to established protocols.[55]

$[Rh(NH_3)_4(chrysi)]OTf_3$. $Rh(NH_3)_6OTf_3$ was prepared as described by Sargeson.[56,57] $Rh(NH_3)_6OTf_3$ (200 mg, 0.3 mmol) was reacted with chrysene-5,6-dione (78 mg, 0.3 mmol) in 150 mL of acetonitrile and 50 mL of water with 0.6 mL of 1N NaOH as a catalyst. The reaction mixture (an orange suspension) was left stirring for 16 h at room temperature and turned into a dark orange-red suspension. Hydrochloric acid was added until the pH reached neutral. Acetonitrile was removed under vacuum and the resulting suspension filtered to remove unreacted chrysene quinone. The product was separated from unreacted $Rh(NH_3)_6OTf_3$ on a Sep-Pak C18 cartridge eluting with 1:1:0.1% H_2O:CH_3CN:TFA. The eluant was lyophilized to recover the solid product (50 mg, 38%). ^{1}H-NMR (300 MHz, d_6-DMSO): δ 13.5 (s, 1H), 12.9 (s, 1H), 8.7–8.5 (m, 3H), 8.45 (dd, 2H), 8.2 (d, 1H), 8.0–7.6 (m, 4H), 4.4 (s, 3H), 4.35 (s, 3H), 3.7 (s, 6H). ESI-MS: calc. 427.11, obs. 427.0 (M-2H$^+$), 410.0 (M-NH_3-2H$^+$), 391.1 (M-2NH_3-2H$^+$), 374.0 (M-3NH_3-2H$^+$), 356.9 (M-4NH_3-2H$^+$).

***rac*-[Rh(DAP)$_2$(chrysi)]OTf$_3$.** $Rh(NH_3)_4chrysi^{3+}$ (20 mg, 0.02 mmol) was reacted with 1,12-diazaperylene (DAP) (20 mg, 0.08 mmol, excess) in 45 mL of ethanol and 45 mL of water. The bright orange solution was heated under reflux for 16 h. The reaction mixture turned a darker orange color upon heating. Ethanol was removed under vacuum and the resulting solution filtered to remove any residue. The filtrate was concentrated on a Sep-Pak C18 cartridge eluting with 1:1:0.1% H_2O:CH_3CN:TFA, lyophilized and purified on an alumina column eluting with 5% MeOH in CH_2Cl_2. The fractions were collected and dried in vacuum to give an orange-brown solid (6.3 mg, 30%). ESI-MS: calc. 865.2 (M-2H$^+$), obs. 865.3 (M-2H$^+$), 611.1 (M-DAP-2H$^+$), 433.2 (M-H^{2+}). UV/vis (H_2O, pH 5): 267 nm (53100 M^{-1} cm^{-1}), 479 nm (16200 M^{-1} cm^{-1}), 509 nm (16000 M^{-1} cm^{-1}).

***rac*-[Rh(HDPA)$_2$(chrysi)]OTf$_3$.** $Rh(NH_3)_4chrysi^{3+}$ (15 mg, 0.02 mmol) was reacted with HDPA (20 mg, 0.12 mmol, excess) in 20 mL ethanol and 20 mL water. The dark red

solution was heated under reflux for 16 h. The reaction mixture turned reddish brown upon heating. Ethanol was removed under vacuum and the resulting solution filtered to remove any residue. The filtrate was concentrated on a Sep-Pak C18 cartridge eluting with 1:1:0.1% H_2O:CH_3CN:TFA, lyophilized and purified on an alumina column eluting with 2% MeOH in CH_2Cl_2. The fractions were collected and dried under vacuum to give an orange-brown solid (8mg, 39%). ^{1}H-NMR (300 MHz, d_6-DMSO): δ 12.84 (s, 1H), 12.34 (s, 1H), 11.78 (s, 1H), 10.32 (d, 1H, 8.7 Hz), 8.63 (d, 1H, 6.9 Hz), 8.40 (d, 1H, 8.4 Hz), 8.31 (d, 1H, 9.3 Hz), 8.14 (m, 2H), 8.07 (d, 1H, 8.7 Hz), 8.04 (d, 1H, 5.4 Hz), 7.94 (m, 4H), 7.77 (m, 5H), 7.58 (m, 2H), 7.48 (d, 1H, 8.1 Hz), 7.41 (d, 1H, 8.4 Hz), 7.32 (s, 1H), 7.14 (m, 2H), 7.04 (t, 1H, 6.8 Hz), 6.98 (t, 1H, 6.9 Hz), 6.81 (t, 1H, 6.5 Hz) ppm. ESI-MS: calc. 699.2 (M-2H$^+$), obs. 699.2 (M-2H$^+$), 350.1 (M-H^{2+}). UV/vis (H_2O, pH 5): 287 nm (42200 M^{-1} cm^{-1}), 321 nm (23000 M^{-1} cm^{-1}), 442 nm (8800 M^{-1} cm^{-1}).

***rac*-[Rh(DIP)$_2$(NH$_3$)$_2$]OTf$_3$.** $RhCl_3$ and 2 equiv. of DIP were combined in 1:1 ethanol:water and refluxed overnight. The solvent was removed *in vacuo*, and the product was recrystallized by dissolving in acetonitrile at 60 °C and cooling to −20 °C. The precipitate was collected by filtration, washed in diethyl ether, and dissolved in neat triflic acid. The solution was again cooled and added dropwise to NH_4OH at −20 °C. The pale white precipitate was collected by filtration and washed with a small amount of water to give [Rh(DIP)$_2$(NH$_3$)$_2$]OTf$_3$.

***rac*-[Rh(DIP)$_2$chrysi]Cl$_3$.** *rac*-[Rh(DIP)$_2$(NH$_3$)$_2$]OTf$_3$ was combined with a 10% excess of chrysene-5,6-quinone and a catalytic amount of NaOH in acetonitrile and stirred at room temperature overnight. The condensation reaction was terminated by addition of a stoichiometric amount of HCl. The solvent was removed *in vacuo*, and the product was purified by alumina column chromatography. Unbound chrysi ligand eluted first with ethyl acetate, and the purified product then eluted with acetonitrile. Finally, the compound was dissolved in 3:2 CH_3CN:H_2O, and the triflate counterion was exchanged for chloride ion with Sephadex QAE-125 ion-exchange resin. ESI-MS (cation): calc. 1023 m/z (M-H^{2+}), obs. 1020.9 m/z (M-2H$^+$), 511.0 m/z (M-H^{2+}). UV/vis (H_2O, pH 5): 290 nm (104000 M^{-1} cm^{-1}), 335 nm (43900 M^{-1} cm^{-1}), 373 nm (22300 M^{-1} cm^{-1}).

1.2.4 Photocleavage titrations

The oligonucleotide was ^{32}P-labeled at the 5'-end by incubating DNA with ^{32}P-γATP and polynucleotide kinase (PNK) at 37 °C for 2 h, followed by purification using gel electrophoresis.[55] A small amount of the labeled DNA (less than 1% of the total amount of DNA) was added to 2 μM DNA in 100 mM NaCl, 20 mM NaPi, pH 7.1 buffer. The DNA was annealed by heating at 90 °C for 10 min and cooling down slowly to room temperature over a period of 2 h. Rhodium complex solutions ranging from nanomolar to micromolar concentration were made in Milli-Q water. 10 μL of annealed 2 μM DNA and 10 μL of Rh solution at each concentration was mixed in an eppendorf tube and incubated at 37 °C for 10 min. A light control (LC), in which the DNA was mixed with 10 μL of water and irradiated, and a dark control (DC), in which the DNA was mixed with the highest concentration of Rh complex without irradiation, were also prepared. The samples were left in the heat block and irradiated on an 1000-W Hg/Xe arc lamp (320–440 nm, Oriel) for 5 min. The irradiated samples were dried and electrophoresed in a 20% denaturing polyacrylamide gel. The gel was then exposed to a phosphor screen, and the relative amounts of DNA in each band were quantitated by phosphorimagery (ImageQuant).

1.2.5 Binding constant determination

The fraction of DNA cleaved in each lane on the gel was normalized and plotted against the log of the concentration of rhodium complex. At least three photocleavage titrations were carried out for each racemic metal complex. The pooled data were fit to a sigmoidal curve using OriginPro 6.1. The resulting midpoint value (i.e., the log of [rhodium complex] at the inflection point of the curve) was converted to units of concentration ([Rh50%]). The dissociation constant was calculated according to K_D = [Rh50%] – 0.5[DNA], and the binding constant was defined as $K_B = 1/K_D$. The errors were derived from the errors associated with the midpoint values. For complexes that did not photocleave DNA, a binding competition titration was carried out with a constant amount (1 μM) of *rac*-$Rh(bpy)_2chrysi^{3+}$added to each sample. The binding and dissociation constants of the non-photocleaving complex were calculated by solving simultaneous binding equlibiria involving DNA, $Rh(bpy)_2chrysi^{3+}$, and the complex in question in Mathematica 6.0.

1.2.6 MALDI-TOF mass spectrometry

Irradiation samples were prepared similarly to those used in photocleavage titrations, except that 2 μM of unlabeled DNA and 2 μM of Rh complex were used instead of 1 μM. The samples were heated at 90 °C for 30 min after irradiation to convert any metastable photocleavage products to stable one(s). Water (30 μL) was added to each sample, and the entire volume was passed through a Bio-Rad Microbio-spin chromatography column. The samples were dried and desalted using the ZipTip procedure (Millipore). The desalted oligonucleotides were then dried and redissolved in 1 μL of water. MALDI-TOF mass spectra were taken on a PerSeptive Biosystem Voyager-DE Pro instrument. The samples were prepared by the dry droplet method, using 3-hydroxypicolinic acid and diammonium citrate as matrix. Several scans of 100 shots each were taken and averaged.

1.2.7 Fluorescence spectroscopy

Steady state fluorescence spectra were recorded on an ISS-K2 fluorimeter at ambient temperatures in aerated solution (5mM Tris, 50 mM NaCl, pH 7.5).

1.2.8 Structural modeling

Geometries of metal complexes were optimized in ChemDraw3D (CambridgeSoft) using MM2 minimization. All modeling sessions were performed in PyMol using the DNA crystal structure (PDB entry 2O1L).[43] Metal complexes were combined with the DNA structure by superimposing the Rh atom with that in $Rh(bpy)_2chrysi^{3+}$ in the crystal structure and maximally overlapping the chrysi ligands. For clarity only one Rh complex is shown in each model.

1.2.9 Cell culture

HCT116N and HCT116O cells were grown in RPMI medium 1640 supplemented with 10% FBS, 2 mM L-glutamine, 0.1 mM nonessential amino acids, 1 mM sodium pyruvate, 100 units/mL penicillin, 100 μg/mL streptomycin, and 400 μg/mL Geneticin (G418). Cells were grown in tissue culture flasks and dishes (Corning Costar, Acton, MA) at 37 °C under 5% CO_2 atmosphere.

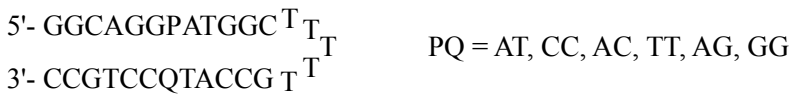

Figure 1.7. Sequence of the DNA hairpin used in Rh(chrysi) complex-DNA binding experiments.

1.2.10 Cellular proliferation ELISA

HCT116N and HCT116O cells were plated in 96-well plates at 2000 cells/well and allowed 24 h to adhere. The cells were then incubated with rhodium complexes for the durations specified. For incubation less than 72 h, the Rh-containing medium was replaced with fresh medium, and the cells were grown for the remainder of the 72 h period. Cells were labeled with BrdU 24 h before analysis. The BrdU incorporation was quantified by antibody assay according to established procedures.[58,59] Cellular proliferation was expressed as the ratio of the amount of BrdU incorporated by the treated cells to that of the untreated cells.

1.3 Results

1.3.1 Binding affinities of metal complexes at single base mismatches

The binding constants of the family of $Rh(L)_2chrysi^{3+}$ complexes at a CC, AC or TT mismatch in a 29-mer DNA hairpin (Figure 1.7) were measured. The hairpin sequence allows cleavage site determination on either strand around the DNA mismatch site. By irradiating samples of DNA titrated with varying concentrations of a rhodium complex, a photocleavage titration curve is obtained, from which the binding constant of the Rh complex is determined. A typical autoradiogram of electrophoresced samples in a photocleavage titration with $Rh(bpy)_2chrysi^{3+}$ and CC-containing DNA is shown in Figure 1.8. The position of the photocleavage band indicates that $Rh(bpy)_2chrysi^{3+}$ cleaves one base away from the mismatch site near the 3'-end.

MALDI-TOF mass spectrometry of similar irradiation samples (but without the radioactive label) shows peaks corresponding to the parent DNA and one major cleavage product (Figure 1.9), which is assigned to 5'-GGCAGGCATGGCTTTTTGCCATC-Pi-3'. The assignment agrees with the band position on the autoradiogram and is consistent with previous work on the determination of photocleavage products using MALDI-TOF

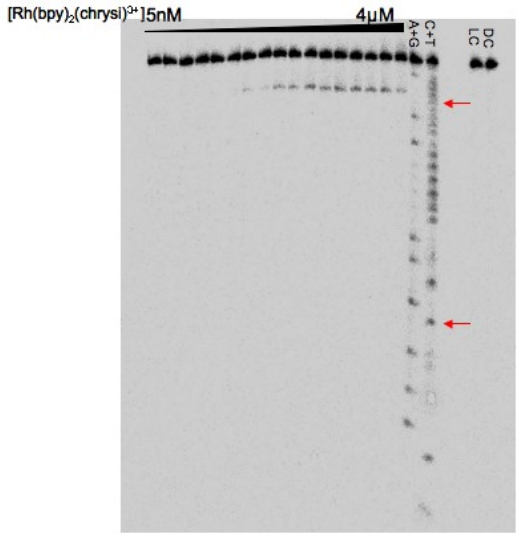

Figure 1.8. Autoradiogram of a denaturing 20% polyacrylamide electrophoresis gel showing a representative photocleavage titration. Conditions are DNA (CC mismatch, 1 μM), $Rh(bpy)_2chrysi^{3+}$ (lanes 1 to 17: 5 nM, 10 nM, 20 nM, 50 nM, 0.1 μM, 0.2 μM, 0.3 μM, 0.4 μM, 0.5 μM, 0.6 μM, 0.7 μM, 0.8 μM, 0.9 μM, 1 μM, 2 μM, 3 μM, 4 μM, lane 20: no Rh complex, lane 21: 4 μM), NaCl 50 mM, NaPi 10 mM, pH 7.1 at room temperature. Samples were irradiated at 365 nm on a 1000W Hg/Xe lamp for 5 min. The dark control in lane 21 was not irradiated. Lanes 18 and 19 are Maxam-Gilbert sequencing reactions. The mismatched sites are marked with red arrows.

mass spectrometry.[53] This cleavage pattern is found to be true of $Rh(phen)_2chrysi^{3+}$ and $Rh(DIP)_2chrysi^{3+}$ as well. No other photocleavage bands are visible, demonstrating the high specificity of Rh(chrysi) complexes binding to the mismatch. The photocleavage titration curve is generated from the autoradiogram by quantitating the amount of photocleavage relative to the total amount of DNA at each Rh concentration. Pooled data from at least three repeats were fitted to a sigmoidal curve (Figure 1.10). The dissociation constant for $Rh(bpy)_2chrysi^{3+}$ at a CC mismatch is found to be (30 $\pm$ 3) nM, which translates into a binding constant of (3.4 $\pm$ 0.3) $\times$ 10^7 M^{-1}. At an AC and TT mismatch, the respective binding constants are (2.2 $\pm$ 0.2) $\times$ 10^6 M^{-1} and (6.3 $\pm$ 2.0) $\times$ 10^6 M^{-1}. The dissociation constant for $Rh(phen)_2chrysi^{3+}$ is found to be (320 $\pm$ 20) nM at a CC mismatch, which corresponds to a binding constant of (3.2 $\pm$ 0.3) $\times$ 10^6 M^{-1}. The binding affinity of $Rh(phen)_2chrysi^{3+}$ to AC is (1.4 $\pm$ 0.2) $\times$ 10^6 M^{-1}. At a TT mismatch, the photocleavage efficiency of $Rh(phen)_2chrysi^{3+}$ is too low to allow meaningful quantification.

In the case of $Rh(DIP)_2chrysi^{3+}$, the quantitation of the fraction of DNA bound to the metal complex is complicated by the presence of a slower-running band above the parent

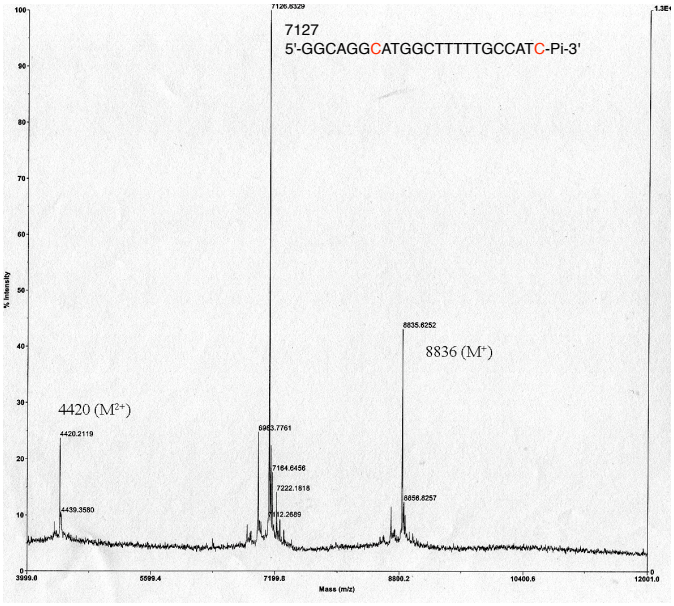

Figure 1.9. MALDI-TOF mass spectrum of CC-containing DNA after irradiation in the presence of $Rh(bpy)_2chrysi^{3+}$.

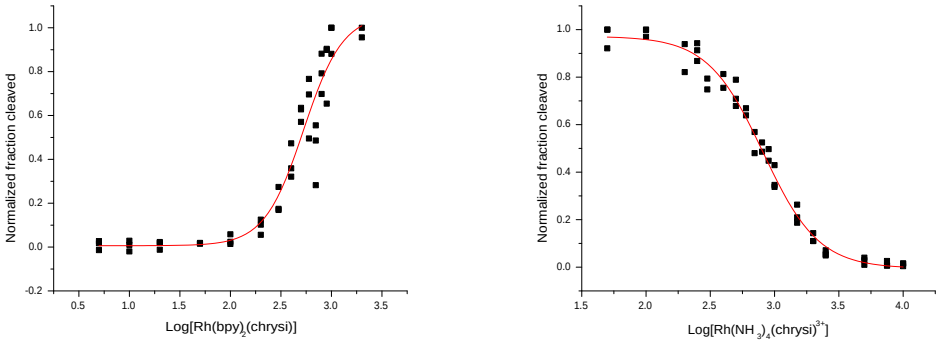

Figure 1.10. Left: plot of normalized fractions of DNA cleaved versus the log of $Rh(bpy)_2chrysi^{3+}$ concentration in nM from three repeats of a photocleavage titration at 37 °C. The pooled data are fit to a sigmoidal function. Right: plots of normalized fraction of DNA cleaved versus the log of $Rh(NH_3)_4chrysi^{3+}$ concentration in nanomolar from three repeats of a binding competition titration at 37 °C. The pooled data are fit to a sigmoidal function.

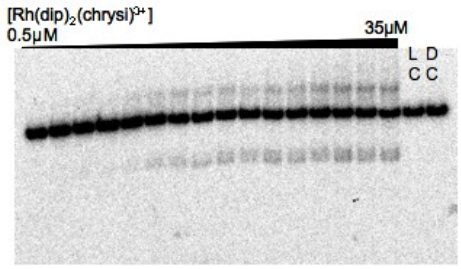

Figure 1.11. Autoradiogram of a denaturing 20% polyacrylamide electrophoresis gel showing photocleavage titration using $Rh(DIP)_2chrysi^{3+}$. Conditions are DNA (1.5 μM), $Rh(DIP)_2chrysi^{3+}$ (lanes 1 to 16: 0.5 μM, 1 μM, 2 μM, 3 μM, 4 μM, 5 μM, 6 μM, 7 μM, 8 μM, 9 μM, 10 μM, 15 μM, 20 μM, 25 μM, 30 μM, 35 μM, lane 17: no Rh complex, lane 18: 40 μM), NaCl 50 mM, NaPi 10 mM, pH 7.1 at 37 °C. Samples were irradiated on a 1000-W Hg/Xe lamp (320–440 nm) for 5 min except for the dark control in Lane 9. In addition to the photocleavage band, a slower-running band above the parent band is visible.

band (Figure 1.11). The intensity of this band is proportional to that of the photocleavage band, which suggests that its origin is somewhat mismatch related. This is confirmed by irradiating samples of $Rh(DIP)_2chrysi^{3+}$ and a DNA hairpin with a matched AT base pair in place of CC (Figure 1.12). Without a mismatch, the slower-running band is not observed.

Piperidine treatment after irradiation shows that a small fraction of the slower-running band is due to the formation of a lesion prone to cleavage by piperidine, perhaps 8-oxo-guanine (Figure 1.12). MALDI-TOF mass spectrometry detects an additional cluster of peaks around m/z $\approx$ 9601 (m/z for parent DNA = 8836). These peaks are tentatively assigned to covalent Rh-DNA adducts with both DIP ligands but without the chrysi ligand (calculated mass for DNA+Rh+2DIP = 9603). Thus, the quantitation of the fraction of DNA photocleaved is carried out by dividing the photocleavage band intensity over the total DNA in a given lane including the slower-running band. The dissociation constant for $Rh(DIP)_2chrysi^{3+}$ is found to be (11 $\pm$ 2) μM and the binding constant is (9 $\pm$ 1) $\times$ 10^4 M^{-1} (Table 1.1). It should be noted that if we treat the slower-running band as a mismatch-specific photoreaction product and combine it with the normal photocleavage band, the measured binding constant will not differ much, since the two bands are proportional to each other and will give similar normalized fractions regardless of whether the slower-running band is included. With an AC mismatch, $Rh(DIP)_2chrysi^{3+}$ does not yield any photocleavage up to 100 μM; thus, its K_D value is estimated to be greater than that. In the case of TT mismatch, again no photocleavage band was observed. For both the AC and TT mismatches, the intensity of the parent DNA band decreases and that of the

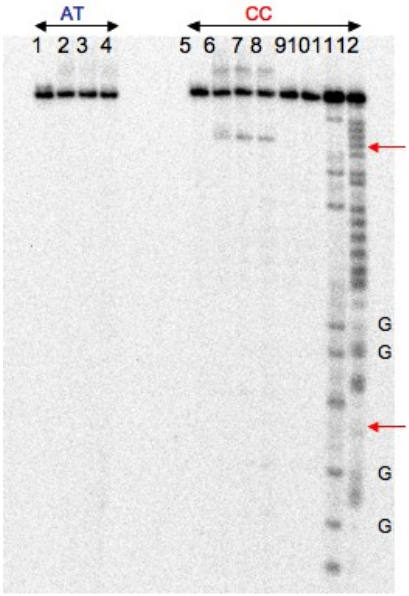

Figure 1.12. Autoradiogram of a denaturing 20% polyacrylamide electrophoresis gel comparing $Rh(DIP)_2chrysi^{3+}$ reaction with matched (AT) and mismatched (CC) DNA. Conditions are DNA (1 μM), $Rh(DIP)_2chrysi^{3+}$ (lanes 1 and 5: 3 μM, lanes 2–4, 6–8 and 10: 40 μM, lane 9: no Rh complex), NaCl 50 mM, NaPi 10 mM, pH 7.1 at 37 °C. Samples were irradiated on a 1000-W Hg/Xe lamp (320–440 nm) for 5 min except for the dark control in Lane 10. Samples in lanes 3 and 7 were heated at 90 °C for 30 min after irradiation. Samples in lanes 4 and 8 were treated with piperidine after irradiation. The mismatched sites are marked with red arrows. Guanine doublets are labeled. Lanes 11 and 12 are Maxam-Gilbert sequencing reactions.

slower-running band increases as the concentration of $Rh(DIP)_2chrysi^{3+}$ increases, until the entire parent band disappears.

$Rh(DAP)_2chrysi^{3+}$ photocleaves DNA; however, instead of producing a single photocleavage band, a smear is seen in the autoradiogram, implying extremely nonspecific binding and cleavage (Figure 1.13). The same smear is seen from irradiations at 313, 320–440, or 495 nm. We attribute this nonspecific interaction with DNA to the shape of the DAP ligand: the DAP ligand resembles a phi ligand in terms of its size and distance from the Rh center. Thus, it is not surprising that it can intercalate and cleave at multiple positions in the duplex. More interestingly, $Rh(DAP)_2chrysi^{3+}$ is found to be luminescent in water, emitting at 560 nm. The luminescence intensity is not proportional to its concentration, with the intensity at 1 μM being much less than 100-fold of the intensity at 10 nM, which implies that the complex is self-quenching. When DNA is added to a buffered solution of $Rh(DAP)_2chrysi^{3+}$, its luminesence decreases as the amount of DNA added increases. The extent of the decrease is similar in the presence of matched or mismatched DNA (Figure 1.14). Consistent with the results from irradiation experiments, these observations again point to nonspecific interactions with DNA and the quenching of the DAP ligand in a hydrophobic environment (in this case propbably stacked between base pairs). Thus, due to its nonspecific interactions with DNA, it was not feasible to extract mismatch-specific binding constant for $Rh(DAP)_2chrysi^{3+}$.

As with phenanthrenequinone diimine complexes of rhodium containing saturated amine ligands, $Rh(NH_3)_4chrysi^{3+}$ and *rac*-$Rh(HDPA)_2chrysi^{3+}$ promote relatively little DNA cleavage upon irradiation.[60] As a result, their binding affinities were determined through binding competition titrations with 1 μM *rac*-$Rh(bpy)_2chrysi^{3+}$. A typical autoradiogram of electrophoresced samples in a binding competition titration is shown in Figure 1.15. On the basis of the binding constant of $Rh(bpy)_2chrysi^{3+}$, the binding constant of $Rh(NH_3)_4chrysi^{3+}$ is calculated by solving simultaneous equilibria at the inflection point of the photocleavage titration curve. Through this competitive titration, the binding constant of $Rh(NH_3)_4chrysi^{3+}$ at a CC mismatch is found to be $(1.0 \pm 0.2) \times 10^8$ M^{-1}. The binding constant is $(3.4 \pm 0.3) \times 10^6$ M^{-1} at an AC mismatch, and $(8.8 \pm 2.0) \times 10^6$ M^{-1} at a TT mismatch. From similar binding competition titrations, the binding constant of *rac*-$Rh(HDPA)_2chrysi^{3+}$ is found to be $(2.0 \pm 0.3) \times 10^7$ M^{-1} at a CC mismatch and $(2.6 \pm 0.2) \times 10^6$ M^{-1}at an AC mismatch. The dissociation and binding constants of the entire series of Rh(chrysi)

Figure 1.13. Autoradiogram of a denaturing 20% polyacrylamide electrophoresis gel showing $Rh(DAP)_2chrysi^{3+}$ photoreaction. Conditions are DNA (1 μM), $Rh(DAP)_2chrysi^{3+}$ (lanes 1–5: 0.25 μM, 1.25 μM, 2.5 μM, 6 μM, 12.5 μM, lane 7: 0.6 μM, lane 8: 6 μM,), $Rh(bpy)_2chrysi^{3+}$ (lanes 6–8: 1 μM), NaCl 50 mM, NaPi 10 mM, pH 7.1 at 37 °C. Samples were irradiated on a 1000-W Hg/Xe lamp (320–440 nm) for 10 min.

complexes are summarized in Table 1.1.

As $Rh(NH_3)_4chrysi^{3+}$ exhibits very tight binding to CC and AC mismatches, its ability to recognize guanine-containing mismatches was also investigated. The metallointercalator $Rh(bpy)_2phi^{3+}$ was used to photocleave a DNA hairpin containing either an AG or a GG mismatch in a nonspecific manner. $Rh(NH_3)_4chrysi^{3+}$ was added to compete for binding with $Rh(bpy)_2phi^{3+}$. The binding of $Rh(bpy)_2phi^{3+}$ at the mismatch site decreased significantly in the case of AG mismatch and to a lesser extent in the case of GG mismatch, as evident in the reduction in photocleavage around the mismatched sites (Figure 1.16). Photocleavage by $Rh(bpy)_2phi^{3+}$ at other sites in DNA was not as significantly affected.

1.3.2 Inhibition of cellular proliferation by enzyme-linked immunosorbent assay (ELISA)

An ELISA for DNA synthesis was used to quantify the effects of the metalloinsertors on the proliferation of HCT116N cells (MMR-proficient) and HCT116O cells (MMR-deficient).[49] Both cell lines were incubated with 0-25 μM of each member of the $Rh(L)_2chrysi^{3+}$ complexes family except $Rh(DIP)_2chrysi^{3+}$, which was administered at 0-5 μM concentrations due to its greater uptake characteristics. Incubations were performed for 12, 24, 48, or 72

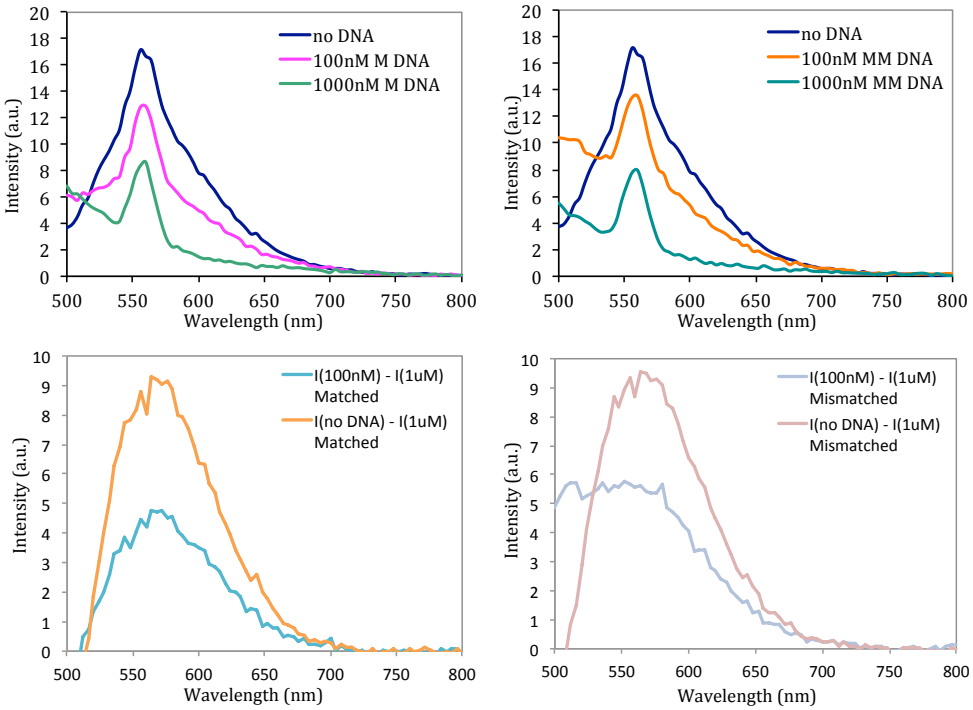

Figure 1.14. Emission spectra of $Rh(DAP)_2chrysi^{3+}$ in the absence and presence of matched (top left) or mismatched (top right) DNA (excitation wavelength = 470 nm). The sharp peak at 560 nm is due to Raman scattering of solvent water. The difference spectra (i.e., the difference in intensity, I, between the spectra recorded in the presence of 100 nM and 1 μM DNA, as well as the difference in I between the spectra in the absence and presence of 1 μM DNA) are shown in the bottom row. Qualitatively there is no difference between the fluorescence response in the presence of matched versus mismatched DNA. The fluorescence intensity (I) decreases with increasing amounts of either matched or mismatched DNA.

h. After the 12, 24, and 48 h incubations, the medium containing Rh was replaced with fresh medium, and the cells were grown for the remainder of the 72 h period. The extent of cellular proliferation is expressed as the ratio of BrdU incorporated by the rhodium-treated cells compared to untreated controls. Figure 1.17 shows representative data for $Rh(NH_3)_4chrysi^{3+}$ at various incubation times. No significant preferential inhibition of the HCT116O cell line is seen at incubation times less than 24 h, consistent with previous results for $Rh(bpy)_2chrysi^{3+}$, with the exception of $Rh(DIP)_2chrysi^{3+}$, which displays a small differential effect at 12 h.[49] With longer incubation times, however, $Rh(NH_3)_4chrysi^{3+}$ displays a strong differential effect with preferential inhibition of the MMR-deficient HCT116O cell line over the MMR-proficient HCT116N cell line. In particular, 48 h treatment with 10 μM $Rh(NH_3)_4chrysi^{3+}$ inhibits the proliferation of the HCT116O line by 82 $\pm$ 2% while

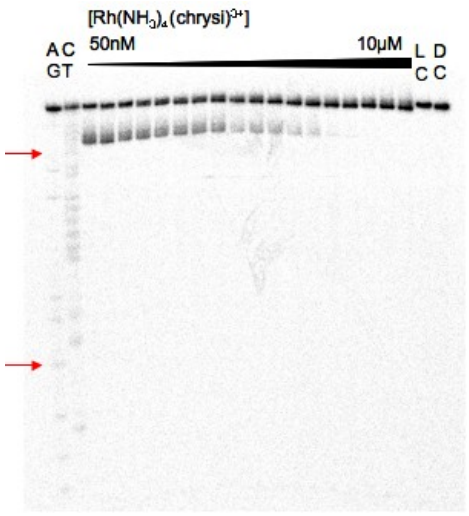

Figure 1.15. Autoradiogram of a denaturing 20% polyacrylamide electrophoresis gel showing a representative binding competition titration. Conditions are DNA (1 μM), $Rh(bpy)_2chrysi^{3+}$ (1 μM except for the light control), $Rh(NH_3)_4chrysi^{3+}$ (lanes 3 to 20: 50nM, 0.1 μM, 0.2 μM, 0.25 μM, 0.3 μM, 0.4 μM, 0.5 μM, 0.6 μM, 0.7 μM, 0.8 μM, 0.9 μM, 1 μM, 1.5 μM, 2 μM, 2.5 μM, 5 μM, 7.5 μM, 10 μM, lane 21: no Rh complexes, lane 22: no $Rh(NH_3)_4chrysi^{3+}$), NaCl 50 mM, NaPi 10 mM, pH 7.1 at 37 °C. Samples were irradiated on a 1000-W Hg/Xe arc lamp (320–440 nm) for 5 min. The dark control in lane 21 was not irradiated. Lanes 1 and 2 are Maxam-Gilbert sequencing reactions. The mismatched sites are marked with red arrows.

exerting little to no effect on the HCT116N line (7 ± 6% inhibition).

Figure 1.18 shows the ELISA results for members of the metalloinsertor family as a function of incubation time. We have shown previously that the Λ-enantiomer of $Rh(bpy)_2chrysi^{3+}$ is biologically inactive[49] and that structurally binding to a mismatch site is enantiospecific for the Δ-isomer.[43] For this reason, treatment with the 10 μM achiral tetraammine complex was compared to treatment with 20 μM racemic mixtures of the $Rh(L)_2chrysi^{3+}$ complexes (L = HDPA, bpy, or phen). The differential effect of rhodium treatment between the cells lines was quantified by subtracting the normalized percentages of cellular proliferation for each cell line. Notably, the optimal incubation time for each compound is inversely related to the hydrophobicity of the ancillary ligands, with *rac*-$Rh(phen)_2chrysi^{3+}$ exhibiting an optimal incubation time of 24 h. This trend also continues with *rac*-$Rh(DIP)_2chrysi^{3+}$, which exhibits differential effects in as little as 12 h at concentrations as low as 2 μM (Figure 1.19). Based on the early effect at 12 h, the HDPA complex may have different uptake characteristics. With the exception of the HDPA complex, this variation in activity with incubation time for the family of complexes parallels closely results seen earlier for uptake in

Table 1.1. Binding constants[a,b] of $Rh(L_2)chrysi^{3+}$ complexes[c] to a single mismatch

Complex	Structure	K_B(CC)/M^{-1}	K_B(AC)/M^{-1}	K_B(TT)/M^{-1}
$Rh(NH_3)_4chrysi^{3+}$	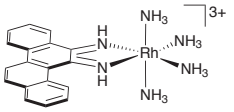	1.0×10^8	3.4×10^6	8.8×10^6
$Rh(bpy)_2chrysi^{3+}$	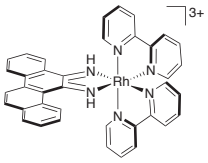	3.4×10^7	2.2×10^6	6.3×10^6
$Rh(HDPA)_2chrysi^{3+}$	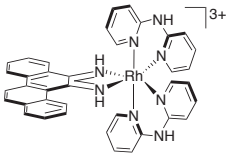	2.0×10^7	2.6×10^6	n.d.[d]
$Rh(phen)_2chrysi^{3+}$	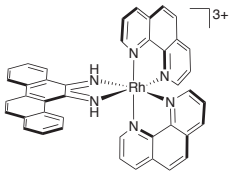	3.2×10^6	1.4×10^6	n.d.[d]
$Rh(DIP)_2chrysi^{3+}$	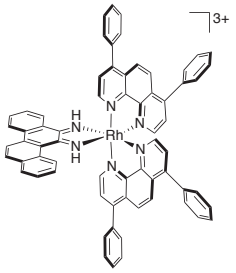	9×10^4	$<10^4$	$<10^4$

[a]Uncertainties are estimated to be 10%–15%. [b]Binding constants are determined from photocleavage or binding competition titrations using a DNA hairpin with the sequence 5'-GGCAGGXATGGCTTTTTGCCATYCCTGCC-3' (XY = CC, AC, or TT). Samples were irradiated with a solar simulator (320–440 nm) at 37 °C in 50 mM NaCl, 10 mM NaPi, pH 7.1, as described in the Experimental Protocols. [c]For the polypyridyl complexes, values are given for racemic mixtures. [d]Not determined.

HeLa cells by $Ru(bpy)_2dppz^{2+}$, $Ru(phen)_2dppz^{2+}$, and $Ru(DIP)_2dppz^{2+}$, where the most rapid uptake is apparent with the lipophilic DIP complex.[51]

Figure 1.20 summarizes the differential effects on cell proliferation and the incubation

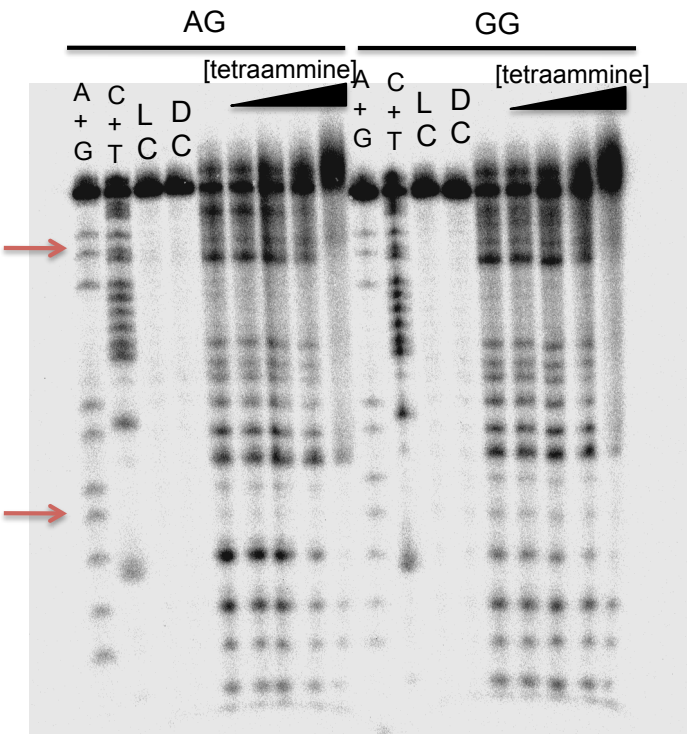

Figure 1.16. Autoradiogram of a denaturing 20% polyacrylamide electrophoresis gel showing binding competition between $Rh(NH_3)_4chrysi^{3+}$ and $Rh(bpy)_2phi^{3+}$ to a DNA hairpin containing an AG or GG mismatch. Conditions are DNA (500 nM), $Rh(bpy)_2phi^{3+}$ (10 μM except for the light control), $Rh(NH_3)_4chrysi^{3+}$ (0 nM, 100 nM, 500 nM, 1 μM, 5 μM), NaCl 50 mM, NaPi 10 mM, pH 7.1. Samples were irradiated on a 1000W Hg/Xe arc lamp (320 - 440 nm) for 30 min and heated at 90 °C for 25 min after irradiation. The light controls were irradiated without Rh complexes. The dark controls were not irradiated. Lanes "A+G" and "C+T" are Maxam-Gilbert sequencing reactions. The mismatched sites are marked with red arrows.

time for the family of complexes. Clear correlations with the binding constants for these complexes are evident (Table 1.1). Significantly, the differential effect in inhibiting cell proliferation in MMR-deficient cells is directly correlated to the binding affinity of the compound for DNA mismatches. $Rh(NH_3)_4chrysi^{3+}$($K_B = 1 \times 10^8$ M^{-1} at a CC mismatch), for example, shows the largest differential effect in inhibiting proliferation of MMR-deficient versus MMR-proficient HCT116 cells after 72 h (79 ± 5%), while $Rh(phen)_2chrysi^{3+}$($K_B = 3.2 \times 10^6$ M^{-1} at a CC mismatch) shows a small differential effect (17 ± 7%). The DIP complex is rapidly taken up by the cells but also shows only a small differential inhibitory effect correlating with its poor specific binding at the mismatch site.

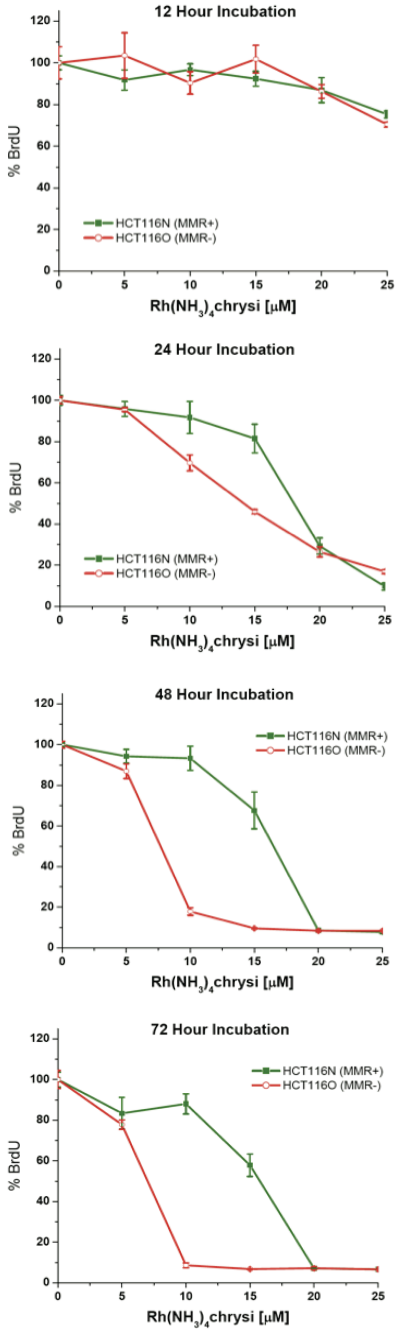

Figure 1.17. Inhibitory effects of $Rh(NH_3)_4chrysi^{3+}$ as a function of incubation time on cellular proliferation. Shown are plots of BrdU incorporation (a measure of DNA synthesis and therefore cellular proliferation) normalized to the BrdU incorporation of untreated cells as a function of rhodium concentration. Standard error bars for 5 trials are shown. MMR-proficient HCT116N cells (green) and MMR-deficient HCT116O cells (red) were plated and allowed 24 hours to adhere before incubation with 0-25 μM $Rh(NH_3)_4chrysi^{3+}$ for 12, 24, 48, or 72 hours. At the end of the 12, 24, and 48 hour incubations, the media containing Rh was replaced with fresh media for the remainder of the 72 hours, followed by ELISA analysis. BrdU was added to the media 24 hours prior to analysis.

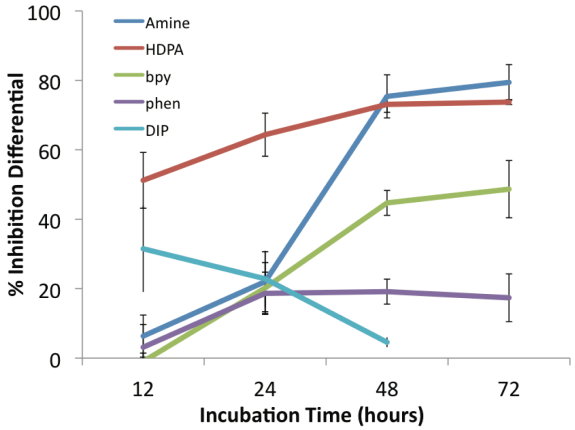

Figure 1.18. Inhibitory effects of rhodium metalloinsertors as a function of incubation time. Shown are plots of BrdU incorporation normalized to the BrdU incorporation of untreated cells as a function of rhodium concentration. The inhibition differential is the difference of the normalized percentages of cellular proliferation for each cell line, with standard error bars (S_{N-O}=$\sqrt{s_N^2 + s_O^2}$). ELISA were performed as in Figure 1.17. Cells were incubated with no rhodium, 2 μM *rac*-Rh(DIP)$_2$chrysi^{3+}, 10 μM Rh(NH$_3$)$_4$chrysi^{3+}, or 20 μM *rac*-Rh(L)$_2$chrysi^{3+} (L = HDPA, bpy, or phen).

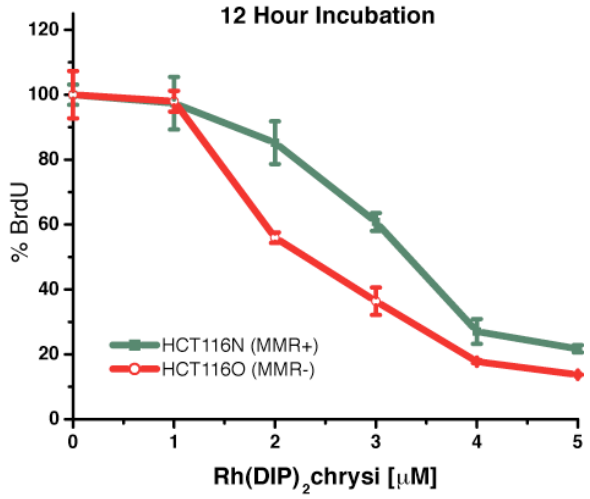

Figure 1.19. Inhibitory effects of *rac*-Rh(DIP)$_2$chrysi^{3+}. Shown are plots of BrdU incorporation normalized to the BrdU incorporation of untreated cells as a function of rhodium concentration. Standard error bars for 5 trials are shown. MMR-proficient HCT116N cells (green) and MMR-deficient HCT116O cells (red) were plated and allowed 24 hours to adhere before incubation with 0-5 μM *rac*-Rh(DIP)$_2$chrysi^{3+}for 12 hours. At the end of the incubation, the media containing Rh was replaced with fresh media and cells were grown for an additional 60 hours before ELISA analysis. BrdU was added to the media 24 hours prior to analysis.

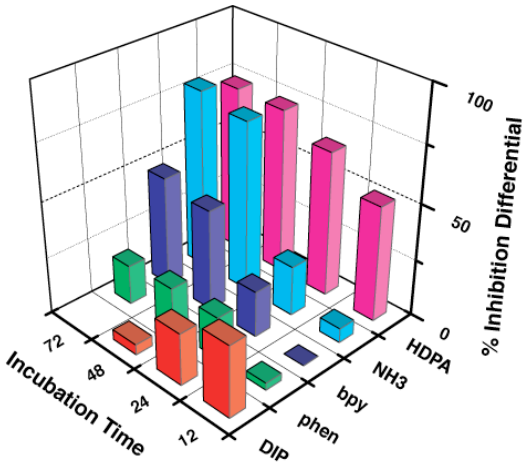

Figure 1.20. Inhibitory effects of rhodium metalloinsertors as a function of metal complex identity. Shown are bar graphs of BrdU incorporation normalized to the BrdU incorporation of untreated cells as a function of rhodium concentration. The inhibition differential is the difference of the normalized percentages of cellular proliferation for the two cell lines, HCT116O versus HCT116N. ELISA were performed as in Figure 1.17. Cells were incubated with no rhodium, 2 μM *rac*-Rh(DIP)$_2$chrysi^{3+}, 10 μM Rh(NH$_3$)$_4$chrysi^{3+}, or 20 μM *rac*-Rh(L)$_2$chrysi^{3+} (L = HDPA, bpy, or phen). A correlation between mismatch binding affinity and differential inhibition of MMR-deficient cells is evident.

1.4 Discussion

A clear trend emerges when comparing the binding constants of the series of rhodium complexes to mismatched sites: the DNA mismatch binding affinity increases as the size of the ancillary ligand decreases. This trend is consistent with what we have learned from the structural studies, specifically that mismatch binding by insertion via the minor groove is subject to stringent space constraints. With major groove intercalation, the base rise is increased, and the major groove offers space to accommodate the ancillary ligands. In contrast, with insertion, there is no increase in base pair rise; the mismatched bases are instead ejected and replaced by the deeply inserted chrysi ligand. Moreover, the minor groove, small even for hydrophobic groove binding molecules, offers little space for the ancillary ligands. While little enantioselectivity is apparent for intercalation of bpy complexes into B-form DNA, Δ-Rh(bpy)$_2$chrysi^{3+} binds enantiospecifically to single base mismatches.[43,61] Thus, steric interactions of the ancillary ligands are seen as an extremely important factor governing the binding affinity of a metal complex at the mismatch site.

We have previously demonstrated that mismatch binding affinity is correlated with ther-

modynamic destabilization over all mismatch identities and sequence contexts.[47,62] Here, we see for all the complexes that binding to the CC mismatch is tighter than binding to the AC mismatch. This is consistent with our previous observations, since AC is the thermodynamically more stable mismatch and, in this case, the melting temperature of the AC hairpin is 5 °C higher than that of the CC hairpin (Table 2.1). We assume, then, that the general trend holds for all members of this metalloinsertor family. This stabilization is translated into a higher dissociation constant (smaller binding affinity) for the entire series of rhodium complexes. This decrease in binding affinity depends upon the greater energy required to eject the mismatched bases from the base pair stack, as evident crystallographically and by NMR.[43,45] Nonetheless, for the family of chrysi complexes, the inverse relationship between the size of the ancillary ligand and the binding affinity still holds, with the smallest complex $Rh(NH_3)_4chrysi^{3+}$ showing the highest affinity and that of the largest complex, $Rh(DIP)_2chrysi^{3+}$, more than 2 orders of magnitude lower.

Figure 1.21 compares the crystal structure of Δ-$Rh(bpy)_2chrysi^{3+}$ bound to the mismatch site[43] with models of Δ-$Rh(DIP)_2chrysi^{3+}$ and $Rh(NH_3)_4chrysi^{3+}$ similarly bound via the minor groove through metalloinsertion. Preserving the DNA conformation from the crystal structure, we see that Δ-$Rh(DIP)_2chrysi^{3+}$ runs into substantial steric hindrance, as its axial phenyl rings extend up and down into the groove, directly clashing with the bases. However, its equatorial phenyl rings do not pose any steric problems, as they point away from the DNA. These observations are supported by the small binding constant measured for $Rh(DIP)_2chrysi^{3+}$. $Rh(phen)_2chrysi^{3+}$, intermediate in size, shows binding affinities for the mismatches that are an order of magnitude lower than those of the bpy derivative but more than an order of magnitude higher than those of the DIP complex. $Rh(HDPA)_2chrysi^{3+}$ is slightly larger in size than the bpy derivative, but the HDPA ligands are more flexible, and there is an opportunity for hydrogen bonding; as a result, $Rh(bpy)_2chrysi^{3+}$ and $Rh(HDPA)_2chrysi^{3+}$ have comparable affinities for the mismatch. Analogously, the large binding constant of $Rh(NH_3)_4chrysi^{3+}$ can be mostly attributed to its small size. Here it is reasonable to suggest that the axial ammines may also hydrogen bond with the neighboring base pairs to form additional stabilizing interactions. Nonetheless, as evident in Figure 1.21, the small cone size of the tetraammine structure clearly facilitates deep insertion within the minor groove site. In fact, the clear inverse correlation of binding affinity with ancillary ligand size, and the finding that $Rh(DIP)_2chrysi^{3+}$, despite its cumbersome size, is able to

bind at all to a mismatch site with some specificity, corroborate our understanding of the driving force and the dynamics of mismatch recognition: the π-stacking between the inserted chrysi ligand and the adjacent bases provides the major stabilizing force for binding, and both the metal complex and DNA distort their conformations to accommodate each other in the bound state.

Importantly, the DNA mismatch binding affinities of the $Rh(L)_2chrysi^{3+}$ family correlate well with the differential biological effects seen between the repair-proficient HCT116N and repair-deficient HCT116O cell lines. This correlation supports the hypothesis that DNA mismatches are the target of rhodium metalloinsertors *in vivo*. Because of this correlation, we may attribute the preferential inhibitory effect on MMR-deficient cells to binding of the complexes to DNA mismatches. Since the MMR-deficient cells contain more mismatches, the tighter binding complexes would be expected to display a greater inhibitory effect. It should be noted that finding any inhibitory effect with these complexes was at first surprising, since they bind DNA noncovalently and might be expected to be readily displaced. Although the mechanism of inhibition is not yet fully understood, it is likely that protein recognition of the metal-mismatch complex, perhaps by RNA polymerase or topoisomerase, may generate a covalent protein-DNA lesion and contribute to the cellular response.

The differential inhibitory effect seen with $Rh(HDPA)_2chrysi^{3+}$ cannot be understood simply on the basis of binding affinities. Despite having essentially the same mismatch binding affinity as $Rh(bpy)_2chrysi^{3+}$, the HDPA complex preferentially inhibits the MMR-deficient cell line almost as well as $Rh(NH_3)_4chrysi^{3+}$ with long incubation times; with short times of incubation, the differential inhibitory effect by $Rh(HDPA)_2chrysi^{3+}$ is greatest. Both the HDPA ligand and the amine group have the potential to form hydrogen bonds. This hydrogen bonding capability and flexibility of the ligands might serve to make them more effective inhibitors of any protein-DNA interactions. Indeed, ruthenium complexes bearing HDPA ligands have been shown to exhibit DNA binding and cytotoxicity.[63]

Certainly, as with any pharmaceutical design, cellular uptake must also be considered. In the case of the HDPA complex, based upon the variations in inhibitory effect with incubation time, the amine ligands may facilitate nuclear uptake. For the bpy complexes, the 48 h incubation time required for $Rh(bpy)_2chrysi^{3+}$ to exert its antiproliferative effect matches the 48 h requirement observed for $Ru(bpy)_2dppz^{2+}$ uptake in HeLa cells.[49,51,52] The more lipophilic $Rh(DIP)_2chrysi^{3+}$ here is found to exert anti-proliferative effects at

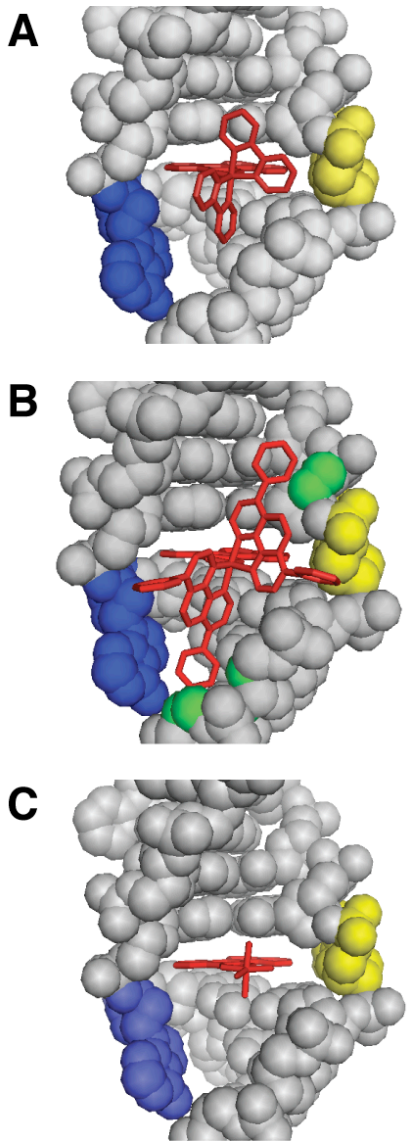

Figure 1.21. Crystal and model structures of rhodium metalloinsertors bound to the mismatch site. Rhodium insertors (red) are shown bound to the DNA (gray) from the minor groove at the mismatch site with the bases (adenine in blue, cytosine in yellow) ejected and the chrysi ligand stacked fully with the adjacent base pairs. The crystal structure of Δ-$Rh(bpy)_2chrysi^{3+}$ bound to the CA mismatch is shown in panel (A), along with structural models of Δ-$Rh(DIP)_2chrysi^{3+}$ (B) and $Rh(NH_3)_4chrysi^{3+}$ (C) binding based on the crystal structure. Superposition of the DIP complex upon the rhodium center of the bpy complex leads to steric clashes with the sugar-phosphate backbone (possible atoms involved in green), whereas the tetraammine complex is easily accommodated.

much shorter incubation times and lower concentrations, which also matches the accelerated uptake observed for $Ru(DIP)_2dppz^{2+}$. Cellular uptake is surely a rate-limiting factor in biological activity of the rhodium metalloinsertors, yet cellular uptake is not the only challenge: proper subcellular localization must also be achieved in order for any drug to act on its target. It has been well established that lipophilic cations preferentially target the mitochondria, whereas hydrophilic cations do not.[64,65] It may be that $Rh(HDPA)_2chrysi^{3+}$ and $Rh(NH_3)_4chrysi^{3+}$ lack the lipophilicity required for mitochondrial accumulation, allowing a greater proportion of these compounds to reach the nucleus once inside the cell. This difference in intracellular partitioning could then account for the differential effects of $Rh(HDPA)_2chrysi^{3+}$.

1.5 Conclusions

In the development of octahedral rhodium complexes as anticancer agents, the choice of ancillary ligand can be seen as a design trade-off, with the binding affinity for a DNA mismatch greatly outweighing uptake properties as the critical factor in the successful targeting of repair-deficient cells. Beyond their effects on DNA binding and overall cellular uptake, it is highly likely that the ancillary ligands affect the cellular response in other ways, including the potential for hydrogen bonding and differences in uptake and intracellular distribution. Here we are confronted with a trade-off that may seem inevitable: more hydrophobic ligands facilitate cellular uptake but impede mismatch binding. Perhaps this trade-off can be avoided by making conjugates arranged with functional moieties tethered with consideration of the structure of the DNA-bound complex associated snugly in the minor groove. Most importantly, these data support the contention that the cell-specific inhibitory effect we observe depends upon binding to the DNA mismatch inside the cell. This cell-specific strategy thus represents a promising direction in the development of small metal complexes that react preferentially in MMR-deficient cells, those susceptible to cancerous transformation.

Bibliography

[1] R. R. Iyer, A. Pluciennik, V. Burdett, and P. L. Modrich. DNA mismatch repair: Functions and mechanisms. *Chemical Reviews*, 106(2):302–323, 2006.

[2] Paul Modrich. Mechanisms in eukaryotic mismatch repair. *Journal of Biological Chemistry*, 281(41):30305–30309, 2006.

[3] John W. Drake. A constant rate of spontaneous mutation in DNA-based microbes. *Proceedings of the National Academy of Sciences*, 88(16):7160–7164, 1991.

[4] John W. Drake. The distribution of rates of spontaneous mutation over viruses, prokaryotes, and eukaryotes. *Annals of the New York Academy of Sciences*, 870(1):100–107, 1999.

[5] Lawrence A. Loeb. A mutator phenotype in cancer. *Cancer Research*, 61(8):3230–3239, 2001.

[6] Nitai P. Bhattacharyya, Adonis Skandalis, Anil Ganesh, Joanna Groden, and Mark Meuth. Mutator phenotypes in human colorectal carcinoma cell lines. *Proceedings of the National Academy of Sciences*, 91(14):6319–6323, 1994.

[7] Bernard S. Strauss. Frameshift mutation, microsatellites and mismatch repair. *Mutation Research/Reviews in Mutation Research*, 437(3):195–203, 1999.

[8] Nickolas Papadopoulos and Annika Lindblom. Molecular basis of HNPCC: Mutations of MMR genes. *Human Mutation*, 10(2):89–99, 1997.

[9] Päivi Peltomäki. Deficient DNA mismatch repair: A common etiologic factor for colon cancer. *Human Molecular Genetics*, 10(7):735–740, 2001.

[10] D. A. Lawes, S. SenGupta, and P. B. Boulos. The clinical importance and prognostic implications of microsatellite instability in sporadic cancer. *European Journal of Surgical Oncology (EJSO)*, 29(3):201–212, 2003.

[11] James G. Herman, Asad Umar, Kornelia Polyak, Jeremy R. Graff, Nita Ahuja, Jean-Pierre J. Issa, Sanford Markowitz, James K. V. Willson, Stanley R. Hamilton, Kenneth W. Kinzler, Michael F. Kane, Richard D. Kolodner, Bert Vogelstein, Thomas A. Kunkel, and Stephen B. Baylin. Incidence and functional consequences of hMLH1 promoter hypermethylation in colorectal carcinoma. *Proceedings of the National Academy of Sciences*, 95(12):6870–6875, 1998.

[12] Iordanis I. Arzimanoglou, Fred Gilbert, and Hugh R. K. Barber. Microsatellite instability in human solid tumors. *Cancer*, 82(10):1808–1820, 1998.

[13] Klaus Pors and Laurence H. Patterson. DNA mismatch repair deficiency, resistance to cancer chemotherapy and the development of hypersensitive agents. *Current Topics in Medicinal Chemistry*, 5(12):1133–1149, 2005.

[14] Anna Maria Valentini, Raffaele Armentano, Michele Pirrelli, and Maria L. Caruso. Chemotherapeutic agents for colorectal cancer with a defective mismatch repair system: The state of the art. *Cancer Treatment Reviews*, 32(8):607–618, 2006.

[15] J. M. Carethers, M. T. Hawn, D. P. Chauhan, M. C. Luce, G. Marra, M. Koi, and C. R. Boland. Competency in mismatch repair prohibits clonal expansion of cancer cells treated with N-methyl-N'-nitro-N-nitrosoguanidine. *The Journal of Clinical Investigation*, 98(1):199–206, 1996.

[16] Daniel Fink, Sibylle Nebel, Stefan Aebi, Hua Zheng, Bruno Cenni, Alissar Nehmé, Randolph D. Christen, and Stephen B. Howell. The role of DNA mismatch repair in platinum drug resistance. *Cancer Research*, 56(21):4881–4886, 1996.

[17] John M. Carethers, Dharam P. Chauhan, Daniel Fink, Sibylle Nebel, Robert S. Bresalier, Stephen B. Howell, and C. Richard Boland. Mismatch repair proficiency and in vitro response to 5-fluorouracil. *Gastroenterology*, 117(1):123–131, 1999.

[18] S. Aebi, D. Fink, R. Gordon, H. K. Kim, H. Zheng, J. L. Fink, and S. B. Howell. Resistance to cytotoxic drugs in DNA mismatch repair-deficient cells. *Clinical Cancer Research*, 3(10):1763–1767, 1997.

[19] André Fedier, Viola A. Schwarz, Heinrich Walt, Renato Delli Carpini, Urs Haller, and Daniel Fink. Resistance to topoisomerase poisons due to loss of DNA mismatch repair. *International Journal of Cancer*, 93(4):571–576, 2001.

[20] D. Fink, S. Aebi, and S. B. Howell. The role of DNA mismatch repair in drug resistance. *Clinical Cancer Research*, 4(1):1–6, 1998.

[21] Peter Karran, Judith Offman, and Margherita Bignami. Human mismatch repair, drug-induced DNA damage, and secondary cancer. *Biochimie*, 85(11):1149–1160, 2003.

[22] Irina V. Nesterova, S. Sibel Erdem, Serhii Pakhomov, Robert P. Hammer, and Steven A. Soper. Phthalocyanine dimerization-based molecular beacons using near-ir fluorescence. *Journal of the American Chemical Society*, 131(7):2432–2433, 2009.

[23] Daniela Baumstark and Hans-Achim Wagenknecht. Perylene bisimide dimers as fluorescent "glue" for DNA and for base-mismatch detection. *Angewandte Chemie International Edition*, 47(14):2612–2614, 2008.

[24] Nina Moran, Dario M. Bassani, Jean-Pierre Desvergne, Sonja Keiper, Philip A. S. Lowden, Joseph S. Vyle, and James H. R. Tucker. Detection of a single DNA base-pair mismatch using an anthracene-tagged fluorescent probe. *Chem. Commun.*, pages 5003–5005, 2006.

[25] Kazushige Yamana, Yoshikazu Ohshita, Yudai Fukunaga, Mitsunobu Nakamura, and Atsushi Maruyama. Bis-pyrene-labeled molecular beacon: A monomer–excimer switching probe for the detection of DNA base alteration. *Bioorganic & Medicinal Chemistry*, 16(1):78–83, 2008.

[26] T. Santhosh Kumar, Jesper Wengel, and Patrick J. Hrdlicka. 2-N-(pyren-1-yl)acetyl-2-amino-α-L-LNA: Synthesis and detection of single nucleotide mismatches in DNA and RNA targets. *ChemBioChem*, 8(10):1122–1125, 2007.

[27] Anthony G. Frutos, Santona Pal, Mark Quesada, and Joydeep Lahiri. Method for detection of single-base mismatches using bimolecular beacons. *Journal of the American Chemical Society*, 124(11):2396–2397, 2002.

[28] Minseon Cho, Suhman Chung, Seong-Dal Heo, Jakang Ku, and Changill Ban. A simple fluorescent method for detecting mismatched DNAs using a MutS–fluorophore conjugate. *Biosensors and Bioelectronics*, 22(7):1376–1381, 2007.

[29] Kazuhiko Nakatani, Shinsuke Sando, and Isao Saito. Scanning of guanine-guanine mismatches in DNA by synthetic ligands using surface plasmon resonance. *Nat Biotech*, 19(1):51–55, 2001.

[30] Kazuhiko Nakatani, Shinya Hagihara, Yuki Goto, Akio Kobori, Masaki Hagihara, Gosuke Hayashi, Motoki Kyo, Makoto Nomura, Masaki Mishima, and Chojiro Kojima. Small-molecule ligand induces nucleotide flipping in $(CAG)_n$ trinucleotide repeats. *Nat Chem Biol*, 1(1):39–43, 2005.

[31] Akio Kobori, Souta Horie, Hitoshi Suda, Isao Saito, and Kazuhiko Nakatani. The SPR sensor detecting cytosinecytosine mismatches. *Journal of the American Chemical Society*, 126(2):557–562, 2004.

[32] Anton Granzhan and Marie-Paule Teulade-Fichou. A fluorescent bisanthracene macrocycle discriminates between matched and mismatch-containing DNA. *Chemistry–A European Journal*, 15(6):1314–1318, 2009.

[33] Brian M. Zeglis, Valerie C. Pierre, and Jacqueline K. Barton. Metallo-intercalators and metallo-insertors. *Chem Commun (Camb)*, (44):4565–4579, 2007.

[34] T. Brown, W. N. Hunter, G. Kneale, and O. Kennard. Molecular structure of the G.A base pair in DNA and its implications for the mechanism of transversion mutations. *Proceedings of the National Academy of Sciences*, 83(8):2402–2406, 1986.

[35] J. V. Skelly, K. J. Edwards, T. C. Jenkins, and S. Neidle. Crystal structure of an oligonucleotide duplex containing G.G base pairs: Influence of mispairing on DNA backbone conformation. *Proceedings of the National Academy of Sciences*, 90(3):804–808, 1993.

[36] William N. Hunter, Tom Brown, and Olga Kennard. Structural features and hydration of a dodecamer duplex containing two C.A mispairs. *Nucleic Acids Research*, 15(16):6589–6605, 1987.

[37] W. N. Hunter, T. Brown, G. Kneale, N. N. Anand, D. Rabinovich, and O. Kennard. The structure of guanosine-thymidine mismatches in B-DNA at 2.5-a resolution. *Journal of Biological Chemistry*, 262(21):9962–9970, 1987.

[38] Nicolas Peyret, P. Ananda Seneviratne, Hatim T. Allawi, and John SantaLucia. Nearest-neighbor thermodynamics and NMR of DNA sequences with internal AA, CC, GG, and TT mismatches. *Biochemistry*, 38(12):3468–3477, 1999.

[39] John SantaLucia and Donald Hicks. The thermodynamics of DNA structural motifs. *Annual Review of Biophysics and Biomolecular Structure*, 33(1):415–440, 2004.

[40] Frances H. Arnold, Steven Wolk, Phillip Cruz, and Ignacio Tinoco. Structure, dynamics, and thermodynamics of mismatched DNA oligonucleotide duplexes $d(CCCAGGG)_2$ and $d(CCCTGGG)_2$. *Biochemistry*, 26(13):4068–4075, 1987.

[41] Richard J. Isaacs, William S. Rayens, and H. Peter Spielmann. Structural differences in the NOE-derived structure of G–T mismatched dna relative to normal DNA are correlated with differences in ^{13}C relaxation-based internal dynamics. *Journal of Molecular Biology*, 319(1):191–207, 2002.

[42] D. J. Patel, S. A Kozlowski, and K. Ikuta, S.and Ikuta. Dynamics of DNA duplexes containing internal GT, GA, AC, and TC pairs—hydrogen-exchange at and adjacent to mismatch sites. *Federation Proceedings*, 43(11):2663–2670, 1984.

[43] Valerie C. Pierre, Jens T. Kaiser, and Jacqueline K. Barton. Insights into finding a mismatch through the structure of a mispaired DNA bound by a rhodium intercalator. *Proceedings of the National Academy of Sciences*, 104(2):429–434, 2007.

[44] Brian M. Zeglis, Valerie C. Pierre, Jens T. Kaiser, and Jacqueline K. Barton. A bulky rhodium complex bound to an adenosine-adenosine DNA mismatch: General architecture of the metalloinsertion binding mode. *Biochemistry*, 48:4247–4253, 2009.

[45] Christine Cordier, Valérie C. Pierre, and Jacqueline K. Barton. Insertion of a bulky rhodium complex into a DNA cytosinecytosine mismatch: An NMR solution study. *Journal of the American Chemical Society*, 129(40):12287–12295, 2007.

[46] L. S. Lerman. Structural considerations in the interaction of DNA and acridines. *Journal of Molecular Biology*, 3(1):18–30, 1961.

[47] Brian A. Jackson, Viktor Y. Alekseyev, and Jacqueline K. Barton. A versatile mismatch recognition agent: Specific cleavage of a plasmid DNA at a single base mispair. *Biochemistry*, 38(15):4655–4662, 1999.

[48] Brian A. Jackson and Jacqueline K. Barton. Recognition of DNA base mismatches by a rhodium intercalator. *Journal of the American Chemical Society*, 119(52):12986–12987, 1997.

[49] Jonathan R. Hart, Oleg Glebov, Russell J. Ernst, Ilan R. Kirsch, and Jacqueline K. Barton. DNA mismatch-specific targeting and hypersensitivity of mismatch-repair-deficient cells to bulky rhodium(III) intercalators. *Proceedings of the National Academy of Sciences*, 103(42):15359–15363, 2006.

[50] Minoru Koi, Asad Umar, Dharam P. Chauhan, Sajeev P. Cherian, John M. Carethers, Thomas A. Kunkei, and C. Richard Boland. Human chromosome 3 corrects mismatch repair deficiency and microsatellite instability and reduces N-Methyl-N-nitro-N-nitrosoguanidine tolerance in colon tumor cells with homozygous hMLH1 mutation. *Cancer Research*, 54(16):4308–4312, 1994.

[51] Cindy A. Puckett and Jacqueline K. Barton. Methods to explore cellular uptake of ruthenium complexes. *Journal of the American Chemical Society*, 129(1):46–47, 2007.

[52] Cindy A. Puckett and Jacqueline K. Barton. Mechanism of cellular uptake of a ruthenium polypyridyl complex. *Biochemistry*, 47(45):11711–11716, 2008.

[53] Jens Brunner and Jacqueline K. Barton. Targeting DNA mismatches with rhodium intercalators functionalized with a cell-penetrating peptide. *Biochemistry*, 45(40):12295–12302, 2006.

[54] Oliver Schmelz, Alf Mews, Thomas Basché, Andreas Herrmann, and Klaus Müllen. Supramolecular complexes from CdSe nanocrystals and organic fluorophors. *Langmuir*, 17(9):2861–2865, 2001.

[55] Brian M. Zeglis and Jacqueline K. Barton. DNA base mismatch detection with bulky rhodium intercalators: synthesis and applications. *Nature Protocol*, 2(2):357–371, 2007.

[56] Nicholas E. Dixon, Geoffrey A. Lawrance, Peter A. Lay, and Alan M. Sargeson. (Trifluoromethanesulfonato-O)pentaammine complexes: Versatile synthetic intermediates. *Inorganic Chemistry*, 22(5):846–847, 1983.

[57] Nicholas E. Dixon, Geoffrey A. Lawrance, Peter A. Lay, and Alan M. Sargeson. Synthetically versatile (trifluoromethanesulfonato)metal amine complexes. *Inorganic Chemistry*, 23(19):2940–2947, 1984.

[58] Armin H. Reitmair, Robert Risley, Robert G. Bristow, Teresa Wilson, Anil Ganesh, Anne Jang, James Peacock, Samuel Benchimol, Richard P. Hill, Tak W. Mak, Richard Fishel, and Mark Meuth. Mutator phenotype in Msh2-deficient murine embryonic fibroblasts. *Cancer Research*, 57(17):3765–3771, 1997.

[59] H. G. Gratzner. Monoclonal antibody to 5-bromo- and 5-iododeoxyuridine: A new reagent for detection of DNA replication. *Science*, 218(4571):474–475, 1982.

[60] Achim H. Krotz, Louis Y. Kuo, Thomas P. Shields, and Jacqueline K. Barton. Dna recognition by rhodium(III) polyamine intercalators: Considerations of hydrogen bonding and van der Waals interactions. *Journal of the American Chemical Society*, 115(10):3877–3882, 1993.

[61] Jacqueline K. Barton. Metals and DNA: Molecular left-handed complements. *Science*, 233(4765):727–734, 1986.

[62] Brian A. Jackson and Jacqueline K. Barton. Recognition of base mismatches in DNA by 5,6-chrysenequinone diimine complexes of rhodium(III): A proposed mechanism for preferential binding in destabilized regions of the double helix. *Biochemistry*, 39(20):6176–6182, 2000.

[63] Venugopal Rajendiran, Mariappan Murali, Eringathodi Suresh, Mallayan Palaniandavar, Vaiyapuri Subbarayan Periasamy, and Mohammad Abdulkader Akbarsha. Non-covalent DNA binding and cytotoxicity of certain mixed-ligand ruthenium(II) complexes of 2,2'-dipyridylamine and diimines. *Dalton Trans.*, pages 2157–2170, 2008.

[64] Josephine S. Modica-Napolitano and June R. Aprille. Delocalized lipophilic cations selectively target the mitochondria of carcinoma cells. *Advanced Drug Delivery Reviews*, 49(1-2):63–70, 2001.

[65] Michael P. Murphy and Robin A. J. Smith. Drug delivery to mitochondria: The key to mitochondrial medicine. *Advanced Drug Delivery Reviews*, 41(2):235–250, 2000.

Chapter 2

Sensitivity of Ruthenium Luminescence to DNA Defects

Adapted from Mi Hee Lim, Hang Song, Eric D. Olmon, Elizabeth E. Dervan, and Jacqueline K. Barton, *Inorganic Chemistry*, **2009**, *48*, 5392–5397. M. H. L., H. S. and E. E. D. performed the steady state fluorescence experiments. E. D. O. performed lifetime measurements.

2.1 Introduction

Cells have evolved intricate enzymatic pathways to screen for and repair DNA lesions such as base pair mismatches and abasic sites to maintain the integrity of the genome.[1,2] Because unrepaired DNA defects can lead to cancerous transformation,[3–5] a means of recognizing DNA lesions is a crucial step in the development of early cancer diagnostics. Many approaches have been developed to target DNA lesions and particularly single base mismatches in DNA.[6–20] As discussed in Chapter 1, our laboratory has focused on the design of bulky metalloinsertors as probes of DNA mismatches.[21] Although these bulky complexes target mismatches with high specificity, they have not yet achieved sufficient sensitivity to serve as luminescent probes for mismatches in cellular assays.[20] In this chapter, we explore the use of the simple luminescent probe for DNA, $Ru(bpy)_2dppz^{2+}$, in targeting single base mismatches and abasic sites.

$Ru(bpy)_2dppz^{2+}$, which has been dubbed a "molecular light switch for DNA," displays a remarkable increase in luminescence upon intercalation into duplex DNA (Figure 2.1).[22–26] In nonaqueous solvents, the complex luminesces brightly owing to the excitation to a metal-to-ligand charge transfer state, but in water the luminescence is quenched through hydrogen bonding with the phenazine nitrogen atoms.[27,28] Studies have shown that the Ru complex binds well-matched duplex DNA avidly through intercalation, where the planar dppz ligand intercalates into the helix, stacking with the DNA but not disturbing base pairing.[22–24,29] Our results have indicated that the complex, like other metallointercalators,[30] binds the duplex from the major groove side.[29] Others have provided some evidence in support of minor groove association.[31–33] In any case, through this intercalative stacking, the phenazine nitrogen atoms of the dppz become somewhat protected from water, and hence, bound to DNA in aqueous solution, $Ru(bpy)_2dppz^{2+}$ shows luminescence.

Our laboratory has also carried out extensive studies to explore rhodium diimine complexes that contain a bulky ligand that is inhibited from binding duplex DNA by intercalation; owing to the expanse of the ligand, the complex instead targets single base mismatches in DNA through metalloinsertion (for details, see Chapter 1).[18] $Rh(bpy)_2chrysi^{3+}$ (chrysi = 5,6-chrysenequinone diimine), for example, binds both single base mismatches and abasic sites in DNA with high specificity through metalloinsertion (Figure 2.1).[34–36] X-ray crystallography and NMR studies have shown that, in contrast to intercalation, in this

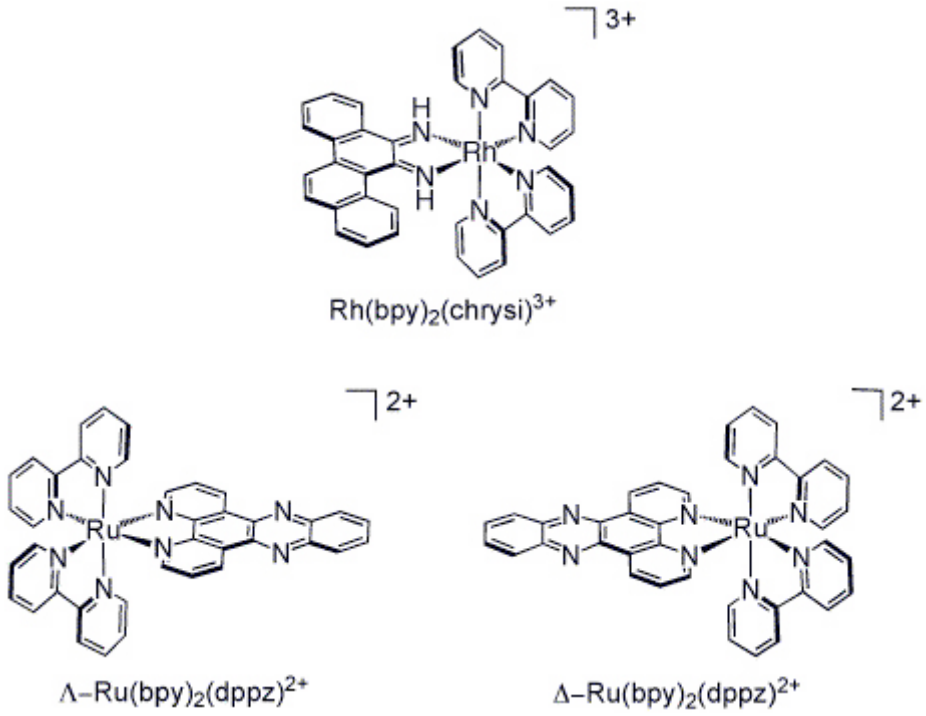

Figure 2.1. Chemical structures of $Rh(bpy)_2chrysi^{3+}$ and $Ru(bpy)_2dppz^{2+}$ isomers.

metalloinsertion mode, the sterically expansive chrysi ligand binds deeply into the mismatch site from the minor groove with complete ejection of the mismatched base pair into the major groove.[37,38] In short, the Rh complex behaves as a π-stacking replacement of the mismatched pair in the DNA base stack. Upon light activation, the Rh complexes promote direct strand cleavage adjacent to the DNA lesion. DNA photocleavage studies on the full range of single base mismatches in all sequence contexts have shown a strong correlation between mismatch binding affinity by the metal complex and the thermodynamic destabilization associated with the mismatch.[34–36] Thus, the easier it is to eject the mismatched base pairs, the tighter the binding through metalloinsertion.

The intercalating dppz ligand of $Ru(bpy)_2dppz^{2+}$ is narrow and long compared with the chrysi ligand and therefore does not seem suitable for binding through metalloinsertion (Figure 2.1). Moreover extensive studies have shown the tight binding of dppz complexes to well-matched DNA through classical intercalation.[22–26,29,31–33] Here we explore the luminescent properties of $Ru(bpy)_2dppz^{2+}$ in the presence of DNA duplexes that contain a single base mismatch or an abasic site. We find significant luminescent enhancements associated with binding to these defects compared to binding to well-matched duplex DNA. Our

results suggest binding to these defects is through metalloinsertion. These data indicate a powerful new application of $Ru(bpy)_2dppz^{2+}$ in probing DNA defects.

2.2 Experimental protocols

2.2.1 Materials

All reagents and solvents were purchased from commercial suppliers and used without further purification. The DNA-binding organic fluorophores, ethidium bromide (EB) and TO-PRO-3 were obtained from Sigma-Aldrich and Invitrogen, respectively. Ruthenium complexes were prepared and enantiomers separated by previously reported methods; all complexes were utilized as chloride salts.[22–24,39] The oligonucleotides used for measurements of steady state luminescence and excited state lifetimes were synthesized on an ABI 3400 DNA synthesizer (Applied Biosystems) and purified as previously described.[40] The copper complex $Cu(phen)_2^{2+}$ was generated *in situ* by reacting the phen ligand with $CuCl_2$ in a ratio of 3:1.[41,42]

2.2.2 Steady state fluorescence

Luminescence spectra with emission intensities ranged from 560 to 800 nm were recorded on an ISS-K2 spectrophotometer at ambient temperature in aerated solutions and then integrated. For all titrations, the experiments were performed at least three times. UV-visible spectra were taken on a Beckman DU7400 spectrophotometer.

2.2.3 Time-resolved fluorescence

Time-resolved emission measurements were carried out at the Beckman Institute Laser Resource Center where samples were excited using a Nd:YAG-pumped OPO (Spectra-Physics Quanta-Ray).[43–45] Laser power at 470 nm ranged from 4.0 to 4.5 mJ per pulse at 10 Hz. Emitted light was collected and focused onto the entrance slit of an ISA double grating (100 mm) monochromator and detected by a PMT (Hamamatsu R928). Each measurement is the average of 500 shots. Emission decays were fit to biexponential functions using nonlinear least-squares minimization.[43–45]

5' – GAC CAG CTT ATC ACC CCT AGA TAA GCG – 3'

Matched: 3' – CTG GTC GAA TAG TGG GGA TCT ATT CGC – 5'

Mismatched: 3' – CTG GTC GAA TAG TCG GGA TCT ATT CGC – 5'

Abasic: 3' – CTG GTC GAA TAG TRG GGA TCT ATT CGC – 5'

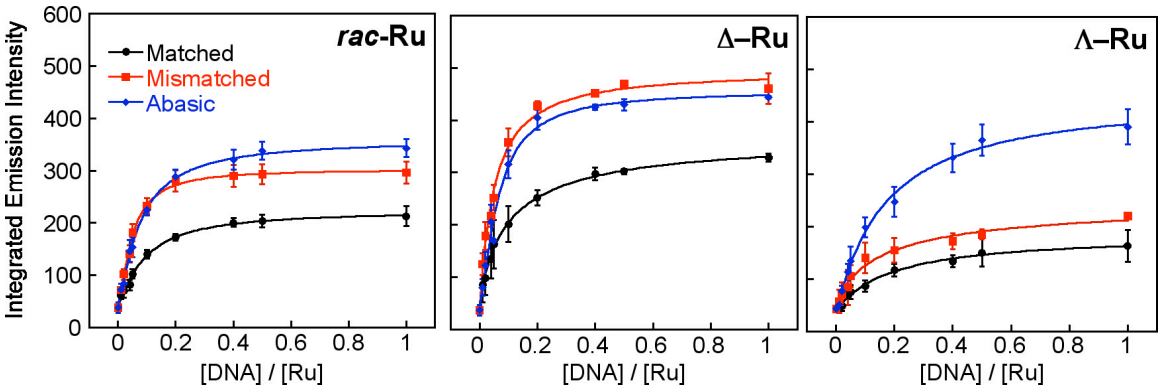

Figure 2.2. Titrations of $Ru(bpy)_2dppz^{2+}$ with DNAs containing defects. Top: DNA sequences of matched, mismatched and abasic 27-mer duplex DNA (R denotes a tetrahydrofuranyl abasic site). Bottom: plots of the integrated emission intensity (λ_{ex} = 440 nm) of *rac*- (left), Δ- (middle) and Λ-$Ru(bpy)_2dppz^{2+}$ (right) (100 nM) upon increasing the concentration of DNA in 50 mM NaCl, 5 mM Tris, pH 7.5. Error bars indicate standard deviations in the measurements.

2.3 Results and discussion

2.3.1 Steady state luminescence of *rac*-, Δ-, and Λ-$Ru(bpy)_2dppz^{2+}$ bound to oligonucleotides

We first investigated the luminescent response of $Ru(bpy)_2dppz^{2+}$in the presence of increasing concentrations of 27-mer oligonucleotide duplexes that were either fully matched or contained a single base mismatch or an abasic site (Figure 2.2). After adding the Ru complex (100 nM, *rac*-, Δ-, or Λ-) to a solution containing various concentrations of DNA (0-100 nM oligomer) in 50 mM NaCl, 5 mM Tris, pH 7.5, the resulting steady state luminescence was measured. We find a marked increase in Ru luminescence as the concentration of DNA increases until saturating conditions are reached. Significantly, the luminescence increase is greater with those oligonucleotides containing the single site defect.

Both Λ- and Δ-Ru enantiomers exhibit an increase in luminescence in the presence of DNA defects versus well matched DNA (Figure 2.2). Specifically, *rac*- and Δ-Ru show a 1.5-fold enhancement in luminescence with DNA containing a CC mismatch or an abasic site

compared to well-matched DNA. It should be noted that Δ-Ru exhibits higher integrated luminescence intensity with all three duplexes, reflecting that the Δ-enantiomer binds more tightly than the Λ-enantiomer to right-handed B-form DNA.[25,26,46] Nonetheless, for rac- and Δ-Ru, 90% saturation is reached at a Ru/DNA ratio of 3:1 with the matched duplex and 4:1 with the mismatched duplex. This stoichiometry reveals that an additional Ru is bound to the mismatch without affecting the loading of Ru at matched sites. Interestingly, Λ-Ru, unlike *rac*-Ru and Δ-Ru, presents a significant increase in luminescence with abasic DNA over well-matched DNA (2.5-fold) or mismatched DNA (1.8-fold), as shown in Figure 2.2 (bottom right). This characteristic of Λ-Ru suggests that it may be useful in the detection of abasic sites in DNA.

2.3.2 Comparison with other DNA-binding fluorophores

To compare the luminescent properties of the Ru complex to other commonly used DNA-binding fluorescent probes, we employed ethidium bromide (EB)[47] and TO-PRO-3[48] (Figure 2.3). When the intercalator EB is incubated with each DNA duplex, no distinguishable difference in luminescence intensity is observed among the three oligonucleotides (Figure 2.3, bottom left). TO-PRO-3, a known minor groove binding agent, shows a small decrease in luminescence in the presence of DNA containing a mismatch or abasic site compared with well-matched DNA. Neither of these two commonly used luminescent DNA binding agents show any evidence of luminescence enhancement with DNAs containing a defect.

The different luminescence behavior of Ru in the presence of mismatched and abasic DNA versus the well matched duplex reports on its structural characteristics at the defect binding site: the defect sites afford the complex a higher degree of protection from solvent water molecules versus a well-matched duplex site. This result also suggests that Ru binding at mismatches and abasic sites is fundamentally different from intercalation between matched bases or groove binding, because if $Ru(bpy)_2dppz^{2+}$ were to bind to mismatches or abasic sites through classical intercalation or groove binding, we might expect the luminescence response to resemble that of EB or TO-PRO-3.

2.3.3 Luminescence behavior of Ru with different base mismatches

We investigated also the ability of Ru to report on other types of DNA base mismatches by using a short hairpin oligonucleotide containing a mismatch near the center of the duplex.

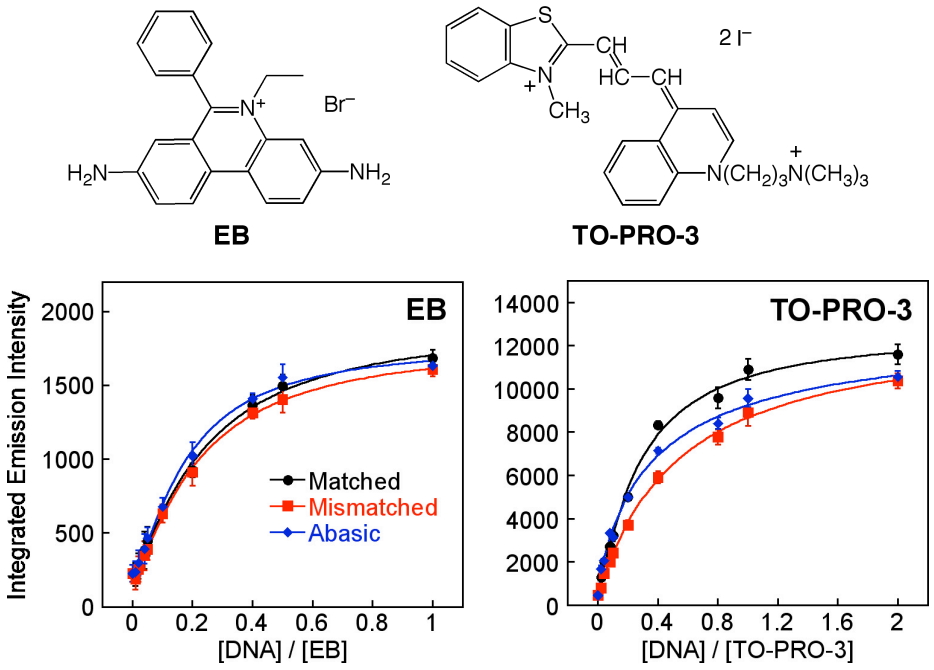

Figure 2.3. Comparisons with common DNA-binding fluorophores. Structures of EB and TO-PRO-3 are shown along with plots of the integrated emission intensity of EB (100 nM) and TO-PRO-3 (100 nM) in the presence of 27-mer duplex DNAs (Figure 2.2; λ_{ex} for EB = 512 nm, λ_{ex} for TO-PRO-3 = 642 nm) in 50 mM NaCl, 5 mM Tris, pH 7.5. Error bars indicate standard deviations in the measurements.

Table 2.1. Melting temperatures (T_m) of DNA hairpins containing a single mismatch[a]

Mismatch	T_m (°C)[b]
CT	65
CC	65
TT	66
AA	67
AC	70
GT	70
AG	71
GG	73
AT (well-matched)	75

[a]Absorbance at 260 nm was monitored as a function of temperature to determine the T_m. DNA hairpins (Figure 2.4) were used. [b]Uncertainties are ±1 °C.

As evident in Figure 2.4, we detect enhanced luminescence intensities with AA, AC, and CC mismatches, which are relatively destabilized compared to Watson-Crick base pairs (Table 2.1).[49] With the thermodynamically stable G-containing mismatches (GG, GA, GT), the Ru complex acts in a manner similar to that with well matched DNA (AT). Indeed, the luminescence intensity of Ru is correlated with the relative thermodynamic stability of each mismatch.

An exception to this thermodynamic correlation that must be noted is that there is no significant increase in the luminescence of Ru with CT and TT mismatches, even though the dppz ligand may insert into pyrimidine-pyrimidine mismatches more easily than purine-purine ones (Figure 2.4). The absence of an increase in luminescence with CT and TT may be related to an intermolecular hydrogen bonding interaction between thymine and the phenazine moiety of dppz, which, like hydrogen bonding with water, yields quenching.

This dependence on mismatch thermodynamic stability strikingly resembles that observed in DNA binding studies of the metalloinsertor $Rh(bpy)_2chrysi^{3+}$.[34–36] Binding of the chrysi complex to a mismatched site occurs via insertion with the ejection of the mismatched bases, and this binding is correlated with the thermodynamic instability of the mismatch; the easier it is to eject the mismatched base pair from the stack, the tighter the binding of the metalloinsertor. Thus, these luminescence data, showing a similar correlation with mismatch instability, suggest that $Ru(bpy)_2dppz^{2+}$ complexes may bind similarly to thermodynamically destabilized sites via insertion of the dppz ligand from the minor

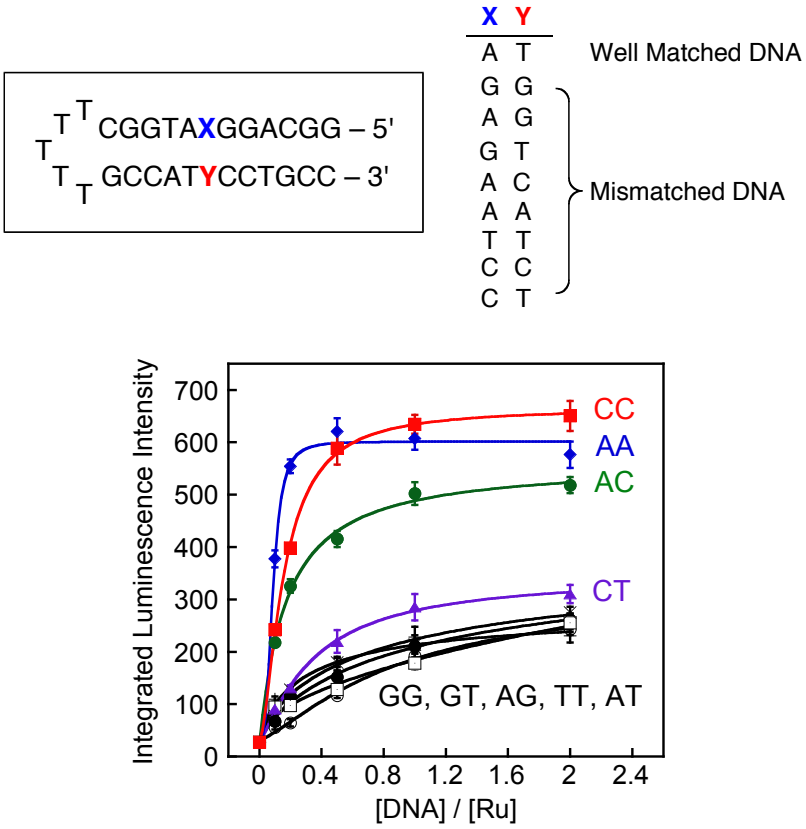

Figure 2.4. Titrations of Ru(bpy)2dppz2+ with hairpin DNAs containing different mismatches. Top: Hairpin DNA sequences. Bottom: plots of the integrated emission intensity (λ_{ex} = 440 nm) of Δ-Ru (100 nM) with with increasing concentrations of hairpin DNA containing mismatches: GG (open circle), GT (open square), AT (filled black circle), AG (×), TT (+), CT (purple triangle), AC (green circle), AA (blue diamond), and CC (red square) in 50 mM NaCl, 5 mM Tris, pH 7.5. Error bars indicate standard deviations in the measurements.

groove, possibly causing the ejection of one or both bases into the major groove. Accordingly, because insertion into the minor groove allows for deeper binding, one could explain the greater luminescence at these mismatched sites.

It should also be noted that a higher differential luminescence intensity of Ru between mismatched and matched DNA is observed with the hairpin oligonucleotides (3-fold increase) compared with the longer 27-mer duplex (1.5-fold increase) for the same mismatch (CC). This observation is expected; only one Ru complex can bind to the single mismatch on both duplexes, while the longer duplex can accommodate more Ru in matched duplex sites. Thus, shortening the DNA increases the probability of binding to the destabilized site which in turn enhances the differential in luminescence intensity.

2.3.4 Excited state lifetimes of Ru

To elucidate further the luminescent characteristics of the Ru complexes bound to DNA defects, we examined their excited state lifetimes in the presence of the 27-mer oligonucleotides. The excited state decay profiles for the Ru complexes have been fit to biexponential luminescent decays (Table 2.2). We have previously seen biexponential decays for the Ru complexes with B-form DNAs and, through quenching studies and NMR experiments, have characterized this biexponential decay structurally in terms of side-on and perpendicular components.[22–24,29] In the perpendicular binding mode, the dppz ligand intercalates such that the Ru-dppz axis lies along the DNA dyad axis; in contrast, when Ru intercalates via a side-on approach, the Rudppz axis lies along the long axis of the base pairs. As a result of these intercalative differences, the perpendicular binding mode places the phenazine moiety between the base pairs in a way that is more protected from quenching by water compared to the side-on bound phenazine moiety, yielding a longer fluorescent lifetime for the perpendicular versus side-on mode.

In the presence of a DNA mismatch, the Δ-Ru complex shows an increase in the long-lived excited state lifetime (Table 2.2). This observation is consistent with binding through metalloinsertion, where the complex is expected to be more deeply held and certainly more protected from water in the small minor groove. $Rh(bpy)_2chrysi^{3+}$ appears to bind a mismatched site in a strictly perpendicular orientation,[37,38] but the longer dppz complex enjoys a higher degree of rotational freedom than the short chrysi complex, likely allowing both orientations of the inserting dppz ligand (Figure 2.1). For the Λ-Ru complex, little signif-

Table 2.2. Luminescence Decay Parameters for *rac*-, Δ- and Λ-Ru(bpy)$_2$dppz^{2+} with DNA[a]

Complex	DNA	τ_1 (ns)[b]	τ_2 (ns)[b]	τ_1:τ_2[c]
rac-Ru	Matched	72	212	83:17
	Mismatched	74	213	77:23
	Abasic	86	192	69:31
Δ-Ru	Matched	83	245	88:12
	Mismatched	91	296	86:14
	Abasic	90	204	79:21
Λ-Ru	Matched	41	199	89:11
	Mismatched	37	156	78:22
	Abasic	69	167	41:59

[a]Samples containing 10 μM Ru and 20 μM DNA (5 mM Tris, pH 7.5, 50 mM NaCl) were used for the excited state lifetime measurements (λ_{ex} = 470 nm, λ_{em} = 610 nm). The 27-mer oligonucleotides (matched, mismatched and abasic DNA, Figure 2.2) were used. [b]Uncertainties in excited state lifetimes are <10%. [c]Relative contributions of each lifetime to the overall decay.

icant difference is evident with the mismatch; this result is not surprising based upon the steady state titration. It is noteworthy here that Δ-Rh(bpy)$_2$chrysi^{3+} binds enantiospecifically through metalloinsertion at the mismatched site because of the very small size of the right-handed minor groove at the mismatched binding site.[34–38]

We have previously found for Rh(bpy)$_2$chrysi^{3+} that binding to an abasic site resembles closely binding to a mismatched site.[50,51] We see similar results for Δ-Ru(bpy)$_2$dppz^{2+}. It appears that the luminescent enhancement associated with binding to the abasic site is reflected in an increase in the excited state lifetime of the side-on component but a higher population of the perpendicular component. For the Λ-isomer these effects are still more substantial. These enhancements likely reflect a looser binding of the Λ-isomer within the abasic site pocket.

2.3.5 Luminescence response of Ru toDNA in the presence of Cu(phen)$_2^{2+}$

To explore further whether the Ru complex interacts with DNA defects from the minor groove, we measured the steady state luminescence of Ru with DNA in the presence of the DNA-binding quencher, Cu(phen)$_2^{2+}$. Upon increasing the concentration of Cu(phen)$_2^{2+}$,[41,42] the luminescence intensity of Ru with matched DNA is unchanged, while that with mismatched and abasic DNA decreases to the same level as that with matched

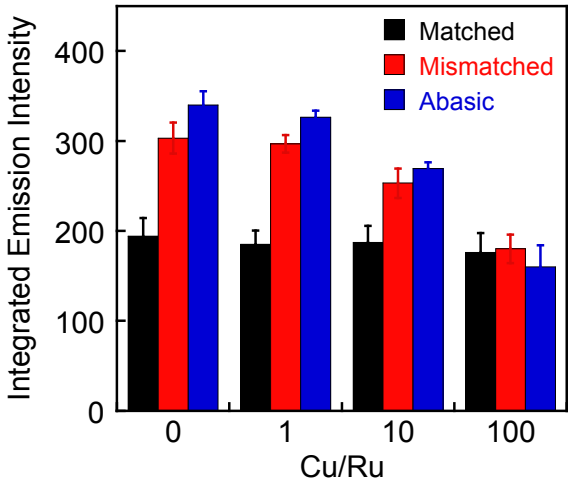

Figure 2.5. Plot of the integrated emission intensity of *rac*-Ru(bpy)$_2$dppz^{2+} (100 nM) with increasing concentration of Cu(phen)$_2^{2+}$ in the presence of 27-mer duplex DNA (Figure 2.2, λ_{ex} = 440 nm). The Ru complex was incubated with DNA previously treated with Cu(phen)$_2^{2+}$ for 30 min (5 mM Tris, pH 7.5, 50 mM NaCl). Error bars indicate standard deviations in the measurements.

DNA (Figure 2.5). Thus Cu binding selectively quenches the luminescence from Ru bound at the defect sites but not of Ru bound at well-matched sites. Since the Cu complex binds in the minor groove,[41,42] these data further support binding by Ru(bpy)$_2$dppz^{2+} to well matched DNA in the major groove. Moreover, since the quenching is selectively at the defect sites, these data also indicate that binding of the Ru complex to the defect sites appears to occur from the minor groove side. We expect that Cu quenching at these sites is the result of paramagnetic quenching rather than displacement of the Ru complex, since titrations indicate binding to the mismatched DNA is comparable in affinity to binding to well-matched DNA and thus far tighter than weak minor groove association by the copper complex. Nonetheless, irrespective of the quenching mechanism, this loss of the enhanced luminescence associated with Ru binding to defects by the minor groove–binding Cu(phen)$_2^{2+}$ strongly implies that Ru binds to the DNA defects via the minor groove. Like the metalloinsertor Rh(bpy)$_2$chrysi^{3+}, the binding mode of Ru into the destabilized site thus is likely to be insertion from the minor groove.[37,38]

2.3.6 Selective quenching of Ru luminescence with matched DNA by NaI

To improve the luminescence differential of bound Ru between matched and mismatched or abasic DNA, we used NaI to quench preferentially the Ru luminescence associated with matched DNA (Figure 2.6). Iodide is an anionic luminescent quencher, and its efficiency in quenching a small molecule bound to DNA depends upon how closely the small molecule is protected from the quencher by the DNA polyanion.[52] On the basis of the electrostatic profile of B-DNA, along with the greater exposure of a Ru complex bound to the major groove versus the minor groove, we might expect greater quenching by I^- of Ru bound in the major versus minor groove. Appropriate amounts of nonquenching KCl were added to maintain a constant ionic strength in all samples. Upon initial addition of KCl alone, we observe a marked decrease in luminescence for all three duplexes; and interestingly, simply increasing this ionic strength leads to some increase in the ratio of luminescence for mismatched:matched DNAs. The increased counterion concentration of the solution must inhibit Ru binding electrostatically and more so for the matched versus mismatched binding. Moreover, as the concentration of the quencher NaI increases, Ru luminescence with all three duplexes decreases further. As a result, in comparing the luminescence ratios without 200 mM salt versus with 200 mM NaI, the relative differential luminescence improves from 1.5-fold to 4-fold. At constant ionic strength, comparing ratios for 200 mM KCl versus 200 mM NaI, we see the ratio for mismatched to matched luminescence change from 2.3 to 3.8. Thus we see some preferential quenching of matched DNA with iodide. This result too suggests that Ru binds to DNA defects from the minor groove. DNA defect-bound Ru is expected to be less accessible to an anionic quencher and thus show less decrease in luminescence upon addition of the quencher.

Changes in the excited state lifetimes for Δ-Ru in the presence of KCl and/or NaI support our conclusions from the steady state measurements (Table 2.3). Again, all data were fit to biexponential decays. Compared with the lifetimes before the addition of salt (Table 2.2), in the presence of 1M KCl, the longer-lived component shows a substantial increase in excited state lifetime for matched, mismatched, and abasic DNA. This increase may reflect deeper perpendicular stacking of the dppz moiety betweenDNA bases. As the NaI concentration increases, the relative proportion of the longer-lived component increases as well, indicating that the shorter-lived species is more accessible to the quencher. The lifetime of

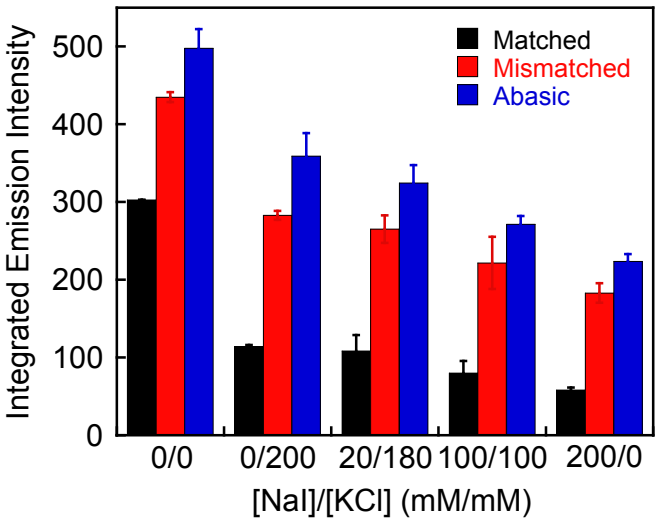

Figure 2.6. Plot of the integrated emission intensity of *rac*-Ru(bpy)$_2$dppz^{2+} (200 nM) with increasing NaI in the presence of 27-mer duplex DNA (Figure 2.2, λ_{ex} = 440 nm). Appropriate amounts of KCl were added to keep the ionic strength constant. Error bars indicate standard deviations in the measurements.

both components decreases with higher quencher concentrations, revealing that the excited state is dynamically quenched by iodide. However, both of the components continue to show a longer lifetime with mismatched DNA even at the highest quencher concentration, thus maintaining a high luminescence differential between matched and mismatched DNA. It should be noted that in all cases the instantaneous emission intensity decreases as iodide concentration increases, suggesting that high concentrations of the quencher also result in sphere of action static quenching. Importantly, this decrease is most substantial in the case of matched DNA for both binding modes. These observations are consistent with the notion that minor groove–bound Ru is buried deeper in the duplex and thus is less likely to be in the proximity of a quencher. Consequently, Ru bound in the major groove is preferentially quenched, thereby accentuating the differential luminescence between defective and matched DNA.

2.4 Conclusions

While small organic DNA binding molecules EB and TO-PRO-3 show either a small decrease or no change in luminescence when combined with defective DNA, Ru(bpy)$_2$dppz^{2+}

Table 2.3. Luminescence Decay Parameters for Δ-Ru(bpy)$_2$dppz^{2+} with DNA in the Presence of NaI[a]

DNA	[NaI]/[KCl] (mM/mM)	τ_1 (ns)[b]	τ_2 (ns)[b]	τ_1:τ_2[c]
Matched	0/1000	83	305	74:26
	500/500	81	295	66:34
	1000/0	76	275	63:37
Mismatched	0/1000	111	448	80:20
	500/500	103	357	74:26
	1000/0	99	325	75:25
Abasic	0/1000	97	300	85:15
	500/500	90	200	75:25
	1000/0	85	177	73:27

[a]Samples containing 2 μM Ru and 4 μM DNA (5 mM Tris, pH 7.5, 50 mM NaCl) were used for the excited state lifetime measurements (λ_{ex} = 470 nm, λ_{em} = 610 nm). The 27-mer oligonucleotides (matched, mismatched and abasic DNA, Figure 2.2) were used. [b]Uncertainties in excited state lifetimes are <10%. [c]Relative contributions of each lifetime to the overall decay.

displays an increase in luminescence in the presence of mismatches and abasic sites. Several observations suggest that binding of Ru into the mismatch or abasic sites occurs in a manner analogous to that of the metalloinsertor Rh(bpy)$_2$chrysi^{3+} (that is, insertion from the minor groove): (i) the correlation of the luminescent enhancement with the thermodynamic instability of mismatched sites, (ii) the preferential quenching of the enhanced luminescence at defects with Cu(phen)$_2^{2+}$ and (iii) the increase in differential luminescence at defects upon iodide quenching. Remarkably, even though the intercalating dppz ligand is structurally very different from the chrysi ligand, its similar manner of binding at mismatches and abasic sites suggests that metalloinsertion may be the general binding mode of octahedral metal complexes into the destabilized mismatched and abasic sites. To obtain direct evidence supporting this proposal, we will examine an atomic-resolution crystal structure of Δ-Ru(bpy)$_2$dppz^{2+} bound to DNA mismatches in the next chapter.

In this chapter, we thus extend the utility of Ru(bpy)$_2$dppz^{2+} to probing small local distortions in the structure of DNA by showing the ability of Ru(bpy)$_2$dppz^{2+} to act as a light-activated signal for DNA defects. Using NaI, we have magnified the luminescence differential with Ru(bpy)$_2$dppz^{2+} between matched and defective DNA by selectively quenching the luminescence from Ru bound to matchedDNA. This selective quenching strategy may prove useful for the direct visualization of biological samples containing DNA defects.

Certainly these data underscore the utility of $Ru(bpy)_2dppz^{2+}$ as a sensitive luminescent reporter of DNA and its defects.

Bibliography

[1] Lawrence J. Marnett and John P. Plastaras. Endogenous DNA damage and mutation. *Trends in Genetics*, 17(4):214–221, 2001.

[2] R. R. Iyer, A. Pluciennik, V. Burdett, and P. L. Modrich. DNA mismatch repair: Functions and mechanisms. *Chemical Reviews*, 106(2):302–323, 2006.

[3] Jan H. J. Hoeijmakers. Genome maintenance mechanisms for preventing cancer. *Nature*, 411(6835):366–374, 2001.

[4] Josef Jiricny and Giancarlo Marra. DNA repair defects in colon cancer. *Current Opinion in Genetics & Development*, 13(1):61–69, 2003.

[5] Josef Jiricny. The multifaceted mismatch-repair system. *Nat Rev Mol Cell Biol*, 7(5):335–346, 2006.

[6] Natalia E. Broude. Stem-loop oligonucleotides: A robust tool for molecular biology and biotechnology. *Trends in Biotechnology*, 20(6):249–256, 2002.

[7] Olaf Köhler, Dilip Venkatrao Jarikote, and Oliver Seitz. Forced intercalation probes (FIT probes): Thiazole orange as a fluorescent base in peptide nucleic acids for homogeneous single-nucleotide-polymorphism detection. *ChemBioChem*, 6(1):69–77, 2005.

[8] Tatsuo Maruyama, Tomoaki Takata, Hirofumi Ichinose, Lian-Chun Park, Noriho Kamaiya, and Masahiro Goto. Simple detection of point mutations in DNA oligonucleotides using SYBR Green I. *Biotechnology Letters*, 25:1637–1641, 2003. 10.1023/A:1025661730518.

[9] Kazuhiko Nakatani, Shinsuke Sando, and Isao Saito. Scanning of guanine-guanine mismatches in DNA by synthetic ligands using surface plasmon resonance. *Nat Biotech*, 19(1):51–55, 2001.

[10] Akio Kobori, Souta Horie, Hitoshi Suda, Isao Saito, and Kazuhiko Nakatani. The SPR sensor detecting cytosinecytosine mismatches. *Journal of the American Chemical Society*, 126(2):557–562, 2004.

[11] Kazuhiko Nakatani, Shinya Hagihara, Yuki Goto, Akio Kobori, Masaki Hagihara, Gosuke Hayashi, Motoki Kyo, Makoto Nomura, Masaki Mishima, and Chojiro Kojima. Small-molecule ligand induces nucleotide flipping in $(CAG)_n$ trinucleotide repeats. *Nat Chem Biol*, 1(1):39–43, 2005.

[12] Linda Valis, Nicole Amann, and Hans-Achim Wagenknecht. Detection of single base mismatches and abasic sites using phenanthridinium as an artificial DNA base and charge donor. *Org. Biomol. Chem.*, 3:36–38, 2005.

[13] G. M. Makrigiorgos, S. Chakrabarti, and A. Mahmood. Fluorescent labelling of abasic sites: A novel methodology to detect closely–spaced damage sites in DNA. *International Journal of Radiation Biology*, 74(1):99–109, 1998.

[14] Maciej Adamczyk, Phillip G Mattingly, and Jeffrey A Moore. O-(Fluoresceinylmethyl)hydroxylamine (OFMHA): A fluorescent reagent for detection of damaged nucleic acids. *Bioorganic & Medicinal Chemistry Letters*, 8(24):3599–3602, 1998.

[15] Nina Moran, Dario M. Bassani, Jean-Pierre Desvergne, Sonja Keiper, Philip A. S. Lowden, Joseph S. Vyle, and James H. R. Tucker. Detection of a single DNA base-pair mismatch using an anthracene-tagged fluorescent probe. *Chem. Commun.*, pages 5003–5005, 2006.

[16] Nicholas J. Greco and Yitzhak Tor. Simple fluorescent pyrimidine analogues detect the presence of DNA abasic sites. *Journal of the American Chemical Society*, 127(31):10784–10785, 2005.

[17] Shanta Dhar, Tetsuya Kodama, and Marc M. Greenberg. Selective detection and quantification of oxidized abasic lesions in DNA. *Journal of the American Chemical Society*, 129(28):8702–8703, 2007.

[18] Brian M. Zeglis, Valerie C. Pierre, and Jacqueline K. Barton. Metallo-intercalators and metallo-insertors. *Chem Commun (Camb)*, (44):4565–4579, 2007.

[19] Eva Rüba, Jonathan R. Hart, and Jacqueline K. Barton. $[Ru(bpy)_2(L)]Cl_2$: Luminescent metal complexes that bind DNA base mismatches. *Inorganic Chemistry*, 43(15):4570–4578, 2004.

[20] Brian M. Zeglis and Jacqueline K. Barton. A mismatch-selective bifunctional rhodiumoregon green conjugate: a fluorescent probe for mismatched DNA. *Journal of the American Chemical Society*, 128(17):5654–5655, 2006.

[21] Brian M. Zeglis and Jacqueline K. Barton. DNA base mismatch detection with bulky rhodium intercalators: synthesis and applications. *Nature Protocol*, 2(2):357–371, 2007.

[22] Alan E. Friedman, Jean Claude Chambron, Jean Pierre Sauvage, Nicholas J. Turro, and Jacqueline K. Barton. A molecular light switch for DNA: $Ru(bpy)_2(dppz)^{2+}$. *Journal of the American Chemical Society*, 112(12):4960–4962, 1990.

[23] Yonchu Jenkins, Alan E. Friedman, Nicholas J. Turro, and Jacqueline K. Barton. Characterization of dipyridophenazine complexes of ruthenium(II): The light switch effect as a function of nucleic acid sequence and conformation. *Biochemistry*, 31(44):10809–10816, 1992.

[24] Richard M. Hartshorn and Jacqueline K. Barton. Novel dipyridophenazine complexes of ruthenium(II): exploring luminescent reporters of DNA. *Journal of the American Chemical Society*, 114(15):5919–5925, 1992.

[25] Catharina Hiort, Per Lincoln, and Bengt Norden. DNA binding of Δ- and Λ-$[Ru(phen)_2DPPZ]^{2+}$. *Journal of the American Chemical Society*, 115(9):3448–3454, 1993.

[26] Ihtshamul Haq, Per Lincoln, Dongchul Suh, Bengt Norden, Babur Z. Chowdhry, and Jonathan B. Chaires. Interaction of Δ- and Λ-$[Ru(phen)_2DPPZ]^{2+}$ with DNA: A calorimetric and equilibrium binding study. *Journal of the American Chemical Society*, 117(17):4788–4796, 1995.

[27] E. J. C. Olson, D. Hu, A. Hörmann, A. M. Jonkman, M. R. Arkin, E. D. A. Stemp, J. K. Barton, and P. F. Barbara. First observation of the key intermediate in the "light-switch" mechanism of $[Ru(phen)_2dppz]^{2+}$. *Journal of the American Chemical Society*, 119(47):11458–11467, 1997.

[28] Björn Önfelt, Per Lincoln, Bengt Nordén, J. Spencer Baskin, and Ahmed H. Zewail. Femtosecond linear dichroism of DNA-intercalating chromophores: Solvation and charge separation dynamics of $[Ru(phen)_2dppz]^{2+}$ systems. *Proceedings of the National Academy of Sciences*, 97(11):5708–5713, 2000.

[29] Cynthia M. Dupureur and Jacqueline K. Barton. Structural studies of Λ- and Δ-$[Ru(phen)_2dppz]^{2+}$ bound to $d(GTCGAC)_2$: Characterization of enantioselective intercalation. *Inorganic Chemistry*, 36(1):33–43, 1997.

[30] Clara L. Kielkopf, Kathryn E. Erkkila, Brian P. Hudson, Jacqueline K. Barton, and Douglas C. Rees. Structure of a photoactive rhodium complex intercalated into DNA. *Nat Struct Mol Biol*, 7(2):117–121, 2000.

[31] Magdalena Eriksson, Mikael Leijon, Catharina Hiort, Bengt Norden, and Astrid Graeslund. Binding of Δ- and Λ-$[Ru(phen)_3]^{2+}$ to $[d(CGCGATCGCG)]_2$ studied by NMR. *Biochemistry*, 33(17):5031–5040, 1994.

[32] Per Lincoln, Anders Broo, and Bengt Nordén. Diastereomeric DNA-binding geometries of intercalated ruthenium(II) trischelates probed by linear dichroism: $[Ru(phen)_2DPPZ]^{2+}$ and $[Ru(phen)_2BDPPZ]^{2+}$. *Journal of the American Chemical Society*, 118(11):2644–2653, 1996.

[33] Antun Greguric, Ivan D. Greguric, Trevor W. Hambley, Janice R. Aldrich-Wright, and J. Grant Collins. Minor groove intercalation of δ-$[Ru(Me_2phen)_2dppz]^{2+}$ to the hexanucleotide $d(GTCGAC)_2$. *J. Chem. Soc., Dalton Trans.*, pages 849–855, 2002.

[34] Brian A. Jackson and Jacqueline K. Barton. Recognition of DNA base mismatches by a rhodium intercalator. *Journal of the American Chemical Society*, 119(52):12986–12987, 1997.

[35] Brian A. Jackson, Viktor Y. Alekseyev, and Jacqueline K. Barton. A versatile mismatch recognition agent: Specific cleavage of a plasmid DNA at a single base mispair. *Biochemistry*, 38(15):4655–4662, 1999.

[36] Brian A. Jackson and Jacqueline K. Barton. Recognition of base mismatches in DNA by 5,6-chrysenequinone diimine complexes of rhodium(III): A proposed mechanism for preferential binding in destabilized regions of the double helix. *Biochemistry*, 39(20):6176–6182, 2000.

[37] Valerie C. Pierre, Jens T. Kaiser, and Jacqueline K. Barton. Insights into finding a mismatch through the structure of a mispaired DNA bound by a rhodium intercalator. *Proceedings of the National Academy of Sciences*, 104(2):429–434, 2007.

[38] Christine Cordier, Valérie C. Pierre, and Jacqueline K. Barton. Insertion of a bulky rhodium complex into a DNA cytosinecytosine mismatch: An NMR solution study. *Journal of the American Chemical Society*, 129(40):12287–12295, 2007.

[39] J. E. Dickeson and L. A. Summers. Derivatives of 1,10-phenanthroline-5,6-quinone. *Australian Journal of Chemistry*, 23:1023–1027, 1970.

[40] Jens Brunner and Jacqueline K. Barton. Targeting DNA mismatches with rhodium intercalators functionalized with a cell-penetrating peptide. *Biochemistry*, 45(40):12295–12302, 2006.

[41] David S. Sigman, Abhijit. Mazumder, and David M. Perrin. Chemical nucleases. *Chemical Reviews*, 93(6):2295–2316, 1993.

[42] Mi Hee Lim, Irvin H. Lau, and Jacqueline K. Barton. DNA strand cleavage near a CC mismatch directed by a metalloinsertor. *Inorganic Chemistry*, 46(23):9528–9530, 2007.

[43] R. Erik Holmlin and Jacqueline K. Barton. $Os(phen)_2(dppz)^{2+}$: A red-emitting DNA probe. *Inorganic Chemistry*, 34(1):7–8, 1995.

[44] R. Erik Holmlin, Eric D. A. Stemp, and Jacqueline K. Barton. $Os(phen)_2dppz^{2+}$ in photoinduced DNA-mediated electron transfer reactions. *Journal of the American Chemical Society*, 118(22):5236–5244, 1996.

[45] Eylon Yavin, Amie K. Boal, Eric D. A. Stemp, Elizabeth M. Boon, Alison L. Livingston, Valerie L. O'Shea, Sheila S. David, and Jacqueline K. Barton. Protein–DNA charge transport: Redox activation of a DNA repair protein by guanine radical. *Proceedings of the National Academy of Sciences of the United States of America*, 102(10):3546–3551, 2005.

[46] Jacqueline K. Barton. Metals and DNA: Molecular left-handed complements. *Science*, 233(4765):727–734, 1986.

[47] Peter B. Dervan. Molecular recognition of DNA by small molecules. *Bioorganic & Medicinal Chemistry*, 9(9):2215–2235, 2001.

[48] Bruce A. Armitage. Cyanine dye–DNA interactions: Intercalation, groove binding, and aggregation. *Top. Curr. Chem.*, 253:55–76, 2005.

[49] John SantaLucia and Donald Hicks. The thermodynamics of DNA structural motifs. *Annual Review of Biophysics and Biomolecular Structure*, 33(1):415–440, 2004.

[50] Brian M. Zeglis, Jennifer A. Boland, and Jacqueline K. Barton. Targeting abasic sites and single base bulges in DNA with metalloinsertors. *Journal of the American Chemical Society*, 130(24):7530–7531, 2008.

[51] Brian M. Zeglis, Jennifer A. Boland, and Jacqueline K. Barton. Recognition of abasic sites and single base bulges in DNA by a metalloinsertor. *Biochemistry*, 48(5):839–849, 2009.

[52] Joseph R. Lakowicz, editor. *Principles of Fluorescence Spectroscopy*. Springer US, 3rd edition, 2006.

Chapter 3

Crystal Structures of Δ-Ru(bpy)$_2$dppz^{2+} Bound to Mismatched and Well-matched DNA

3.1 Introduction

The development of DNA-binding transition metal complexes as diagnostic and therapeutic agents necessitates a thorough understanding of the structural basis of their interactions with target DNA. Octahedral, polypyridyl complexes of second- and third-row transition metals are commonly employed to elucidate noncovalent binding interactions. In particular, dppz complexes of ruthenium have become a subject of particular interest owing to their unique photophysical response to DNA. Typically, these complexes exhibit little luminescence in water, but their luminescence is significantly enhanced upon binding to double-stranded DNA, hence the "light switch" effect.[1] Extensive studies in solution have established that these complexes bind to DNA by intercalation through the planar dppz ligand.[2–6] Due to their highly dynamic and nonspecific nature of DNA binding, solution or crystal structures have largely remained elusive. Although the discovery of the unique photophysical properties of this class of complexes was made over two decades ago, the first crystal structure of the complex bound to DNA was not obtained until very recently,[7] and the crystal structure did not capture dppz intercalation into a native DNA duplex.

Besides binding to well-matched DNA, dppz complexes of ruthenium, exemplified by $Ru(bpy)_2dppz^{2+}$ (Figure 3.1), show further enhanced luminescence in the presence of DNA defects such as base mismatches.[8] Its augmented luminescence sensitivity to DNA mismatches makes it a promising parent complex for the design of luminescence-based mismatch sensors. As mismatch repair (MMR) deficiencies have been linked to increased rate of mutation and several types of cancers,[9–15] a luminescent probe for DNA mismatches would provide a direct, fast and sensitive detection method for MMR deficiency. A better structural understanding of $Ru(bpy)_2dppz^{2+}$ bound to DNA mismatches will undoubtedly aid in the development of future generations of luminescent DNA probes.

We have proposed that the binding of $Ru(bpy)_2dppz^{2+}$ to mismatches occurs by metalloinsertion, in an analogous fashion to how mismatch-specific $Rh(bpy)_2chrysi^{3+}$ recognizes mismatches.[8] In this binding mode, the intercalating ligand (e.g., dppz or chrysi) inserts into the mismatch site and extrudes the mispaired bases out of the helix, effectively taking their place in the base stack.[16–19] Here we report the crystal structure of Δ-$Ru(bpy)_2dppz^{2+}$ bound to mismatched DNA at atomic resolution (1.0 Å, Figure 3.2), as well as a crystal structure of Δ-$Ru(bpy)_2dppz^{2+}$ with well-matched DNA (at 2.2-Å resolution, Figure 3.3).

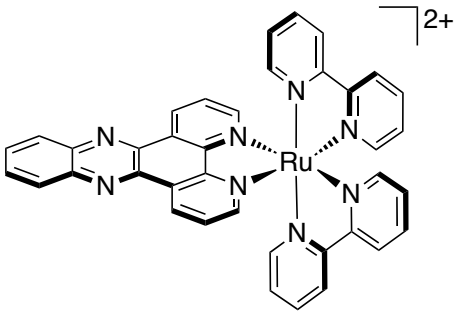

Figure 3.1. Chemical structure of Δ-$Ru(bpy)_2dppz^{2+}$.

These two structures provide several independent views of $Ru(bpy)_2dppz^{2+}$ binding to DNA through dppz intercalation or insertion, illustrating in detail the structural basis of the interactions between DNA and the "light switch" molecule as captured by crystallization in the solid state.

3.2 Experimental procedures

3.2.1 Materials

$[Ru(bpy)_2dppz]Cl_2$ was synthesized according to previously reported procedures.[20] The enantiomers were separated using a CYCLOBOND I 2000 DMP HPLC column (Sigma) on a Hewlett-Packard 1100 HPLC, with an isocratic solvent composition of 60/40 (v/v) CH_3CN:100 mM KPF_6(aq). The Δ-enantiomer eluted first, followed by the Λ-isomer. The assignment of the two fractions was confirmed by circular dichroism.[21] The fractions were lyophilized and washed with water to remove excess KPF_6 and exchanged for chloride salt on a QAE anion-exchange column. Oligonucleotides (Integrated DNA Technologies) were purified by reverse-phase HPLC using a C18 reverse-phase column (Varian) on a Hewlett-Packard 1100 HPLC. Quantification was performed on a Beckman DU 7400 spectrophotometer.

3.2.2 Crystallization and data collection

Oligonucleotides were incubated with Δ-$[Ru(bpy)_2dppz]Cl_2$ before crystallization. Subsequent manipulations were performed with minimal exposure of the complex to light. Crystal **1** was grown from a solution of 1 mM $d(C_1G_2G_3A_4A_5A_6T_7T_8A_9C_{10}C_{11}G_{12})_2$, 2 or 3

mM enantiomerically pure Δ-Ru(bpy)$_2$dppz^{2+}, 20 mM sodium cacodylate (pH 7.0), 6 mM spermine-tetrahydrochloride, 40 mM NaCl or KCl, 10 mM $BaCl_2$, and 5% 2-methyl-2,4-pentanediol (MPD) equilibratd in sitting drops versus a reservoir of 35% MPD at ambient temperature. The crystals grew in space group $P1$ with one biomolecule per asymmetric unit and unit cell dimensions: $a = 24.0$ Å, $b = 24.8$ Å, $c = 37.5$ Å, $\alpha = 74.7°$, $\beta = 84.4°$, and $\gamma = 76.2°$ (Table 3.1).

Crystal **2** was grown from 1 mM d($C_1G_2G_3T_4A_5A_6T_7T_8A_9C_{10}C_{11}G_{12}$)$_2$ and 4 mM enantiomerically pure Δ-Ru(bpy)$_2$dppz^{2+}. Other conditions remained the same as those for crystal **1**. The crystals grew in space group $C121$ with one biomolecule per asymmetric unit and unit cell dimensions: $a = 80.1$ Å, $b = 27.2$ Å, $c = 49.6$ Å, $\alpha = \gamma = 90°$, and $\beta = 115.8°$ (Table 3.1).

The data for crystal **1** were collected from a flash-cooled crystal at 100 K on an R-axis IV image plate using Cu Kα radiation produced by a Rigaku RU-H3RHB rotating-anode generator with double-focusing mirrors and a Ni filter. High-resolution data were subsequently collected from a different crystal on beamline 12-2 at the Stanford Synchrotron Radiation Laboratory (Menlo Park, CA; $\lambda = 0.7749$ Å, 100 K, PILATUS 6M detector). The data were processed with MOSFLM or XDS[22], and SCALA from the CCP4 suite of programs.[23]

The data for crystal **2** were collected from a flash-cooled crystal at 100 K on the Rigaku diffractometer described above, processed with XDS,[22] POINTLESS, and SCALA.[23]

3.2.3 Structure determination and refinement

Both structures were determined by single anomalous dispersion phasing using the anomalous scattering of ruthenium with the Shelxc/d/e suite of programs.[24] For both crystals, five heavy atoms were located per asymmetric unit. Structures were built in COOT[25] and refined with PHENIX version 1.7.[26] For structure **1**, the anomalous contribution of ruthenium was taken into account and alternative conformations of phosphates were included in the refinement; for non-hydrogen atoms, anisotropic temperature factors were refined. For structure **2**, further refinement is underway. Figures were drawn with Pymol.[27] Alignment was performed with LSQMAN.[28]

Table 3.1. Data collection and refinement statistics

	structure **1**	structure **2**
Data collection		
space group	$P1$	$C121$
cell dimensions		
a,b,c (Å)	24.0, 24.8, 37.5	80.1, 27.2, 49.6
α,β,γ (deg)	74.7, 84.4, 76.2	90.0, 115.8, 90.0
wavelength	0.7749	1.5418
resolution	23.3-1.00 (1.05-1.00)	25.5-2.17 (2.32-2.17)
R_{merge}	0.029 (0.212)	0.021 (0.263)
R_{pim}	0.017 (0.124)	0.021 (0.250)
$I/\sigma I$	24.0 (5.6)	19.1 (3.5)
completeness (%)	86.1 (81.4)	99.4 (99.6)
redundancy	3.9	3.0
Refinement		
no. of reflections	37763	5407
$R_{\text{work}}/R_{\text{free}}$	0.125/0.144	0.247/0.305
rmsd for bond lengths (Å)	0.025	0.017
rmsd for bond angles (deg)	1.471	2.954

3.2.4 Steady state fluorescence

Luminescence spectra (excitation wavelength = 440 nm) with emission intensities ranged from 560 to 800 nm were measured in 40 mM sodium cacodylate (pH 7.0), 80 mM KCl, 20 mM $BaCl_2$ on an ISS-K2 spectrophotometer at 4 °C in aerated solutions. $Cu(phen)_2^{2+}$ was formed *in situ* using 1:3 $CuCl_2$ and phenanthroline. Experiments were performed in triplicate.

3.3 Results and discussion

3.3.1 Cocrystallization of Δ-Ru(bpy)$_2$dppz^{2+} with DNA

To elucidate the structural basis for $Ru(bpy)_2dppz^{2+}$ interaction with both mismatched and well-matched DNA, we cocrystallized Δ-$Ru(bpy)_2dppz^{2+}$ with 12-mer palindromic DNA sequences. The sequence used in structure **1**, $d(C_1G_2G_3\underline{A_4}A_5A_6T_7T_8\underline{A_9}C_{10}C_{11}G_{12})_2$, contains two AA mismatches (underlined) and has been previously used to obtain two crystal structures of Δ-$Rh(bpy)_2chrysi^{3+}$ bound to mismatched DNA.[19] The sequence in structure **2**, $d(C_1G_2G_3T_4A_5A_6T_7T_8A_9C_{10}C_{11}G_{12})_2$, was designed to be well matched throughout the

duplex, with a TA base pair in place of the AA mismatch. Both crystals took longer than 8 weeks to appear in the crystallization wells. Although the starting ratio of Ru:duplex was different (2:1 or 3:1 in structure **1** and 4:1 in structure **2**), the crystals each incorporated five ruthenium complexes per DNA duplex, which together forms the asymmetric unit in both cases. For the two sequences, crystals formed in two different space groups. Crystal **1**, diffracted to atomic resolution, revealed three binding modes of the ruthenium complex: (i) metalloinsertion at the mismatched sites with ejection of the mispaired adenosines, (ii) metallointercalation between well-matched base pairs and (iii) end-capping between two (crystallographically related) duplexes (Figure 3.2). To our surprise, crystal structure **2**, which started with a fully complementary DNA sequence, also exhibited the three binding modes in the final structure (Figure 3.3). Interestingly, despite a global resemblance between the two structures, the orientation of the dppz ligand is rather different. These structures, taken together, illustrate the generality of metalloinsertion and the versatile DNA binding modes attainable for dppz complexes, and also point to the force of crystal packing in forming intricate molecular structures.

3.3.2 Structure 1

In crystal **1**, the metal complex and the oligonucleotide containing AA-mismatches cocrystallized in space group $P1$. The biological molecule consists of a full DNA duplex and five ruthenium complexes. All five ruthenium complexes are inserted or intercalated through the dppz ligand from the minor groove, providing five independent views of ruthenium binding to DNA. Crystallographically related duplexes are stacked head to tail, forming parallel long rods in the crystal lattice (Figure 3.4). Aside from the end-stacking interactions between consecutive duplexes, mediated by an end-capping metal complex, neighboring parallel rods do not have detectable contacts with one another.

At destabilized AA mismatches, the metal complex inserts deeply from the minor groove and fully ejects the mispaired adenosines. We had proposed that $Ru(bpy)_2dppz^{2+}$ binds to DNA mismatches through insertion via the minor groove, and that metalloinsertion may be a general binding mode for octahedral metal complexes bearing planar ligands.[8] Here, consistent with our proposal, the ruthenium complex indeed binds tightly to both mismatched sites through metalloinsertion, with the dppz ligand stacked between the two flanking base pairs, effectively replacing the mispaired adenosines in the base stack. All four

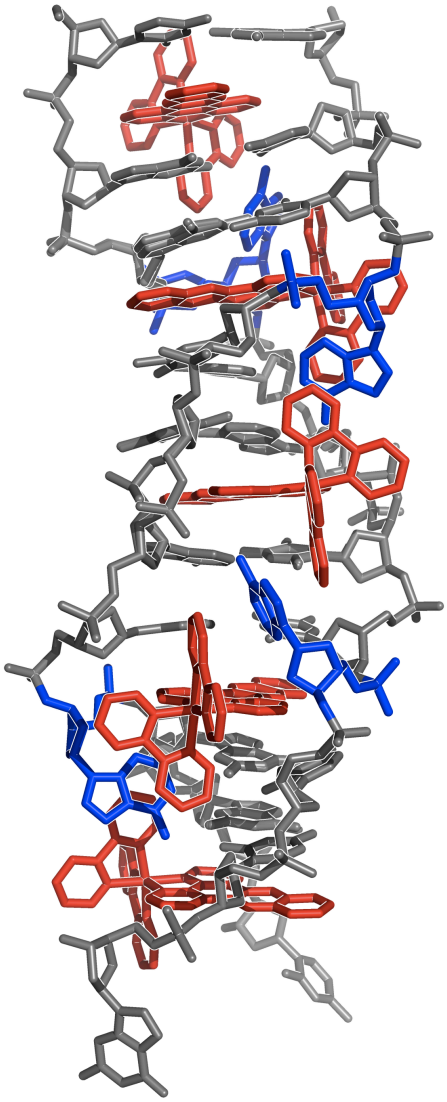

Figure 3.2. Crystal structure (**1**) of Δ-Ru(bpy)$_2$dppz^{2+} (red) bound to the oligonucleotide d(CGGAAATTACCG)$_2$ (gray). The AA mismatches (blue) are extruded out of the helix by inserted ruthenium complexes.

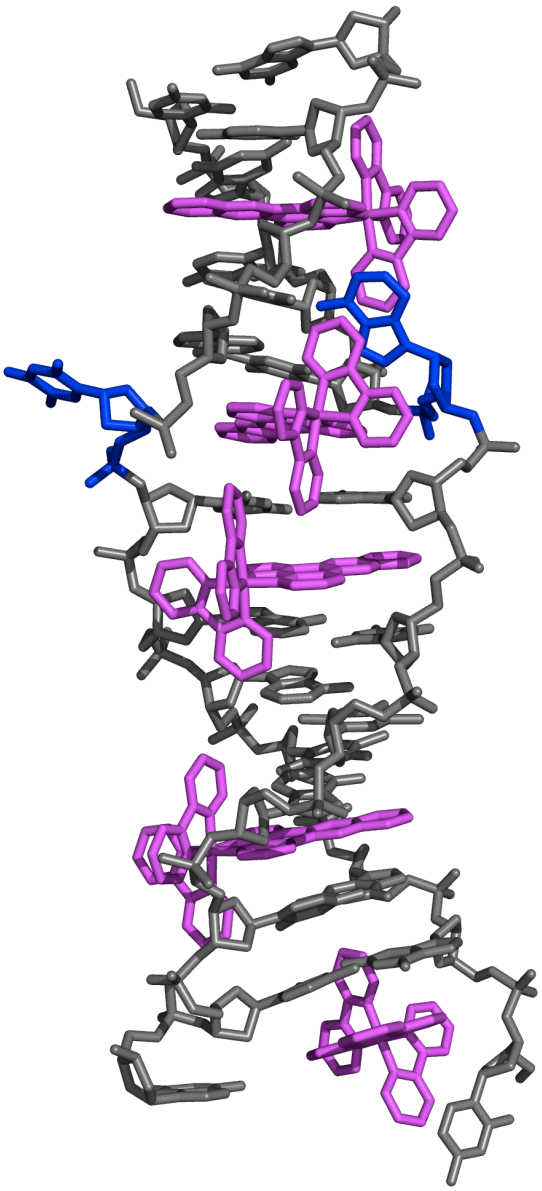

Figure 3.3. Crystal structure (**2**) of Δ-Ru(bpy)$_2$dppz^{2+} (magenta) bound to the oligonucleotide d(CGGTAATTACCG)$_2$ (gray). An AT base pair (blue) is extruded out of the helix by an inserted ruthenium complex.

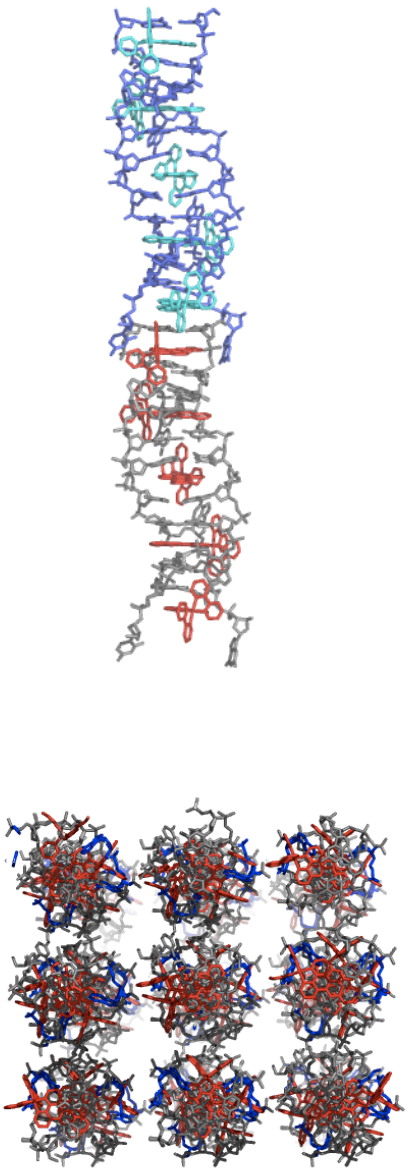

Figure 3.4. Top: one duplex (blue, ruthenium complex in cyan) stacks on top of a symmetry-related duplex (gray, ruthenium complex in red) to form a long rod in the crystal lattice. Bottom: view down the helical axis of nine parallel rods.

ejected adenosines are folded back in the minor groove. They adopt the *syn* conformation and stack with the very ruthenium that is inserted at their respective mismatched site. An overlay of the two separate metalloinsertion sites shows that the local geometry of the DNA and the relative orientation of the ruthenium complex is highly similar between the two sites (Figure 3.5). The dppz is inserted in a head-on fashion, positioned halfway between the phosphate backbones. On the other hand, if we only consider the relative orientation of the dppz with respect to the base pairs above and below the insertion site, the dppz is inserted at an acute angle with respect to either dyad axis of the flanking base pairs. Unlike in the rhodium structure, where the minor groove widens to accommodate the sterically expansive chrysi ligand,[16,19] the insertion of the narrower dppz ligand and the bpy-stacked adenosines do not lead to groove widening.

Of the remaining three ruthenium complexes, two are intercalated between well-matched base pairs, also via the minor groove. This mode of intercalation, namely from the minor groove, is somewhat unexpected, and appears to contrast what we would predict from previous solution studies, in which we had deduced a major groove preference for metallointercalation.[3,6,29] However, we note that in this structure (and structure **2**, *vide infra*), intercalation occurs in conjunction with stacking interactions between an ancillary bpy ligand of the intercalating complex and either an extruded adenosine or the bpy ligand from a neighboring complex. These stacking interactions, likely due to crystal packing, serve to stabilize the intercalated complex in the minor groove, which indicates that the energetic difference between intercalation from the major groove versus the minor groove is small. Computational studies of ruthenium-dppz complexes intercalated into a dinucleotide step also support the notion of very small differences in intercalation energetics from the two grooves.[30] In this intercalative binding mode, the dppz ligand is positioned inside the base stack also in a head-on fashion. The intercalation of the dppz ligand is so deep that the end most distal from the ruthenium center protrudes into the major groove. An overlay of the two independent intercalation sites, aligned using DNA backbone atoms, reveals subtle differences in the relative position of the complex (Figure 3.6). In the 5'-C_1G_2-3' step, the dppz is right in the middle of the two strands and intercalated more deeply, with most of the stacking interactions formed between the central ring of the phenazine portion and the bases. In comparison, at the 5'-A_6T_7-3' step, the dppz is closer to one strand than the other, and both the distal and the central rings of the phenazine are involved in stacking.

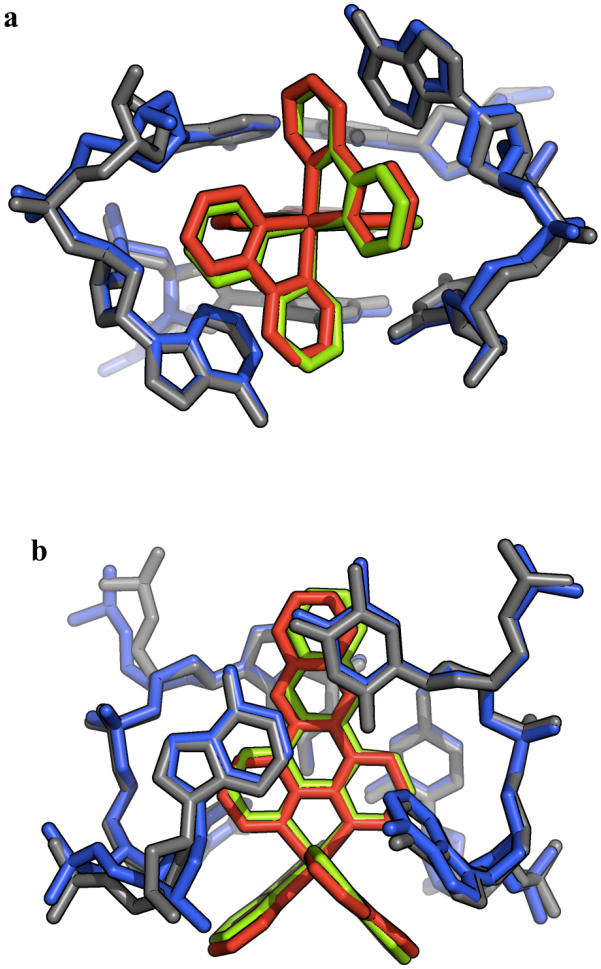

Figure 3.5. Superposition of the two independent views of metalloinsertion by the ruthenium complex at mismatched sites in structure **1**. (a) View from the minor groove of Δ-Ru(bpy)$_2$dppz^{2+} insertion and extrusion of the mismatched adenosines. (b) View down the helix axis. The two binding sites were superimposed using only the DNA backbone atoms (rmsd of 42 atoms = 0.607 Å).

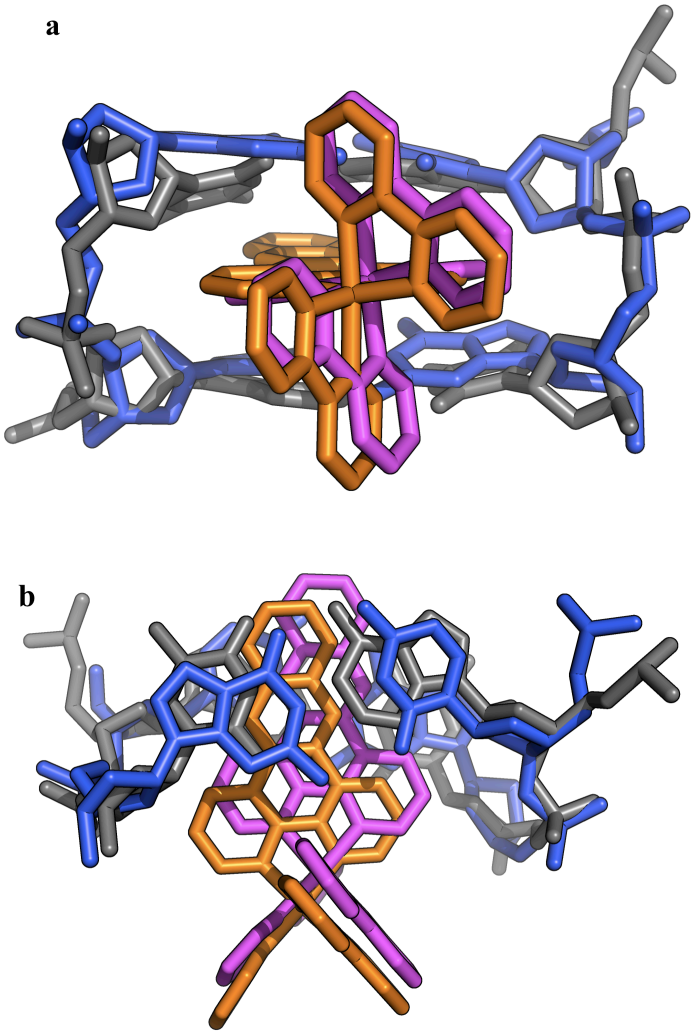

Figure 3.6. Superposition of the two independent views of intercalation by the ruthenium complex in structure **1**. (a) View from the minor groove of Δ-Ru(bpy)$_2$dppz^{2+} intercalation between 5'-C$_1$G$_2$-3' (light blue, Ru in orange) and 5'-A$_6$T$_7$-3' (gray, Ru in magenta). (b) View down the helix axis. The two binding sites were superimposed using only the DNA backbone atoms (rmsd of 27 atoms = 1.001 Å).

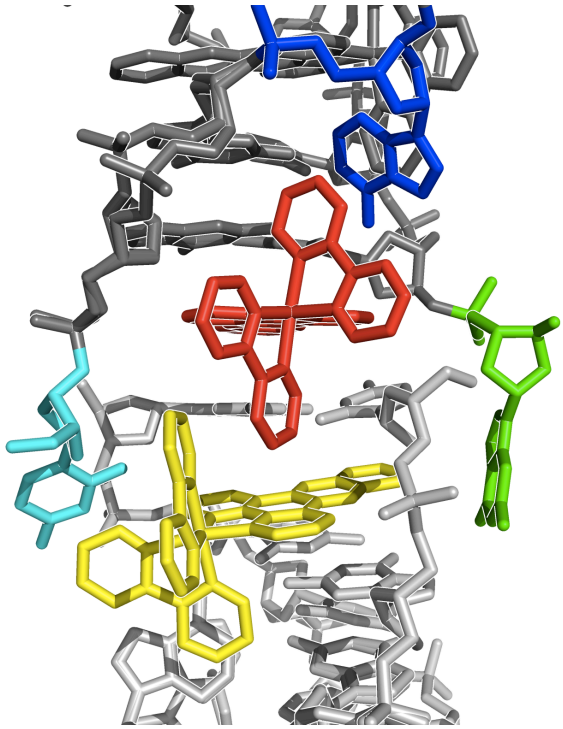

Figure 3.7. The duplex (dark gray) is end-capped by a ruthenium complex (red), which is stacked between an extruded adenosine (blue) and the first complex (yellow) in a crystallographically related duplex (light gray). The last GC base pair (cytidine in cyan and guanosine in green) forms a frayed end.

The fifth ruthenium complex is sandwiched between two crystallographically related duplexes (Figure 3.7). The last GC base pair becomes a frayed end, with the cytidine and the guanidine pointing down into the minor and major groove of the next duplex, respectively. The dppz ligand of the end-capping ruthenium complex effectively replaces this terminal base pair in the helix, providing an anchor for the next duplex to stack on.

Throughout the DNA helix, the minor groove is densely populated by alternating metal complex and extruded adenosines. The five metal complexes are evenly spaced out, binding to DNA at every two base steps. The four mismatched adenosines are sandwiched between the five metal complexes, and the last metal complex makes contact with the first one in the next repeating unit. The DNA maintains its B-form, albeit with some local deviations from ideal B-form geometry (Table 3.2). The overall structure is slightly bent toward the major groove, similar to what we have observed in the rhodium structure with the identical DNA sequence.[19] All base pairs show some degree of unwinding to accommodate inserted and intercalated complexes, as expected, since unwinding of DNA is always associated with

Table 3.2. DNA helical parameters[a] in structure **1**[b]

Step	Ru binding mode	Shift (Å)	Slide (Å)	Rise (Å)	Tilt (°)	Roll (°)	Twist (°)
C_1/G_2	intercalation	0.12	2.08	6.26	13.00	4.42	18.35
G_2/G_3	–	0.91	0.21	2.92	-3.43	-5.89	30.16
G_3/A_5	insertion	0.69	3.42	7.16	7.27	13.01	68.64
A_5/A_6	–	-0.58	-0.14	2.95	0.96	0.28	26.52
A_6/T_7	intercalation	-0.14	0.53	7.09	-1.06	10.82	23.50
T_7/T_8	–	0.41	-0.33	2.84	-1.70	3.88	23.70
T_8/C_{10}	insertion	-0.69	3.46	7.37	-7.19	11.20	69.50
C_{10}/C_{11}	–	-0.94	-0.23	3.02	3.31	-8.85	23.67
B-DNA	–	-0.1	-0.8	3.3	-1.3	-3.6	36

[a]Geometrical relationships between consecutive base pairs: shift, translation into the groove; slide, translation toward the phosphodiester backbone; rise, translation along the helix axis; tilt, rotation about the pseudo-twofold axis relating the DNA strands; roll, rotation about a vector between the C1' atoms; and twist, rotation about the helix axis. [b]Data were calculated using 3DNA.[34]

intercalators.[31–33] The rise is approximately doubled at each ruthenium binding site as the metal complex serves as an additional base pair in the helix, but interestingly, the rise between native consecutive base pairs are less than 3.3 Å. This compression of the vertical space between consecutive base pairs may be an indication that stacking between the bpy ligands and extruded adenosines is a dominating interaction, such that the base pairs between the intercalation sites have to shorten their rise in order for the adenosines and bpy ligands to reach each other. The average distance between a bpy and an adenosine is in fact 3.3 Å. This is consistent with our notion that the adenosine-bpy stacking may be driving ruthenium intercalation from the minor groove. But importantly, the adenosines are extruded in the first place because ruthenium complexes are inserted at the mismatched sites, and we fully anticipate metalloinsertion to occur via the minor groove.

3.3.3 Structure 2

Structure **2** is not fully refined as yet, due to difficulties from possible crystal growth defects and/or radiation damage. Preliminary results are presented and discussed here.

In crystal **2**, the metal complex and the fully complementary oligonucleotide cocrystallized in space group $C121$. The asymmetric unit is a full DNA duplex with five bound ruthenium complex. Again, we are provided with five independent views of ruthenium

binding to DNA. The crystallization conditions are highly similar to those used in crystal **1**, and the sequence is identical except for the previously mismatched base pairs. However, except for the end-capping complex and the 5'-A_6-Ru-T_7-3' step, compared to crystal **1**, the ruthenium molecules are bound at different steps along the DNA (i.e., the sequence context is altered), and the global crystal packing is more intricate, hence the different space group.

The sequence for structure **2** is intended to be self-complementary and thus well matched at all base pairs, but one metal complex is found to bind by metalloinsertion at an AT step (which is a different step than the AA mismatch in structure **1**). Upon ruthenium insertion from the minor groove, the adenosine and thymidine are both ejected from the base stack. Much like the case in structure **1**, the adenosine is folded back into the minor groove and stacks between the inserted and a neighboring complex. The exact conformation of the adenosine, i.e., whether it is *anti* or *syn*, remains to be determined upon further refinement. In contrast, the thymidine is extruded into the major groove and stacks with the same thymidine from a crystallographically related duplex. This unexpected metalloinsertion event suggests that the extruded AT base pair is the least stabilized region of the duplex (besides the frayed end, *vide infra*). Metalloinsertion at this weak point along the helix would then anchor the inserted ruthenium complex and provide additional crystal packing interactions through the extruded bases.

Perhaps more intriguing than metalloinsertion at a well-matched base step is that the inserted complex is separated from a neighboring complex, also in the minor groove, by just a single base pair. In other words, this arrangement appears to violate the nearest-neighbor exclusion principle, which states that intercalators cannot bind at higher loading density than one per two base pairs.[35–38] However, since the inserted ruthenium complex is causing the extrusion of a base pair, we do not consider it a bona fide intercalator that the nearest-neighbor exclusion principle is concerned with. Yet this unusual nearest-neighbor insertion-intercalation binding event shows that local DNA conformations can become very flexible to accommodate multiple ligand binding at high loading density. In this case, the intercalative binding is further complicated by the three-dimensional structure of the octahedral metal complex—the ancillary bpy ligands of these two nearest neighbors are stacked with each other. As a result, the minor groove widens at the intercalation site to allow a rather canted binding orientation for both complexes. Groove widening is only observed for this nearest-neighbor arrangement, and is absent in all the other intercalation

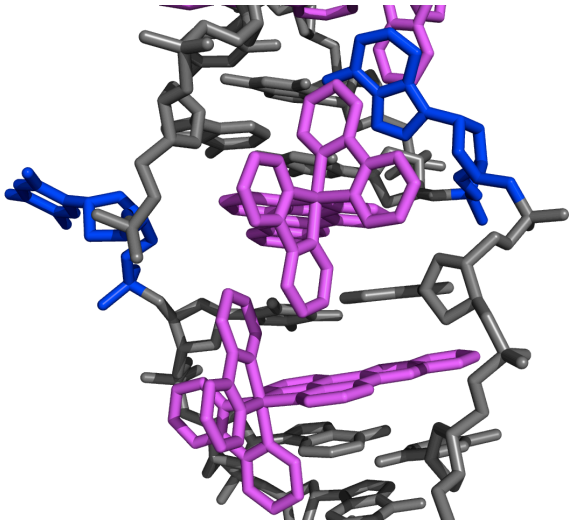

Figure 3.8. Metalloinsertion of Δ-Ru(bpy)$_2$dppz^{2+} (magenta) at an AT base pair (blue). The dppz ligand is inserted into the base stack (gray) from the minor groove, ejecting the adenosine and thymine. The adenosine is stacked with the bpy ligand of the inserted ruthenium. The other bpy ligand is stacked with the next complex, which is located only one base pair away.

or insertion sites. Furthermore, the twist of the helix at the insertion step is about 80°, compared with the normal 72°(= 36° × 2) for two base steps in ideal B-form DNA. This additional positive twist is likely a result of crystal packing, as it is absent in other insertion sites and is directly associated with the extruded thymidine. Fortunately, the extended shape of the dppz ligand enables it to stack effectively with the two almost orthogonal flanking base pairs (Figure 3.8).

Similar to structure **1**, the last GC base pair forms a frayed end rather than being properly hydrogen bonded. However, in this structure, the cytidine is positioned in the minor groove and sandwiched between the end-capping ruthenium and the first complex of the next repeating unit. Thus, much like the case in structure **1**, in structure **2**, four out of the five ruthenium complexes form ancillary stacking interactions with either an extruded base or a neighboring complex, which we have hypothesized to be the driving force behind minor groove intercalation. We notice, however, that there is one exception. The fifth metal complex, which is also intercalated between two well-matched base pairs (5'-A$_9$C$_{10}$-3'), does not appear to have ancillary interactions through its bpy ligands, yet it still binds via the minor groove. It is located approximately halfway between its neighbors, with two base-pair separation on one side and three base-pair separation on the other side. In this

case, we suspect that the preference of the metal complex for the minor groove may be a result of the major groove being less available in the crystal. In this structure, two large densities are present in the major groove, which are tentatively fit to Ba atoms, coordinated by the O6 and N7 of guanines. A Ba atom was also located in the major groove in a recent structure of Λ-Ru(TAP)$_2$dppz^{2+} bound to DNA.[7] One of the Ba atoms is only one base pair away from the 5'-A_9C_{10}-3' intercalation site. At the same time, the ruthenium complex at 5'-A_6T_7-3', intercalated deeply into the DNA base stack, has its dppz ligand protruding out into the major groove. Thus, the space in the major groove becomes rather restricted, which may have prompted the last ruthenium complex to bind in the minor groove even without ancillary interactions.

In this crystal, stacking from extruded thymidines connects two side-by-side, antiparallel, crystallographically related duplexes (Figure 3.9 and 3.10). Symmetry-related duplexes are also stacked head-to-tail to form a rod along the long axis (Figure 3.10). The two rods stemming from the two side-by-side duplexes are at an angle of ∼35° with respect to each other (Figure 3.10). Thus, each duplex within a rod forms thymine-thymine interactions with a different rod in the lattice. Altogether, parallel rods and their thymine-stacking partner rods make up a crisscross pattern in the lattice.

3.3.4 Differences and similarities between the two structures

The foremost difference between the two crystals is the DNA sequence. In crystal **1**, a palindromic 12-mer oligonucleotide containing two AA mismatches were employed, while a fully complementary 12-mer sequence is used for crystal **2**. Crystal **1** formed with an initial ratio of 1:2 or 1:3 duplex-to-ruthenium, but crystal **2** only formed at a ratio of 1:4 duplex-to-ruthenium (1:2 or 1:3 did not yield crystals.) However, the screen conditions are identical and rather similar to the conditions used for previously solved rhodium-DNA structures, suggesting that these conditions may represent a good starting point for metal complex-DNA cocrystallization. In both cases, the stoichiometry of ruthenium complex to DNA is found to be five Ru per duplex, which is higher than the starting metal-to-DNA ratio. This high binding density might in fact be the key to obtaining these structures: as Ru-dppz complexes are known to be nonspecific binders to DNA, DNA with lower binding density may have heterogenous ruthenium distribution and thus less likely to pack uniformly into a single crystal.

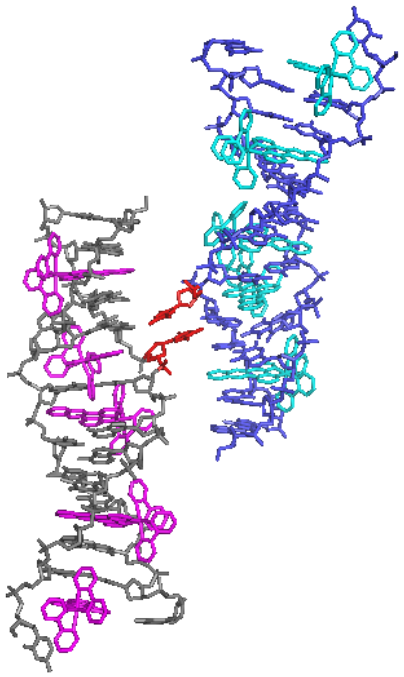

Figure 3.9. Two side-by-side, crystallographically related duplexes are connected through thymine-thymine (red) stacking.

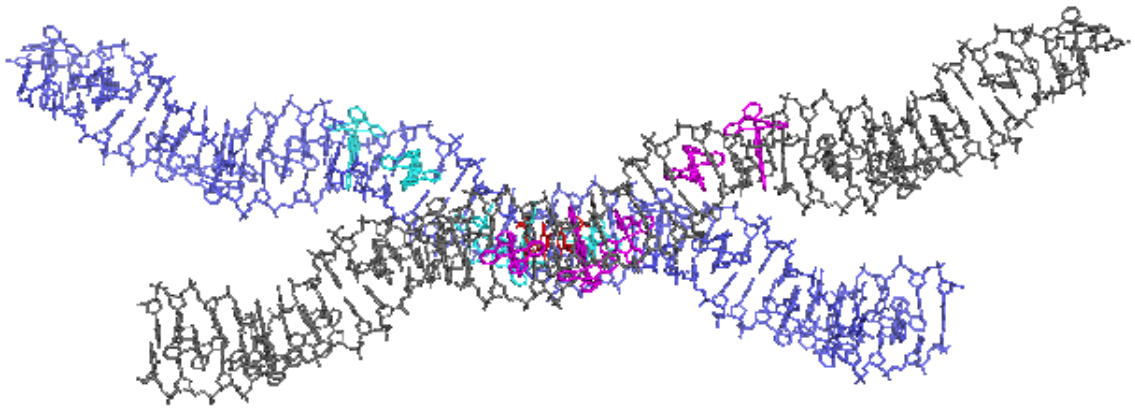

Figure 3.10. Long rods formed by end-to-end stacking of symmetry-related duplexes are positioned at an angle with respect to each other.

Taken together, the two structures offered three independent views of metalloinsertion, five of metallointercalation, and two of end-capping. All binding events occurred from the minor groove, with the dppz ligand inserted deeply into the DNA base stack, π-stacking with the bases above and below the binding site. The orientation of the dppz ligand varies quite significantly among the binding sites. In structure **1**, the dppz ligand is always centered between the sugar-phosphate backbones, but in structure **2**, it is always intercalated sideways (Figure 3.11). Given that dppz is a narrow but long ligand with the entire phenazine portion available for π-π stacking, we had previously proposed these two types of binding orientation based on NMR and luminescence lifetime studies.[6,29] Although our proposal was predicated on binding in the major groove, the crystal structures presented here clearly show that even when the ruthenium complex is restricted in the minor groove, it can bind in either a head-on or canted fashion. In the head-on orientation, the two phenazine nitrogens are equally protected from the solvent; in the canted orientation, one nitrogen is perceivably more solvent accessible than the other. The difference in binding orientation in the crystal structures may have originated from the DNA being more "symmetric" in structure **1** but less so in structure **2**. In the former, the two symmetric AA mismatches are the most destabilized regions of the duplex, where initial binding of ruthenium by metalloinsertion must have occurred. Curiously, in the second crystal, even though the DNA sequence is also palindromic, it appears that once the ruthenium recognizes a weak point (the extruded AT) in the helix, the rest of the helix must have been affected in a way that the previously symmetric AT pair is no longer a weak point (in the case of an AA mismatch, it will always remain destabilized relative to well-matched regions). Consequently, the remaining ruthenium complexes are intercalated along the helix at different steps from those in the mismatched duplex. Furthermore, the two AT pairs are only two base pairs away from each other (versus four base-pair separation for the AA mismatches), and it is possible that this difference ultimately affects binding geometries.

Besides intercalation through the dppz ligand, the most striking similarity between the two structures is the prevailing ancillary interactions between two bpy ligands, or a bpy and an extruded base. Ancillary interactions are present in related rhodium-DNA structures, but this is the first time we observe direct stacking between two neighboring complexes, or between an extruded base and the very complex that has caused its ejection. In two of the rhodium-DNA structures, a $Rh(bpy)_2chrysi^{3+}$ is intercalated between well-matched base

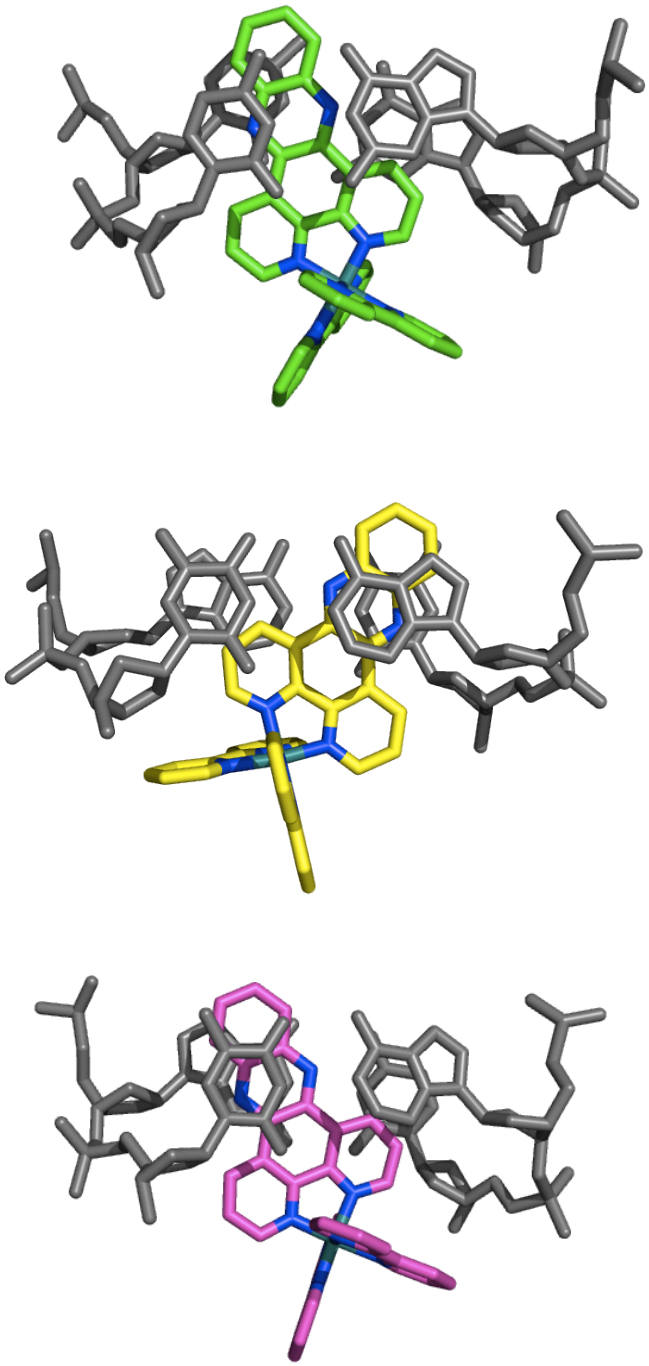

Figure 3.11. Ruthenium intercalation in structure **2** at 5-'G_2G_3-3' (top), 5'-A_6T_7-3' (middle) and 5'-A_9C_{10}-3' (bottom).

Table 3.3. DNA base step parameters in structure **2**[a]

Step	Ru binding mode	Shift (Å)	Slide (Å)	Rise (Å)	Tilt (°)	Roll (°)	Twist (°)
C_1/G_2	–	-0.04	0.88	2.91	-1.06	-0.76	27.48
G_2/G_3	intercalation	-0.13	0.52	7.01	-4.16	15.99	26.76
G_3/T_4	–	-0.57	-0.02	2.91	-1.90	0.66	21.47
T_4/A_6	insertion	0.42	4.60	6.83	-5.95	1.05	80.41
A_6/T_7	intercalation	0.78	-0.07	6.43	3.24	13.50	8.44
T_7/T_8	–	-0.10	0.56	3.19	3.23	4.60	32.20
T_8/A_9	–	-0.53	1.74	3.25	1.63	5.74	34.38
A_9/C_{10}	intercalation	-0.22	0.18	6.65	-19.15	13.88	22.07
C_{10}/C_{11}	–	-0.03	-0.10	3.03	5.22	-0.72	25.37
B-DNA	–	-0.1	-0.8	3.3	-1.3	-3.6	36

[a]Data were calculated using 3DNA.[34]

pairs from the major groove, while its bpy ligands are end-stacked with crystallographically related duplexes.[16,19] The intercalative Rh binding event, absent in solution, was attributed to crystal packing through ancillary interactions. Likewise, in the two ruthenium-DNA structures, these interactions act to stabilize intercalated ruthenium complexes, rigidifying the entire structure and potentially facilitating crystallization.

Overall, the DNA helix in both structures is unwound at almost every step – the majority of the helical twist parameter between two consecutive, stacked base pairs is between 20 and 30° – so as to accommodate the high density of intercalated metal complexes (Table 3.2 and 3.3). Both structures also show a wide range of propeller and buckle angles, as the DNA adapts to multiple ligand binding and base extrusion. All of the sugar pucker is C2'-endo or the closely-related C3'-exo and C1'-exo. Given that five independent views of intercalation are illustrated between the two structures, it seems that alternating C3'-endo/C2'-endo puckering is not a requirement for intercalation.

3.3.5 Comparisons to other structures

The first structure of a ruthenium dppz complex bound to DNA is that of a Λ-enantiomer of $Ru(TAP)_2dppz^{2+}$ (TAP = 1,4,5,8-tetraazaphenanthrene) bound to a 10-mer oligonucleotide.[7] The ruthenium complex is found to bind through semi-intercalation of a TAP ligand between two GC base pairs, as well as intercalation of the dppz ligand between a GC

and a reverse Watson-Crick-paired terminal AT pair, with the adenine and thymine coming from symmetry-related strands. Besides having a different ancillary ligand, this complex is of the opposite chirality of our ruthenium complex. We have demonstrated in our structures that the Δ-isomer intercalates through the dppz ligand between natively well-matched base pairs, but this mode of binding is absent in the TAP structure. This is consistent with early solution studies of the binding of intercalative metal complexes to DNA: the ancillary ligands of the Λ-isomer are sterically repelled by the backbone of right-handed B-form DNA, while the Δ-isomer has complementary shape to fit in the grooves.[39] In the TAP structure, the DNA duplex adopts an overall B-form despite large local distortions, and dppz intercalation occurs only at the interface between two duplexes, which are positioned perpendicular to each other rather than form a continuous helix. At the same time, the semi-intercalation of TAP induces a severe kink in the DNA. Taken together, these observations suggest that the Λ-configuration indeed does not favor intercalation. In contrast, the Δ-isomer, as shown in the structures reported herein, bind avidly to the right-handed helix through full intercalation.

Next, we compare our structures with that of Δ-Rh(Me_2trien)phi^{3+} (Me_2trien = 2*R*,9*R*-diamino-4,7-diazadecane) intercalated in an 8-mer oligonucleotide.[32] The rhodium structure shows only one complex bound per 8-mer duplex, as opposed to five ruthenium complexes per 12-mer duplex in our structures. Functional groups were installed on the rhodium complex to form sequence-specific contacts with the DNA in the major groove, hence the single-site binding at a specific step in the base stack. The ruthenium dppz complex, on the other hand, binds nonspecifically to DNA. Thus, binding at multiple sites along the duplex was observed in both ruthenium structures. The sequence context of the intercalation sites—purine-purine, purine-pyrimidine, and pyrimidine-purine—also speaks to the nonspecific nature of ruthenium dppz binding to DNA.

3.3.6 Solution luminescence

We measured the solution luminescence of Δ-Ru(bpy)$_2$dppz^{2+} bound to the two sequences in order to determine if the crystal structures reflect binding preferences in solution. As the AA mismatch-containing duplex has a low melting temperature of 22 °C, the experiments were conducted at 4 °C to ensure all DNA strands are properly hybridized. The luminescence from Δ-Ru(bpy)$_2$dppz^{2+} bound to mismatched DNA is about three times the luminescence

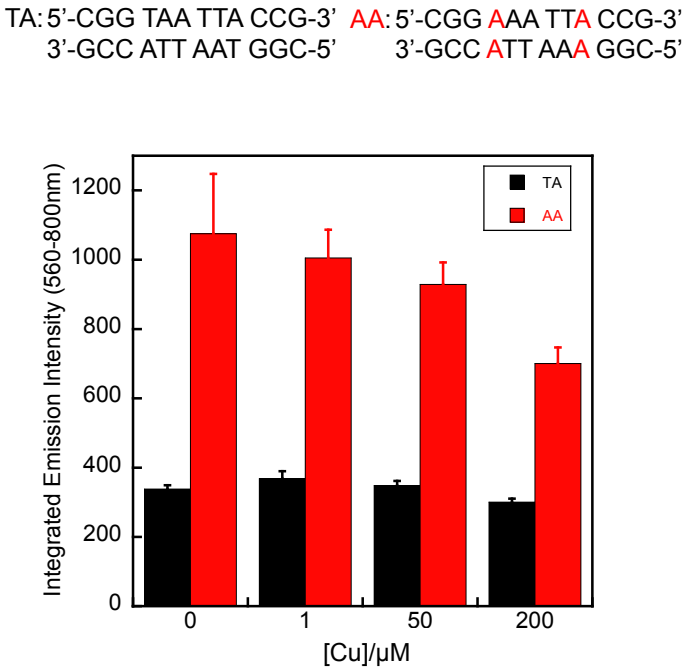

Figure 3.12. Top: DNA sequences used in the solution luminescence measurements and crystallization. Bottom: integrated emission intensity of Δ-Ru(bpy)$_2$dppz^{2+} in the presence of oligonucleotides with increasing concentrations of the minor groove-specific quencher Cu(phen)$_2^{2+}$. Luminescence is quenched more significantly for the AA mismatch-containing DNA. Conditions are 1 μM Δ-Ru(bpy)$_2$dppz^{2+}, 1 μM duplex, 0-200 μM Cu(phen)$_2^{2+}$ in 40 mM sodium cacodylate (pH 7.0), 80 mM KCl, 20 mM $BaCl_2$ at 4 °C. The ruthenium complex is excited at 440 nm and emission intensity from 560 to 800 nm is integrated.

with the well-matched duplex (Figure 3.12), consistent with previously observed higher sensitivity of Ru(bpy)$_2$dppz^{2+} luminescence response to mismatched DNA.

To determine the groove preference of ruthenium complex binding, we employed the minor groove-specific quencher, Cu(phen)$_2^{2+}$,[40,41] to quench the luminescence from ruthenium (Figure 3.12). The luminescence associated with mismatched DNA is significantly quenched (by 34%) with increasing concentrations of Cu(phen)$_2^{2+}$, while luminescence associated with the matched sequence is quenched to a lesser extent (12%). This differential quenching is consistent with the mismatch-bound ruthenium complexes being located in the minor groove, but those bound to well-matched DNA are mostly in the major groove. Therefore, although the crystal structures provide a very detailed picture of metalloinsertion and metallointercalation in the minor groove, they fail to capture intercalation events occurring in the major groove. Perhaps the inherently dynamic nature of ruthenium intercalation

from the major groove, as reflected in the fast exchange and multiple binding conformations revealed in NMR studies,[6] hinders the formation of well-packed crystals. Nonetheless, the crystal structures still provide invaluable insights into intercalation of Δ-Ru(bpy)$_2$dppz^{2+} when it is in the minor groove.

3.4 Conclusions

The two structures presented here, one at 1.0-Å resolution, depict in detail the versatile binding modes attainable for octahedral metal complexes bearing an intercalating ligand. Altogether, the structures showed three independent views of metalloinsertion, five of intercalation, and two of end-capping. At destabilized regions of the DNA, the metal complex binds through metalloinsertion via the minor groove, accompanied by extrusion of the mismatched bases. This binding mode was previously observed with a sterically expansive ligand, but the ruthenium-dppz structures reported here clearly demonstrate that a narrower ligand such as dppz is equally capable of recognizing mismatches by metalloinsertion, pointing to the generality of this binding mode. The smaller size of the dppz ligand also allows the ruthenium complex to bind through classical intercalation between two consecutive well-matched base pairs. Multiple intercalation geometries are displayed between the two structures. Curiously, intercalated complexes are all located in the minor groove as well, for which we hypothesize that the extensive presence of ancillary interactions is responsible; in solution, intercalation takes place in the major groove. This discrepancy notwithstanding, the two structures attest to the remarkable structural flexibility of DNA upon high-density ligand binding, illustrate the nuanced binding geometries sampled by a noncovalently bound small molecule, and highlight the dominance of metalloinsertion as the preferred binding mode to destabilized regions of DNA. We hope these newly garnered structural understandings will help guide the development of future generations of metal complexes as chemical tools and medicinal agents.

Bibliography

[1] Alan E. Friedman, Jean Claude Chambron, Jean Pierre Sauvage, Nicholas J. Turro, and Jacqueline K. Barton. A molecular light switch for DNA: $Ru(bpy)_2(dppz)^{2+}$. *Journal of the American Chemical Society*, 112(12):4960–4962, 1990.

[2] Catharina Hiort, Per Lincoln, and Bengt Norden. DNA binding of Δ- and Λ-$[Ru(phen)_2DPPZ]^{2+}$. *Journal of the American Chemical Society*, 115(9):3448–3454, 1993.

[3] Cynthia M. Dupureur and Jacqueline K. Barton. Use of selective deuteration and ^1H NMR in demonstrating major groove binding of Δ-$[Ru(phen)_2dppz]^{2+}$ to $d(GTCGAC)_2$. *Journal of the American Chemical Society*, 116(22):10286–10287, 1994.

[4] Ihtshamul Haq, Per Lincoln, Dongchul Suh, Bengt Norden, Babur Z. Chowdhry, and Jonathan B. Chaires. Interaction of Δ- and Λ-$[Ru(phen)_2DPPZ]^{2+}$ with DNA: A calorimetric and equilibrium binding study. *Journal of the American Chemical Society*, 117(17):4788–4796, 1995.

[5] Per Lincoln, Anders Broo, and Bengt Nordén. Diastereomeric DNA-binding geometries of intercalated ruthenium(II) trischelates probed by linear dichroism: $[Ru(phen)_2DPPZ]^{2+}$ and $[Ru(phen)_2BDPPZ]^{2+}$. *Journal of the American Chemical Society*, 118(11):2644–2653, 1996.

[6] Cynthia M. Dupureur and Jacqueline K. Barton. Structural studies of Λ- and Δ-$[Ru(phen)_2dppz]^{2+}$ bound to $d(GTCGAC)_2$: Characterization of enantioselective intercalation. *Inorganic Chemistry*, 36(1):33–43, 1997.

[7] James P. Hall, Kyra O'Sullivan, Abeer Naseer, Jayden A. Smith, John M. Kelly, and Christine J. Cardin. Structure determination of an intercalating ruthenium dipyridophenazine complex which kinks DNA by semiintercalation of a tetraazaphenanthrene ligand. *Proceedings of the National Academy of Sciences*, 108(43):17610–17614, 2011.

[8] Mi Hee Lim, Hang Song, Eric D. Olmon, Elizabeth E. Dervan, and Jacqueline K. Barton. Sensitivity of $Ru(bpy)_2dppz^{2+}$ luminescence to DNA defects. *Inorganic Chemistry*, 48(12):5392–5397, 2009.

[9] Lawrence A. Loeb. A mutator phenotype in cancer. *Cancer Research*, 61(8):3230–3239, 2001.

[10] Bernard S. Strauss. Frameshift mutation, microsatellites and mismatch repair. *Mutation Research/Reviews in Mutation Research*, 437(3):195–203, 1999.

[11] Nickolas Papadopoulos and Annika Lindblom. Molecular basis of HNPCC: Mutations of MMR genes. *Human Mutation*, 10(2):89–99, 1997.

[12] Päivi Peltomäki. Deficient DNA mismatch repair: A common etiologic factor for colon cancer. *Human Molecular Genetics*, 10(7):735–740, 2001.

[13] D. A. Lawes, S. SenGupta, and P. B. Boulos. The clinical importance and prognostic implications of microsatellite instability in sporadic cancer. *European Journal of Surgical Oncology (EJSO)*, 29(3):201–212, 2003.

[14] Nitai P. Bhattacharyya, Adonis Skandalis, Anil Ganesh, Joanna Groden, and Mark Meuth. Mutator phenotypes in human colorectal carcinoma cell lines. *Proceedings of the National Academy of Sciences*, 91(14):6319–6323, 1994.

[15] Iordanis I. Arzimanoglou, Fred Gilbert, and Hugh R. K. Barber. Microsatellite instability in human solid tumors. *Cancer*, 82(10):1808–1820, 1998.

[16] Valerie C. Pierre, Jens T. Kaiser, and Jacqueline K. Barton. Insights into finding a mismatch through the structure of a mispaired DNA bound by a rhodium intercalator. *Proceedings of the National Academy of Sciences*, 104(2):429–434, 2007.

[17] Christine Cordier, Valérie C. Pierre, and Jacqueline K. Barton. Insertion of a bulky rhodium complex into a DNA cytosinecytosine mismatch: An NMR solution study. *Journal of the American Chemical Society*, 129(40):12287–12295, 2007.

[18] Brian M. Zeglis, Valerie C. Pierre, and Jacqueline K. Barton. Metallo-intercalators and metallo-insertors. *Chem Commun (Camb)*, (44):4565–4579, 2007.

[19] Brian M. Zeglis, Valerie C. Pierre, Jens T. Kaiser, and Jacqueline K. Barton. A bulky rhodium complex bound to an adenosine-adenosine DNA mismatch: General architecture of the metalloinsertion binding mode. *Biochemistry*, 48:4247–4253, 2009.

[20] Edmond Amouyal, Abdulrazzak Homsi, Jean-Claude Chambron, and Jean-Pierre Sauvage. Synthesis and study of a mixed-ligand ruthenium(II) complex in its ground and excited states: bis(2,2'-bipyridine)(dipyrido[3,2-*a*:2',3'-*c*]phenazine-N^4N^5)ruthenium(II). *J. Chem. Soc., Dalton Trans.*, pages 1841–1845, 1990.

[21] J.-G. Liu, B.-H. Ye, Q.-L. Zhang, X.-H. Zou, Q.-X. Zhen, X. Tian, and L.-N. Ji. Enantiomeric ruthenium(II) complexes binding to DNA: Binding modes and enantioselectivity. *Journal of Biological Inorganic Chemistry*, 5:119–128, 2000.

[22] Wolfgang Kabsch. *XDS. Acta Crystallographica Section D*, 66(2):125–132, 2010.

[23] Collaborative Computational Project Number 4. The *ccp*4 suite: Programs for protein crystallography. *Acta Crystallographica Section D*, 50(5):760–763, 1994.

[24] George M. Sheldrick. A short history of *SHELX*. *Acta Crystallographica Section A*, 64(1):112–122, 2008.

[25] Paul Emsley and Kevin Cowtan. *Coot*: Model-building tools for molecular graphics. *Acta Crystallographica Section D*, 60:2126–2132, 2004.

[26] Paul D. Adams, Pavel V. Afonine, Gábor Bunkóczi, Vincent B. Chen, Ian W. Davis, Nathaniel Echols, Jeffrey J. Headd, Li-Wei Hung, Gary J. Kapral, Ralf W. Grosse-Kunstleve, Airlie J. McCoy, Nigel W. Moriarty, Robert Oeffner, Randy J. Read, David C. Richardson, Jane S. Richardson, Thomas C. Terwilliger, and Peter H. Zwart. *PHENIX*: A comprehensive Python-based system for macromolecular structure solution. *Acta Crystallographica Section D*, 66(2):213–221, 2010.

[27] Schrödinger, LLC. The PyMOL molecular graphics system, version 1.3r1. August 2010.

[28] G. J. Kleywegt. Use of non-crystallographic symmetry in protein structure refinement. *Acta Crystallographica Section D*, 52(4):842–857, 1996.

[29] R. Erik Holmlin, Eric D. A. Stemp, and Jacqueline K. Barton. $Ru(phen)_2dppz^{2+}$ luminescence: Dependence on DNA sequences and groove-binding agents. *Inorganic Chemistry*, 37(1):29–34, 1998.

[30] David Ambrosek, Pierre-François Loos, Xavier Assfeld, and Chantal Daniel. A theoretical study of Ru(II) polypyridyl DNA intercalators: Structure and electronic absorption spectroscopy of $[Ru(phen)_2(dppz)]^{2+}$ and $[Ru(tap)_2(dppz)]^{2+}$ complexes intercalated in guanine–cytosine base pairs. *Journal of Inorganic Biochemistry*, 104(9):893–901, 2010.

[31] Henry M. Sobell, Chun-Che Tsai, Shri C. Jain, and Steven G. Gilbert. Visualization of drug-nucleic acid interactions at atomic resolution: III. Unifying structural concepts in understanding drug-DNA interactions and their broader implications in understanding protein-DNA interactions. *Journal of Molecular Biology*, 114(3):333–365, 1977.

[32] Clara L. Kielkopf, Kathryn E. Erkkila, Brian P. Hudson, Jacqueline K. Barton, and Douglas C. Rees. Structure of a photoactive rhodium complex intercalated into DNA. *Nat Struct Mol Biol*, 7(2):117–121, 2000.

[33] Adrienne Adams, J. Mitchell Guss, William A. Denny, and Laurence P. G. Wakelin. Crystal structure of 9-amino-N-[2-(4-morpholinyl)ethyl]-4-acridinecarboxamide bound to $d(CGTACG)_2$: Implications for structure–activity relationships of acridinecarboxamide topoisomerase poisons. *Nucleic Acids Research*, 30(3):719–725, 2002.

[34] Xiang-Jun Lu and Wilma K. Olson. 3DNA: A software package for the analysis, rebuilding and visualization of three-dimensional nucleic acid structures. *Nucleic Acids Research*, 31(17):5108–5121, 2003.

[35] D. M. Crothers. Calculation of binding isotherms for heterogeneous polymers. *Biopolymers*, 6:575–584, 1968.

[36] P. J. Bond, R. Langridge, K. W. Jennette, and S. J. Lippard. X-ray fiber diffraction evidence for neighbor exclusion binding of a platinum metallointercalation reagent to DNA. *Proceedings of the National Academy of Sciences*, 72(12):4825–4829, 1975.

[37] Donald Voet. Intercalation complexes of DNA. *Nature*, 269(5626):285–286, 1977.

[38] Jeffrey W. Nelson and Ignacio Tinoco. Interacalation of ethidium ion into DNA and RNA oligonucleotides. *Biopolymers*, 23(2):213–233, 1984.

[39] Jacqueline K. Barton, Avis Danishefsky, and Jonathan Goldberg. Tris(phenanthroline)ruthenium(II): stereoselectivity in binding to DNA. *Journal of the American Chemical Society*, 106(7):2172–2176, 1984.

[40] David S. Sigman and Chi-hong B Chen. Chemical nucleases: New reagents in molecular biology. *Annual Review of Biochemistry*, 59(1):207–236, 1990.

[41] Mi Hee Lim, Irvin H. Lau, and Jacqueline K. Barton. DNA strand cleavage near a CC mismatch directed by a metalloinsertor. *Inorganic Chemistry*, 46(23):9528–9530, 2007.

Chapter 4

Ruthenium-Dye Conjugates as Luminescent Reporters of DNA Mismatches

4.1 Introduction

Deficiencies in mismatch repair (MMR) subject cells to a higher rate of mutation and render them more susceptible to the development of cancers (for details, see Chapter 1). Thus, early detection of DNA mismatch accumulation will greatly aid in the diagnosis and prognosis of MMR-deficient cancers. To this end, molecular probes that can detect DNA base mismatches directly in biological samples will be a powerful tool. An attractive choice for probing such biological systems is luminescent small molecules that specifically recognize NDA mismatches, as they offer a rapid and sensitive means of detection.

The "DNA light switch" molecule $Ru(bpy)_2dppz^{2+}$ was recently found to show enhanced luminescence at DNA mismatches (Chapter 2).[1] However, $Ru(bpy)_2dppz^{2+}$ by itself is not an effective reporter of mismatches in biological samples, even with iodide quenching, due to its strong binding affinity to matched DNA and the low frequency of mismatches in cells ($\sim$1000 in the entire genome[2]). Thus, in order for $Ru(L)(L')dppz^{2+}$ complexes to become more sensitive and specific probes of DNA mismatches, we employed a tethering strategy to selectively register the signal from ruthenium bound to mismatched DNA through fluorescence resonance energy transfer (FRET). As matched-DNA binding occurs from the major groove and mismatch binding occurs from the minor groove, we envisioned a design in which a RET acceptor, which emits only when bound to DNA from the minor groove, is tethered to ruthenium, so that emission from the RET acceptor is observed only when ruthenium is also in the minor groove, i.e., in the presence of a mismatch (Figure 4.1). The ideal RET acceptor should (i) be a light switch for DNA, (ii) binds only from the minor groove, and (iii) has good spectral overlap with $Ru(L)(L')dppz^{2+}$ (i.e., absorption close to 620 nm).

Red-absorbing benzothiazole-quinolinium cyanine dyes, which bind DNA and exhibit substantially enhanced fluorescence in the bound form, were considered a promising FRET acceptor in this conjugate design. In particular, TO-PRO-3, a trimethine thiazole orange (TO) derivative with a positively charged side chain (Figure 2.3, Chapter 2),[3] has been shown to effect RET with $Ru(bpy)_2dppz^{2+}$ efficiently when added simultaneously to DNA.[4] A ruthenium-TO-3 (herein abbreviated Ru-TO) conjugate design has two advantages over a ruthenium-only light switch. First, TO-3 has a much higher quantum yield compared to ruthenium, thus the resultant RET signal will be several-fold stronger than the correspond-

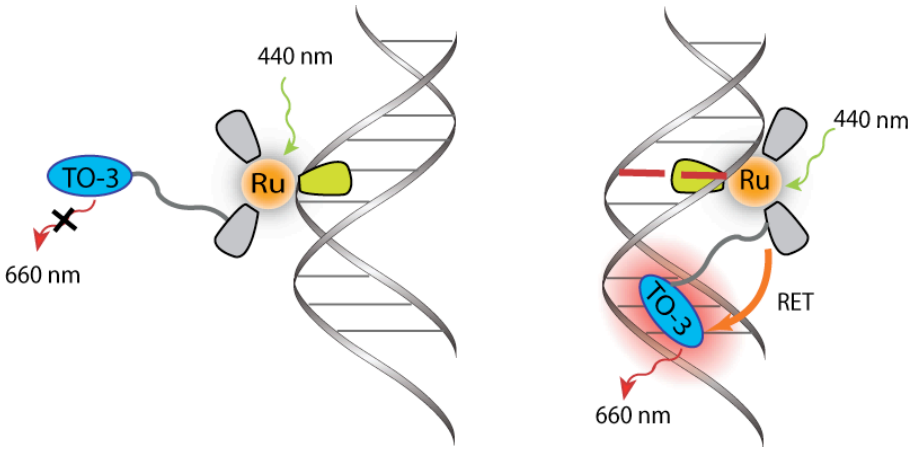

Figure 4.1. Illustration of Ru-TO-3 conjugate binding to well-matched (left) and mismatched (right) DNA. TO-3 emission through RET is detectable only in the presence of a mismatch (red) when both the ruthenium and TO-3 are bound in the minor groove.

ing ruthenium signal without TO-3. Second, ruthenium fluorescence has a long lifetime, which will be translated to a longer lifetime for TO-3 emission through RET. A longer lifetime allows better distinction of probe signal from cellular background fluorescence.[5] Both stronger emission intensity and longer lifetimes have been observed in an untethered system of $Ru(bpy)_2dppz^{2+}$ and TO-PRO-3 simultaneously bound to DNA,[4] and we expect these emission features to be preserved in our conjugated system. In this chapter, we report the synthesis and luminescence properties of four conjugates (**1**, **2**, **3**, **4**, Figure 4.2) in the presence of mismatch-containing oligonucleotides.

4.2 Experimental protocols

4.2.1 Materials

Commercially available chemicals were used as received from Sigma-Aldrich. DNA was synthesized and purified as described in Chapter 1. Amine-modified bpy ligands (**9** and **10**) were laboratory stocks synthesized from established protocols.[6,7]

4.2.2 Synthesis of dye, metal complex, and conjugates

The following compounds were prepared based on literature procedures: DPA-$(CH_2)_6$-COOH,[6] $Ru(L)(phen)(dppz)^{2+}$ (L = $(CO)_2$,[8] HDPA or DPA-$(CH_2)_6$-COOH), TO-COOH **5**,[9] and ethidium-COOH **11**[10]. Amide coupling with HBTU/DIEA was used to link the

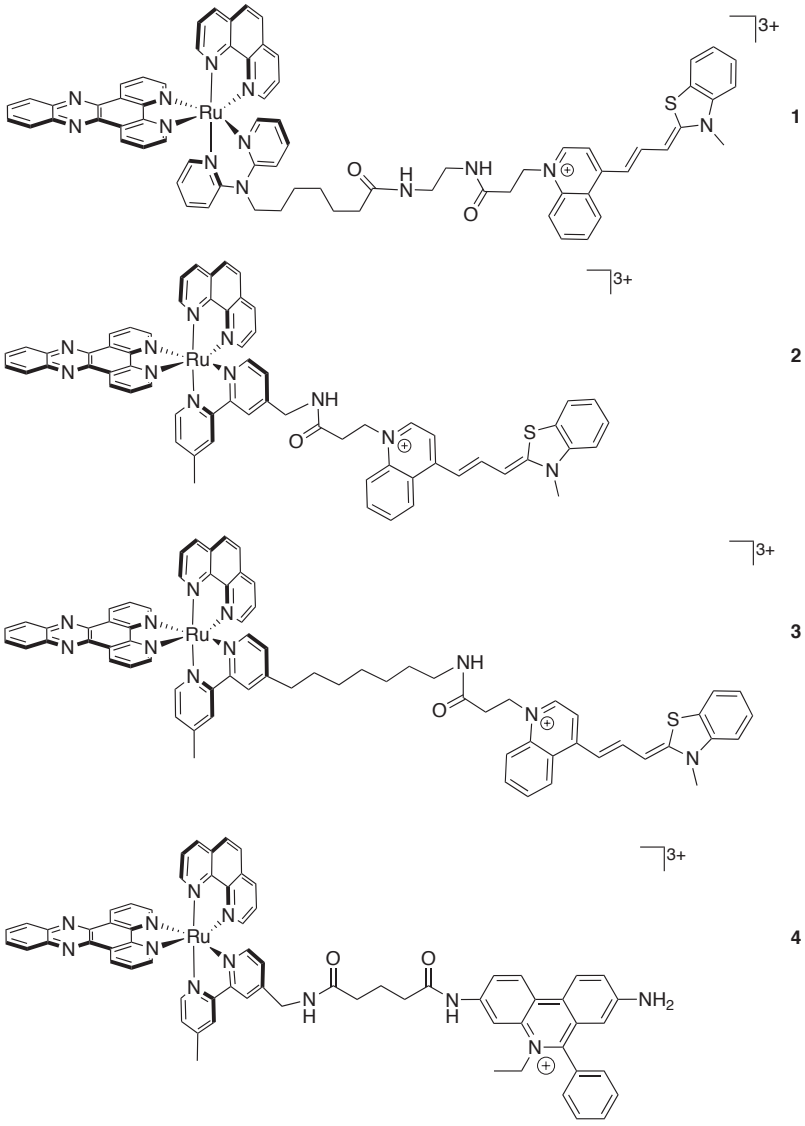

Figure 4.2. Chemical structures of Ru-dye conjugates: Ru-10-TO (**1**), Ru-1-TO (**2**), Ru-7-TO (**3**), Ru-Eth (**4**).

components in all conjugate syntheses.[11,12] Briefly, HBTU was added to the carboxylic acid-terminated moiety and DIEA was added to the amine-terminated moiety, both in a solution of DMF. The two parts were then mixed and the coupling reaction was allowed to proceed overnight at room temperature under a dry Ar atmosphere. The compounds **5**, **9**, **10** and **12** were recrystallized by vapor diffusion of diethyl ether into a MeOH solution. Purity of the final conjugates was checked by analytical HPLC. Characterization of the compounds are reported below.

TO-COOH **5**. ^{1}H-NMR (300 MHz, DMSO) δ 8.51 (d, J = 7.2 Hz, 1H), 8.46 (d, J = 8.6 Hz, 1H), 8.07 (dt, 2H), 7.97–7.89 (t, 1H), 7.83 (m, 2H), 7.73–7.63 (t, 1H), 7.52 (d, 1H), 7.45 (t, 1H), 7.26 (t, 1H), 7.09 (d, J = 13.1 Hz, 1H), 6.41 (d, J = 11.9 Hz, 1H), 4.68 (t, J = 7.1 Hz, 2H), 3.68 (s, 3H), 2.41 (t, 2H). ESI-MS: calc. 389.13, obs. 389.2 (M^+).

Ru(phen)(HDPA)dppz^{2+} **6**. ^{1}H-NMR (300 MHz, CD_3CN) δ 11.64 (s, 1H), 9.77 (dd, J = 8.2, 1.3 Hz, 1H), 9.45 (dd, J = 8.2, 1.3 Hz, 1H), 9.17–9.05 (m, 2H), 8.77 (d, J = 7.1 Hz, 1H), 8.53–8.41 (m, 3H), 8.30 (d, J = 8.9 Hz, 1H), 8.20–8.12 (m, 4H), 8.07–8.01 (m, 1H), 7.91 (dd, J = 5.3, 1.2 Hz, 1H), 7.79 (dd, J = 5.4, 1.3 Hz, 1H), 7.69–7.52 (m, 5H), 7.46 (dd, J = 8.2, 5.3 Hz, 1H), 7.30 (d, J = 5.8 Hz, 1H), 7.20 (d, J = 5.7 Hz, 1H), 6.65–6.50 (m, 2H). ESI-MS: calc. 735.14, obs. 734.2 $(M\text{-}H)^+$, 367.6 (M^{2+}). UV-vis (H_2O): 357 nm (32,000 $M^{-1}cm^{-1}$), 374 nm (36,000 $M^{-1}cm^{-1}$), 410 nm (23,000 $M^{-1}cm^{-1}$).

Ru(phen)(DPA-(CH$_2$)$_6$-COOH)dppz^{2+} **7**. ESI-MS: calc. 863.23, obs. 431.7 (M^{2+}). UV-vis (H_2O): 357 nm (32,000 $M^{-1}cm^{-1}$), 374 nm (35,000 $M^{-1}cm^{-1}$), 410 nm (24,000 $M^{-1}cm^{-1}$).

Ru(phen)(DPA-(CH$_2$)$_6$-CONH-(CH$_2$)$_2$-NH$_2$)dppz^{2+} **8**. ESI-MS: calc. 905.29, obs. 452.7 (M^{2+}).

Ru-10-TO **1**. ESI-MS: calc. 1276.41, obs. 425.8 (M^{3+}).

Bpy-1-TO **9**. ^{1}H-NMR (500 MHz, CD_2Cl_2) δ 8.59 (d, J = 4.9 Hz, 1H), 8.56–8.47 (m, 2H), 8.38 (d, J = 7.4 Hz, 2H), 8.29 (d, J = 8.1 Hz, 2H), 7.98–7.85 (m, 3H), 7.69–7.59 (m, 1H), 7.53–7.46 (m, 1H), 7.39–7.27 (m, 5H), 6.87 (d, J = 13.4 Hz, 1H), 6.25 (d, J = 12.3 Hz, 1H), 4.86 (t, J = 6.8 Hz, 2H), 4.52 (d, J = 6.0 Hz, 2H), 3.71 (s, 3H), 3.15 (t, J = 6.8 Hz, 2H), 2.50 (s, 3H). ESI-MS: calc. 570.23, obs. 570.1 (M^+).

Ru-1-TO **2**. ^{1}H-NMR (500 MHz, CD_3CN) δ 9.63 (d, J = 8.3 Hz, 1H), 9.51 (d, J = 8.3 Hz, 1H), 8.83 (d, J = 19.5 Hz, 2H), 8.71 (d, J = 7.7 Hz, 1H), 8.58 (d, J = 8.0 Hz, 1H), 8.50 (d, J = 8.5 Hz, 1H), 8.44 (d, J = 7.8 Hz, 1H), 8.40 (d, J = 8.6 Hz, 1H), 8.37 (d, J = 7.3

Hz, 1H), 8.28 (d, J = 10.5 Hz, 2H), 8.26–8.22 (m, 3H), 8.21–8.17 (m, 3H), 8.01 (m, 3H), 7.96 (d, J = 8.0 Hz, 1H), 7.94–7.90 (m, 1H), 7.90–7.84 (m, 1H), 7.82 (d, J = 5.9 Hz, 1H), 7.76–7.67 (m, 3H), 7.62–7.55 (m, 2H), 7.50 (d, J = 6.2 Hz, 1H), 7.43 (d, J = 7.4 Hz, 1H), 7.32 (d, J = 6.2 Hz, 1H), 7.27 (d, J = 7.4 Hz, 1H), 7.22 (d, J = 7.5 Hz, 1H), 7.16–7.09 (m, 2H), 6.95-6.90 (m, 2H), 6.22 (d, J = 12.3 Hz, 1H), 4.86 (t, J = 6.2 Hz, 2H), 4.54–4.46 (m, 2H), 3.54 (s, 3H), 2.62 (s, 3H). ESI-MS: calc. 1134.30, obs. 378.3 (M^{3+}), 566.3 $(M\text{-}H)^{2+}$, 623.0 $(M+TFA)^{2+}$.

Bpy-7-TO **10**. ^{1}H-NMR (500 MHz, CD_2Cl_2) δ 8.63–8.48 (m, 2H), 8.46–8.30 (m, 3H), 8.15 (d, 1H), 8.01 (t, 1H), 7.92–7.83 (m, 2H), 7.66-7.60 (m, 2H), 7.51–7.46 (m, 1H), 7.42 (d, 1H), 7.36–7.27 (m, 4H), 6.92 (d, J = 13.4 Hz, 1H), 6.25 (d, J = 12.3 Hz, 1H), 4.81 (t, J = 6.7 Hz, 2H), 3.68 (s, 3H), 3.18 (dd, J = 12.7, 6.9 Hz, 2H), 2.88 (t, J = 6.3 Hz, 2H), 2.79–2.63 (m, 2H), 2.51 (s, 3H), 1.68 (m, 2H), 1.46 (m, 2H), 1.34 (m, 4H), 1.27 (m, 2H). ESI-MS: calc. 654.33, obs. 654.2 (M^+), 327.8 $(M+H)^{2+}$.

Ru-7-TO **3**. ^{1}H-NMR (500 MHz, CD_3CN) δ 9.67 (d, J = 8.3 Hz, 1H), 9.58 (d, J = 8.3 Hz, 1H), 8.69 (d, J = 8.4 Hz, 1H), 8.59 (d, J = 8.2 Hz, 1H), 8.50 (m, 4H), 8.37 (d, J = 8.9 Hz, 1H), 8.28 (m, 3H), 8.23 (d, J = 6.4 Hz, 1H), 8.20–8.16 (m, 2H), 8.09 (d, J = 6.6 Hz, 2H), 7.98 (m, 2H), 7.92 (m, 2H), 7.84 (m, 1H), 7.70 (m, 4H), 7.62 (m, 1H), 7.50 (m, 2H), 7.46 (d, J = 7.2 Hz, 1H), 7.38 (d, J = 7.9 Hz, 1H), 7.30 (t, J = 7.5 Hz,1H), 7.22 (d, J = 5.6 Hz, 1H), 7.14–7.10 (d, J = 5.6 Hz, 1H), 6.94 (d, J = 13.5 Hz, 1H), 6.75–6.70 (m, 1H), 6.30 (d, J = 12.1 Hz, 1H), 4.73 (t, J = 6.5 Hz, 2H), 4.49 (s, 3H), 3.63 (s, 2H), 3.14–3.06 (m, 2H), 2.79 (m, 2H), 2.56 (s, 3H), 1.68 (m, 2H), 1.31 (m, 6H), 1.24–1.18 (m, 2H). ESI-MS: calc. 1218.39, obs. 406.3 (M^{3+}), 608.8 $(M\text{-}H)^{2+}$, 665.0 $(M+TFA)^{2+}$.

Ethidium-COOH **11**. ^{1}H-NMR (300 MHz, CD_3OD) δ 8.73 (d, J = 8.9 Hz, 2H), 8.26 (dd, J = 9.2, 2.3 Hz, 1H), 7.85–7.72 (m, 4H), 7.65–7.62 (m, 2H), 7.43–7.40 (m, 2H), 4.71–4.64 (m, 2H), 2.39–2.27 (m, 2H), 2.18 (t, J = 7.1 Hz, 2H), 1.93–1.83 (m, 2H), 1.53 (t, J = 7.2 Hz, 3H). ESI-MS: calc. 428.20, obs. 428.2 (M^+).

Bpy-ethidium **12**. ^{1}H-NMR (300 MHz, CD_3OD) δ 8.74 (d, J = 9.3 Hz, 2H), 8.55 (d, J = 5.2 Hz, 1H), 8.43 (d, J = 4.9 Hz, 1H), 8.25 (dd, J = 9.1, 2.4 Hz, 1H), 8.18 (d, J = 14.8 Hz, 2H), 7.77 (m, 4H), 7.63 (m, 2H), 7.42 (m, 2H), 7.34 (d, J = 5.2 Hz, 1H), 7.26 (m, 1H), 4.67 (m, 2H), 4.47 (s, 2H), 2.44 (s, 3H), 2.38 (dd, J = 14.2, 7.2 Hz, 4H), 2.00 (m, 2H), 1.53 (t, J = 7.1 Hz, 3H). ESI-MS: calc. 609.30, obs. 609.3 (M^+).

Ru-Eth **4**. ESI-MS: calc. 1173.36, obs. 391.1 (M^{3+}).

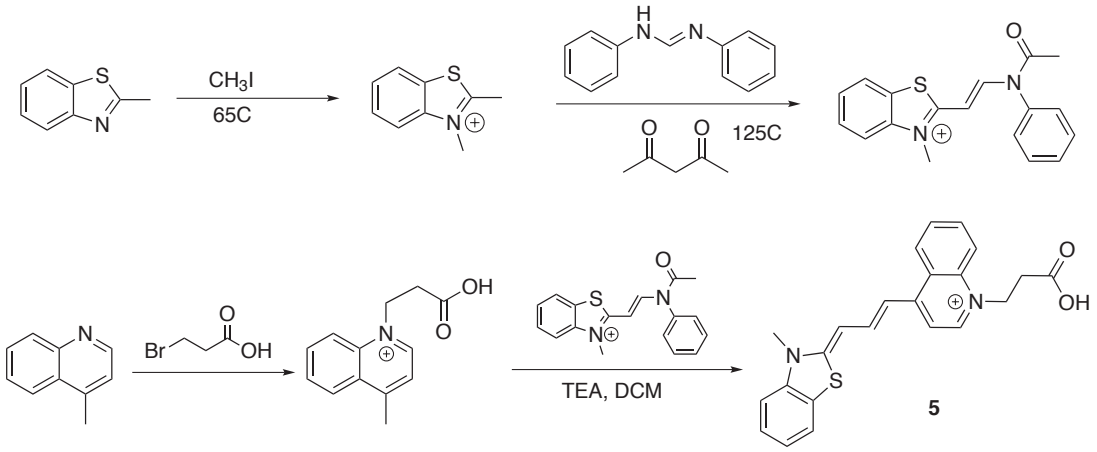

Figure 4.3. Scheme showing the synthesis of TO-COOH **5**.[9]

4.2.3 Steady state fluorescence

Luminescence spectra were recorded on an ISS-K2 spectrophotometer at ambient temperature in aerated solutions. Standard deviations in integrated luminescence intensity were calculated from three samples. Concentrations of Ru-TO conjugates were estimated using ϵ_{630}=102,000 $M^{-1}cm^{-1}$.[9] All DNA concentrations are reported as the duplex concentration. Raman scattering of water at 520 nm (λ_{ex} = 440 nm) is shown in all emission spectra.

4.3 Results and discussion

4.3.1 Ru-TO-3 conjugates

The FRET acceptor TO-3 was modified with a carboxylic acid group[9] (Figure 4.3) to facilitate subsequent coupling with an amine-terminated linker. The synthesis of trisheteroleptic Ru(L)(L')dppz^{2+} complexes is outlined in Figure 4.4.[8] The DPA-derivative was used in the synthesis of conjugate **1** (Ru-10-TO, Figure 4.5). However, it was difficult to obtain shorter linkers derivatized from HDPA. In particular, DPA-CH_2-COOH coordinates poorly to ruthenium and tends to dissociate from the metal center. Thus, in the synthesis of Ru-TO conjugates with shorter linkers (Ru-1-TO **2** and Ru-7-TO **3**, Figure 4.6), a modified bpy was used as the ligand bearing the linker.

Parent ruthenium complexes Ru(phen)(HDPA)dppz^{2+} **6** and Ru(phen)(DPA-$(CH_2)_6$-COOH)dppz^{2+} **7** behave as light switches for DNA (Figure 4.7), as expected. Their luminescence in acetonitrile (λ_{ex} = 440 nm) is approximately 25% of Ru(bpy)$_2$dppz^{2+}, with

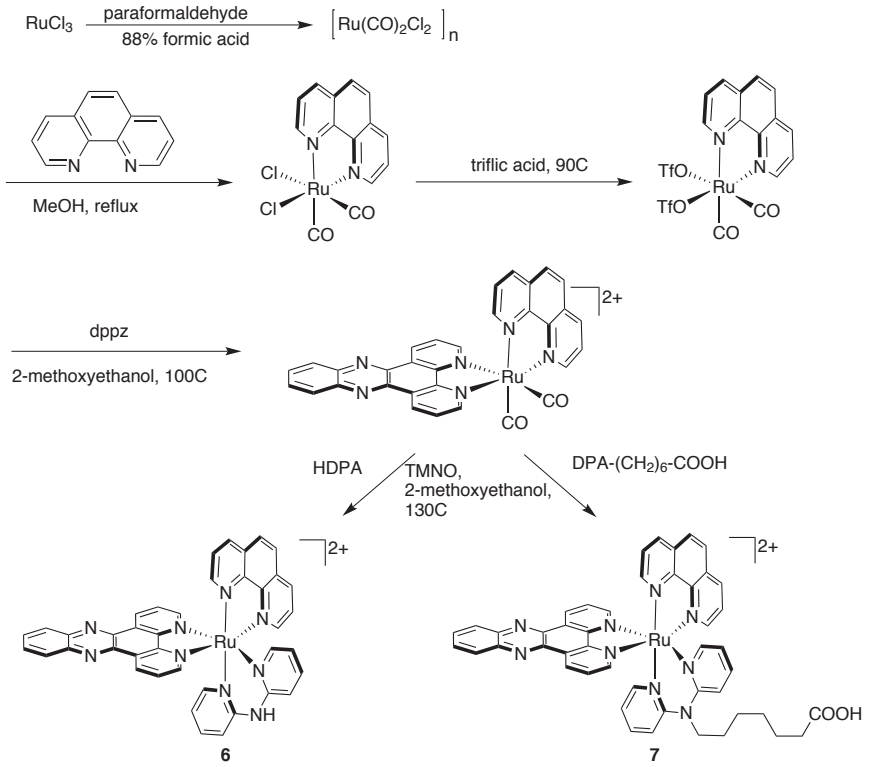

Figure 4.4. Scheme showing the synthesis of trisheteroleptic Ru(L)(L')dppz^{2+}complexes **6** and **7**.[8]

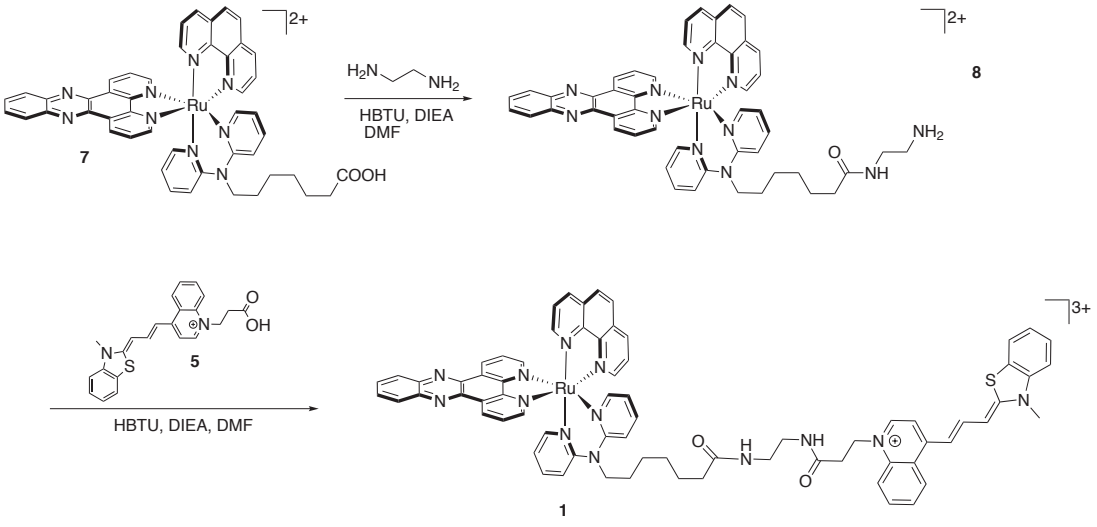

Figure 4.5. Scheme showing the synthesis of conjugate **1** (Ru-10-TO).

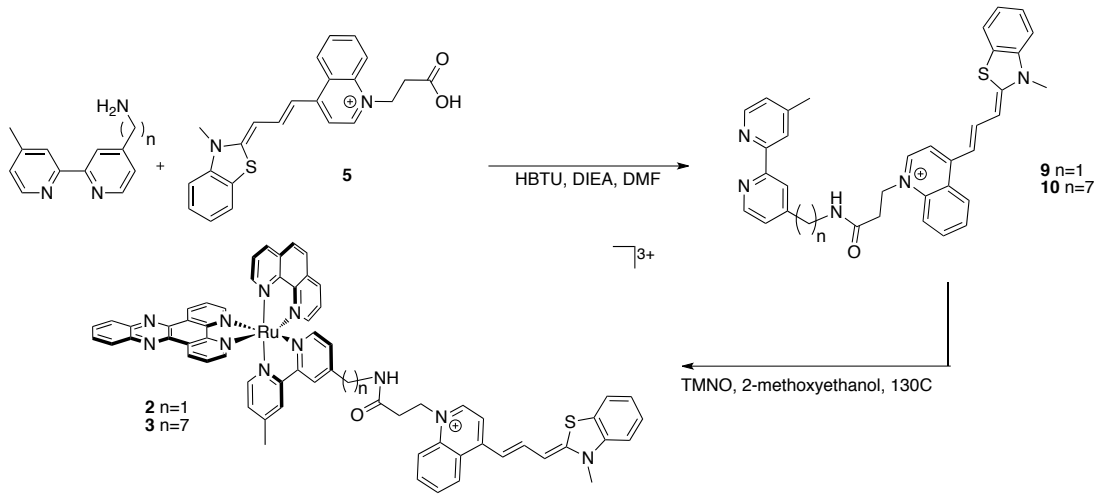

Figure 4.6. Scheme showing the synthesis of conjugates **2** (Ru-1-TO) and **3** (Ru-7-TO).

λ_{max} red-shifted to 650 nm (Figure 4.8). They show moderate luminescence enhancement when bound to mismatched and abasic DNA (Figure 4.7), with **7** apparently binding tighter to mismatches and abasic sites. However, the level of discrimination achieved with **7** was not enough to give any differential luminescence at a matched:mismatched base pair ratio of 2726:1 (Figure 4.9). Thus, a larger innate luminescence differential between ruthenium bound to matched and mismatched DNA is necessary to enable discrimination at higher matched:mismatched ratios relevant to biological samples. The conjugate design, as explained before, was one potential way to achieve such differential.

The first Ru-TO-3 conjugate we synthesized was Ru-10-TO **1**. As amine-terminated DPA derivates did not coordinate to Ru (or Rh), a carboxylic acid-terminated DPA was used as the linker-bearing ligand. The trisheteroleptic Ru complex **7** was then reacted with ethylene diamine to generate an amine-terminated Ru moiety **8**, which was coupled to a carboxylic acid-functionalized TO-3 (TO-COOH **5**) in the final step (Figure 4.5). The entire linker region consists of 14 atoms and, if fully extended, spans 18.8 Å between the amino nitrogen on DPA and the quinolinium nitrogen on the TO-3. The conjugate emits extremely weakly in acetonitrile, indicating that FRET serves to quench Ru luminescence in the absence of DNA. This is consistent with the notion that TO-3 only emits when bound in a rigid form to DNA.[13] Upon excitation at 440 nm in the presence of DNA, the conjugate emission shows a characteristic profile of TO-3 fluorescence, and the resulting emission intensity is much higher than the parent Ru complex at the same concentration

5' – GAC CAG CTT ATC ACC CCT AGA TAA GCG – 3'
Matched: 3' – CTG GTC GAA TAG TGG GGA TCT ATT CGC – 5'
Mismatched: 3' – CTG GTC GAA TAG TCG GGA TCT ATT CGC – 5'
Abasic: 3' – CTG GTC GAA TAG TRG GGA TCT ATT CGC – 5'

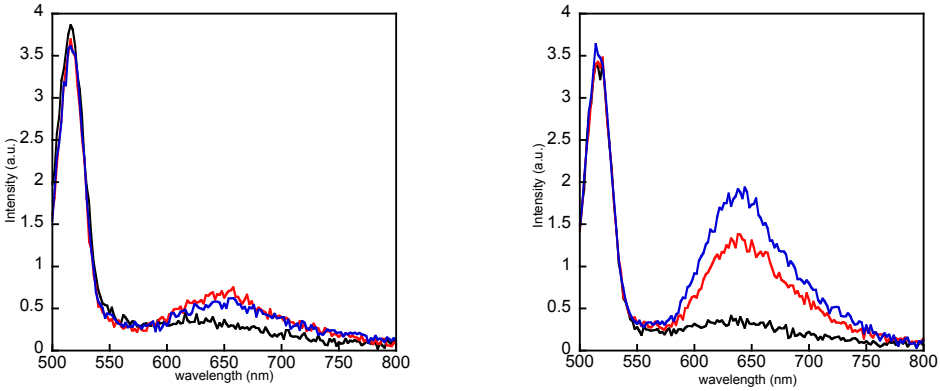

Figure 4.7. Top: DNA duplexes used for all fluorescence measurements. Bottom: emission spectra of Ru(phen)(HDPA)dppz^{2+} **6** (left) and Ru(phen)(DPA-$(CH_2)_6$-COOH)dppz^{2+} **7** (right) in the presence of matched (black), mismatched (red) and abasic (blue) DNA. Conditions are 100 nM Ru complexes, 100 nM duplex in 5 mM Tris, 50 mM NaCl, pH 7.5, λ_{ex} = 440 nm.

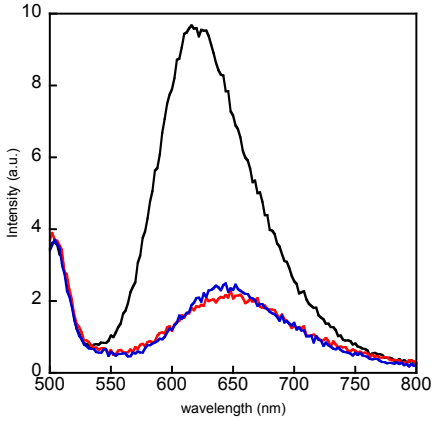

Figure 4.8. Emission spectra of Ru(bpy)$_2$dppz^{2+} (black), Ru(phen)(HDPA)dppz^{2+} **6** (red) and Ru(phen)(DPA-$(CH_2)_6$-COOH)dppz^{2+} **7** (blue) in acetonitrile. λ_{ex} = 440 nm. [Ru complex] = 100 nM.

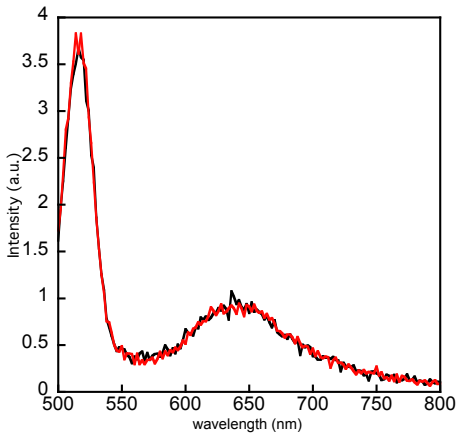

Figure 4.9. Emission spectra of Ru(phen)(DPA-$(CH_2)_6$-COOH)dppz^{2+} **7** (100 nM) in well-matched (M) DNA duplexes only (black, [M] = 1 μM), and a mixture of matched and mismatched (MM) duplexes (red, [M] = 1 μM, [MM] = 10 nM). Conditions are 5 mM Tris, 50 mM NaCl, pH 7.5, λ_{ex} = 440 nm.

(Figure 4.10). In fact, 10 nM of conjugate produces similar levels of luminescence signal to 100 nM Ru complex, demonstrating efficient FRET between Ru and TO-3 as intended. However, this conjugate does not show any luminescence differential between matched and mismatched DNA. We initially suspected that the long linker might allow simultaneously binding of Ru and TO-3 in both grooves, which would lead to signal magnification regardless of the presence of a mismatch.

To correct for the long linker, we subsequently prepared conjugate Ru-1-TO **2**, which bears a 5-atom linker. With this short linker, again no luminescence differential was detected between matched and mismatched DNA when the conjugate is excited at 440 nm (Figure 4.11). Upon excitation at 590 nm, which probes only the luminescence from TO-3 and not from RET, emission intensity was stronger for TO-3 in the presence of fully matched DNA and weaker in the presence of mismatched DNA, indicating that FRET efficiencies are higher in the presence of DNA defects.

The linker in **2** is so short that it is not expected to allow binding of the conjugate in both grooves simultaneously, thus TO-3 must be able to bind in the major groove as well. Given the relative binding affinities of Ru and cyanine dyes to DNA (10^6-10^7 M^{-1} versus 10^4-10^5 M^{-1}),[14,15] we expect the binding preference of ruthenium to dominate. The realiza-

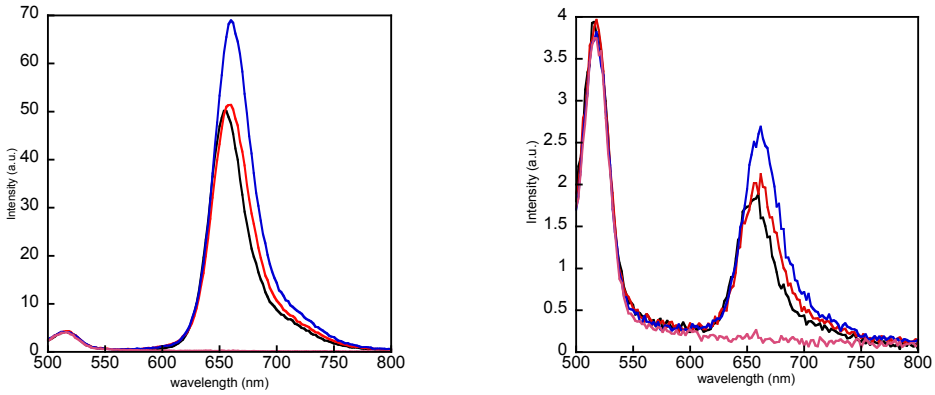

Figure 4.10. Emission spectra of Ru-10-TO **1** in the presence of matched (black), mismatched (red) and abasic (blue) DNA (left: [Ru-10-TO] = 100 nM, [DNA] = 200 nM; right: [Ru-10-TO] = 10 nM, [DNA] = 100 nM). Conditions are 5 mM Tris, 50 mM NaCl, pH 7.5, λ_{ex} = 440 nm. Pink traces are luminescence spectra without DNA.

tion that TO-3 binds in the major groove prompted us to carry out quenching experiments to determine the groove preference of TO-3 binding to DNA in conjugate **1**. Quenching **1** with $Cu(phen)_2^{2+}$, a minor groove binder, shows that the conjugate is more susceptible to quenching in the presence of DNA defects, although quenching was seen with matched duplexes as well. In other words, TO-3 is indeed in the minor groove with the ruthenium when DNA defects are present, but it still binds alongside ruthenium in the major groove in the absence of DNA defects. Alternatively, in light of the minor-groove intercalation revealed in the crystal structures of $Ru(bpy)_2dppz^{2+}$ bound to DNA (Chapter 3), it is possible that the ruthenium complex, now tethered to TO-3, binds to well-matched DNA also in the minor groove. These multiple binding modes significantly complicate the behavior of the conjugates, giving rise to enhanced luminescence with both well-matched and defective DNA.

Finally, the conjugate with an intermediate linker length, Ru-7-TO **3**, restored the luminescence differential between matched and mismatched DNA (Figure 4.11). At regular ionic strength (50 mM NaCl), the luminescence differential (∼1.8-fold) is slightly higher than that shown by $Ru(bpy)_2dppz^{2+}$ (∼1.5-fold); at high ionic strength (500 mM NaCl), the absolute luminescence intensity decreases, but the differential is increased to 3-fold between mismatched and matched DNA (versus 2.3-fold with $Ru(bpy)_2dppz^{2+}$) (Figure

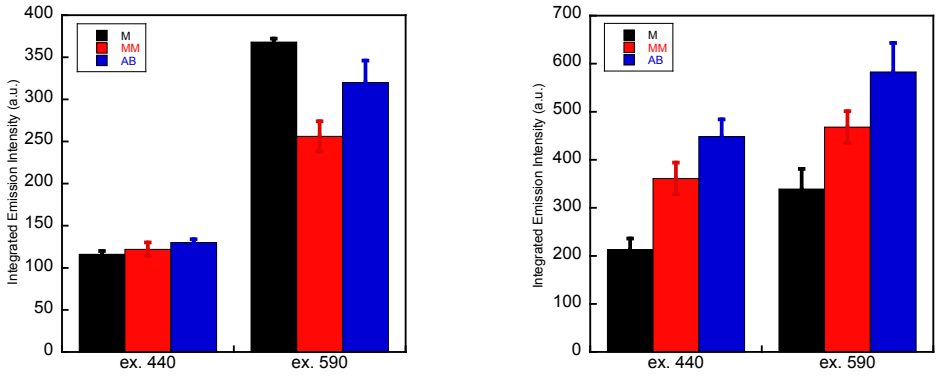

Figure 4.11. Integrated emission intensity of Ru-1-TO **2** (left) and Ru-7-TO **3** (right). Conditions are [conjugate] = 50 nM, [DNA] = 100 nM, 5 mM Tris, 50 mM NaCl, pH 7.5. For λ_{ex} = 440 nm, emission from 560 to 800 nm is integrated. For λ_{ex} = 590 nm, emission from 610 to 800 nm is integrated. Error bars are standard deviation of measurements from three samples.

4.12). The fact that increasing ionic strength improves the luminescence differential (at both 440 nm and 590 nm excitation) suggests that there is a slight preference for TO-3 to bind from the minor groove. High ionic strength leads to dissociation of loose binders from DNA, leaving behind tight binders. At high ionic strength, TO-3 bound to well-matched DNA appears to dissociate more readily than that bound to defective DNA. As a result, the relative amount of conjugate bound to mismatched DNA over matched DNA increases. Again, FRET efficiencies are higher in the presence of DNA defects. Excitation scans of the conjugate shows a strong absorption band at 640 nm, which is indicative of intercalated TO-3.[16] In fact, this absorption band was present in all three Ru-TO-3 conjugates. These observations, together with the differential quenching by $Cu(phen)_2^{2+}$, suggest that TO-3 can bind DNA in both grooves through a mostly intercalative mode, rather than the minor-groove binding mode we initially thought it might prefer. Overall, the three conjugates improved the ruthenium luminescence intensity through FRET, and **3** is a slightly better luminescence reporter of DNA defects than the parent $Ru(bpy)_2dppz^{2+}$ complex.

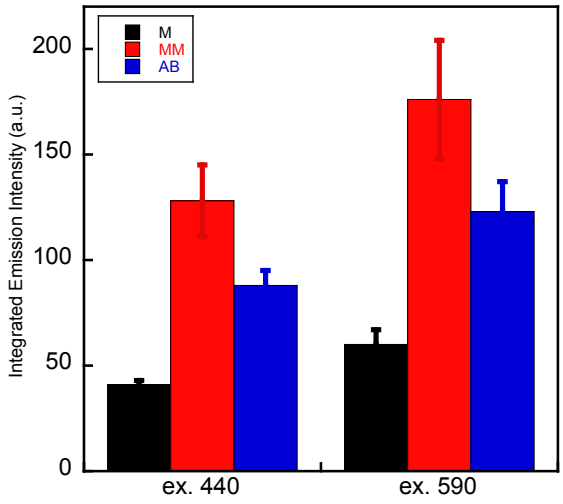

Figure 4.12. Integrated emission intensity of Ru-7-TO **3** (50 nM) at high ionic strength. Conditions are [DNA] = 100 nM, 5 mM Tris, 500 mM NaCl, pH 7.5. For λ_{ex} = 440 nm, emission from 560 to 800 nm is integrated. For λ_{ex} = 590 nm, emission from 610 to 800 nm is integrated. Error bars are standard deviation of measurements from three samples.

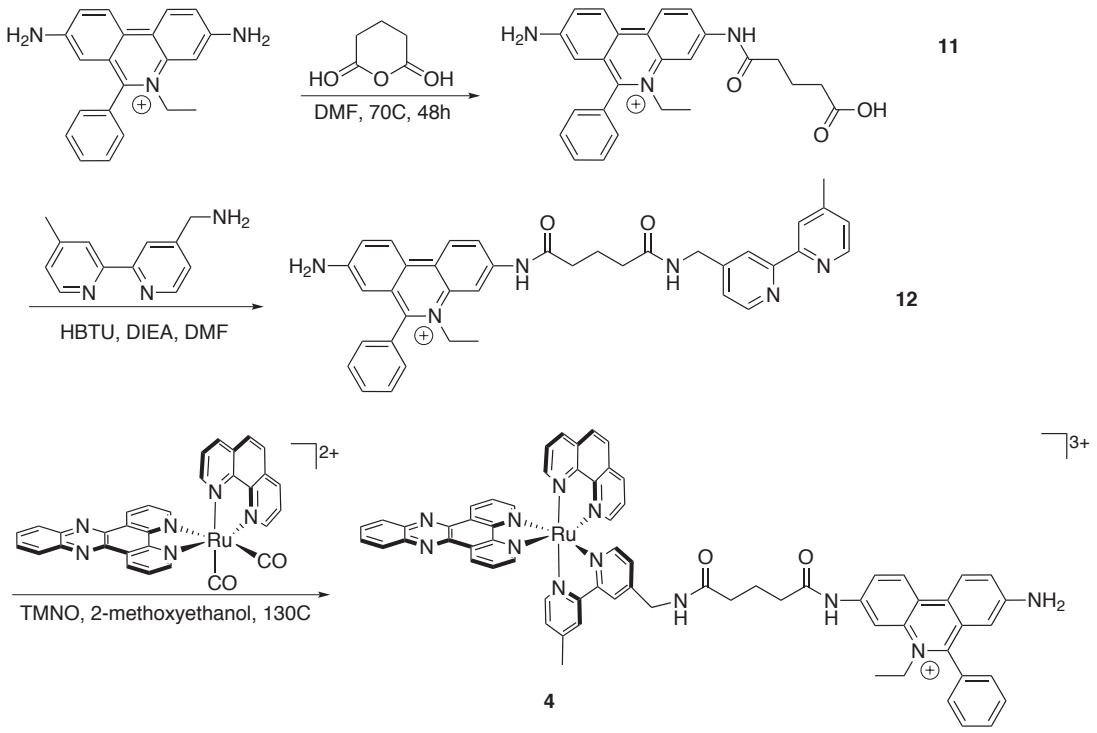

Figure 4.13. Scheme showing the synthesis of conjugate **4** (Ru-Eth).

4.3.2 Ru-Eth conjugate

The choice of ethidium as the FRET acceptor was inspired by a recent paper reporting FRET between phenanthridine and $Ru(bpy)_2phen^{2+}$.[17] Here, instead of following the reported modification scheme, ethidium was tethered at a different position to simplify the synthesis. Moreover, instead of tethering from the alkyl group, ethidium was modified at the 3-amino group to bear a carboxylic acid,[10] which was then tethered to an amine-terminated Ru (Figure 4.13). The modified ethidium (ethidium-COOH or N-glycyl Et, **11**) has a UV-vis spectrum very similar to ethidium, except that the absorption band at 485 nm is blueshifted to 450 nm (Figure 4.14).

Upon excitation of the conjugate at 440 nm (λ_{max} for Ru), the emission profile resembles mostly that of the parent Ru complex (Figure 4.15). Mismatch discrimination is observed at a similar level to Ru only. Upon excitation at 512 nm, which should mostly probe ethidium luminescence, very weak emission is observed, which is, at first, unexpected, given the high quantum yield of the organic fluorophore. Clearly, FRET did not occur for this conjugate.

A careful examination of the deviation of our conjugate from the reported system (the Turro system) reveals three critical differences that may account for the lack of FRET in

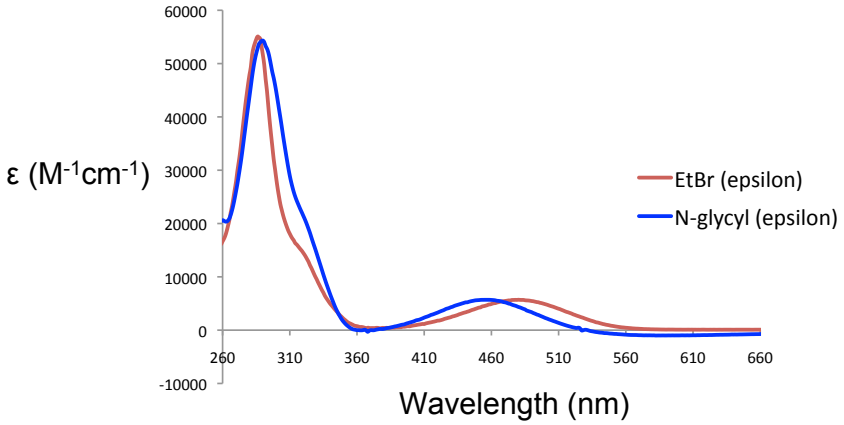

Figure 4.14. UV-vis spectra of ethidium bromide (blue) and ethidium-COOH **11**.

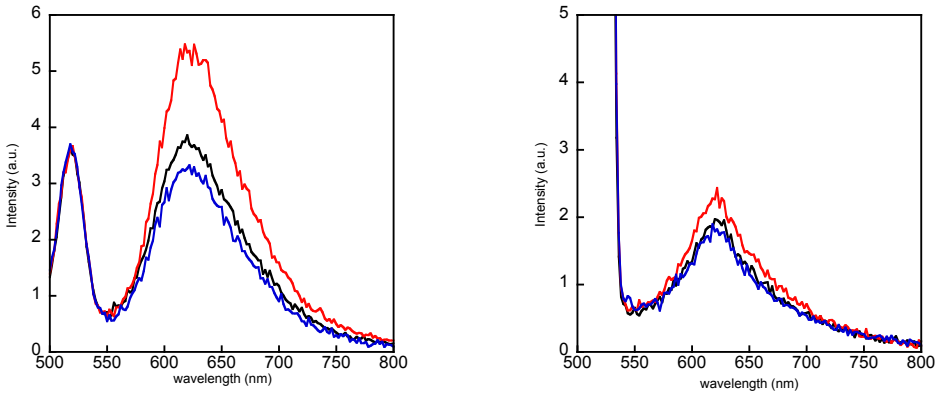

Figure 4.15. Emission spectra of Ru-Eth **4** (100 nM) in the presence of matched (black), mismatched (red) and abasic (blue) DNA (left: λ_{max}= 440 nm; right: λ_{max}= 512 nm). Conditions are 100 nM duplex, 5 mM Tris, 50 mM NaCl, pH 7.5.

the ruthenium-ethidium conjugate. First of all, modifying the ethidium at the amines blueshifted its absorption by 35 nm (Figure 4.14). As Ru emission is already at longer wavelength than ethidium absorption, blueshifting the acceptor absorption would undoubtedly reduce FRET efficiency. In the Turro system, modifying off the alkyl group on ethidium effectively made it more like propidium spectroscopically, which has redshifted absorption. Thus, the Turro system has better spectral overlap, as the acceptor absorption is moved closer to donor emission.

Furthermore, in our system, dppz is used in place of phen. The emission maximum of dppz complexes of ruthenium is redshifted by about 30 nm from that of bpy or phen species. This shift in donor emission further aggravated the already poor spectral overlap by pushing the donor emission further away from the acceptor absorption.

Finally, tethering through the terminal amines on ethidium with a rather short linker probably prevented the proper intercalation of ethidium into the DNA duplex. This is evident from the poor ethidium emission of the conjugate. Intercalation would redshift ethidium absorption, increasing the spectral overlap between ethidium and Ru. Since intercalation of ethidium was not observed, the absorption of ethidium would not be different from that of free ethidium in solution, which is just too far away from Ru emission. Tethering through the alkyl group, even with a short linker such as the one in the Turro system, apparently gives ethidium much greater freedom of movement and does not interfere with its intercalation. To allow intercalation of N-glycyl ethidium while the Ru is bound, a much longer linker might be necessary. Indeed, N-glycyl ethidium was observed to intercalate properly with a linker that was more than twice the length of the one in Ru-Eth.[10]

Although the Ru-Eth conjugate did not show FRET and thus was not an effective conjugate at improving the mismatch specificity, it serves as an example that underscores the sensitivity of FRET efficiency to small structural perturbations.

4.4 Conclusions

In this chapter, we attempted to improve the mismatch selectivity of ruthenium fluorophores through conjugation with a DNA-binding FRET acceptor. A trimethine benzothiazole-quinolinium cyanine dye (TO-3) and ethidium were used as the FRET acceptor, and four conjugates were synthesized. FRET was observed for all three of the Ru-TO conjugates,

significantly enhancing the fluorescence signal intensity of the parent Ru complex. For the conjugate Ru-7-TO **3**, the fluorescence differential in the presence of mismatched versus matched DNA was ∼3-fold at high ionic strength, which was a slight improvement from the unconjugated $Ru(bpy)_2dppz^{2+}$ (∼2.3-fold). Further improvement in mismatch selectivity was hindered by the complexity of conjugate binding to DNA. Clearly, the binding preferences of each component is not necessarily preserved in the final conjugate. In the Ru-Eth conjugate system, FRET was not observed due to poor spectral overlap. The current level of mismatch selectivity may not seem adequate for direct application in imaging mismatch-containing biological samples, but the conjugate strategy illustrated the feasibility of using a FRET acceptor to preferentially enhance the luminescence associated with mismatch-bound ruthenium. Presumably, a more dedicated minor groove binder would make a better FRET acceptor in this conjugate design. In the absence of such a FRET acceptor, the mismatch binding selectivity will be of critical importance.

Bibliography

[1] Mi Hee Lim, Hang Song, Eric D. Olmon, Elizabeth E. Dervan, and Jacqueline K. Barton. Sensitivity of $Ru(bpy)_2dppz^{2+}$ luminescence to DNA defects. *Inorganic Chemistry*, 48(12):5392–5397, 2009.

[2] R. R. Iyer, A. Pluciennik, V. Burdett, and P. L. Modrich. DNA mismatch repair: Functions and mechanisms. *Chemical Reviews*, 106(2):302–323, 2006.

[3] Bruce A. Armitage. Cyanine dye–DNA interactions: Intercalation, groove binding, and aggregation. *Top. Curr. Chem.*, 253:55–76, 2005.

[4] Joseph R. Lakowicz, Grzegorz Piszczek, and Jung Sook Kang. On the possibility of long-wavelength long-lifetime high-quantum-yield luminophores. *Analytical Biochemistry*, 288(1):62–75, 2001.

[5] Angel A. Martí, Cindy A. Puckett, Joanne Dyer, Nathan Stevens, Steffen Jockusch, Jingyue Ju, Jacqueline K. Barton, and Nicholas J. Turro. Inorganicorganic hybrid luminescent binary probe for DNA detection based on spin-forbidden resonance energy transfer. *Journal of the American Chemical Society*, 129(28):8680–8681, 2007.

[6] Brian M. Zeglis. *Investigations into the generality of metalloinsertion at DNA defects.* PhD thesis, California Institute of Technology, 2009.

[7] Cindy A. Puckett. *The cellular uptake of luminescent ruthenium complexes.* PhD thesis, California Institute of Technology, 2010.

[8] Katherine E. Augustyn, E. D. A. Stemp, and Jacqueline K. Barton. Charge separation in a ruthenium-quencher conjugate bound to DNA. *Inorganic Chemistry*, 46(22):9337–9350, 2007.

[9] Jay R. Carreon, Kelly M. Stewart, Kerry P. Mahon Jr., Stephanie Shin, and Shana O. Kelley. Cyanine dye conjugates as probes for live cell imaging. *Bioorganic & Medicinal Chemistry Letters*, 17(18):5182–5185, 2007.

[10] Shana O. Kelley, R. Erik Holmlin, Eric D. A. Stemp, and Jacqueline K. Barton. Photoinduced electron transfer in ethidium-modified DNA duplexes: dependence on distance and base stacking. *Journal of the American Chemical Society*, 119(41):9861–9870, 1997.

[11] Christian A. G. N. Montalbetti and Virginie Falque. Amide bond formation and peptide coupling. *Tetrahedron*, 61:10827–10852, 2005.

[12] Eric Valeur and Mark Bradley. Amide bond formation: Beyond the myth of coupling reagents. *Chemical Society Reviews*, 38:606–631, 2009.

[13] Thomas L. Netzel, Kambiz Nafisi, Min Zhao, Jerome R. Lenhard, and Iain Johnson. Base-content dependence of emission enhancements, quantum yields, and lifetimes for cyanine dyes bound to double-strand DNA: Photophysical properties of monomeric and bichromomphoric DNA stains. *Journal of Physical Chemistry*, 99(51):17936–17947, 1995.

[14] S. M. Yarmoluk, S. S. Lukashov, M. Yu Losytskyy, B. Akerman, and O.S. Kornyushyna. Interaction of cyanine dyes with nucleic acids: XXVI. Intercalation of the trimethine cyanine dye Cyan 2 into double-stranded DNA: study by spectral luminescence methods. *Spectrochimica Acta Part A: Molecular and Biomolecular Spectroscopy*, 58(14):3223–3232, 2002.

[15] Tarita Biver, Angela De Biasi, Fernando Secco, Marcella Venturini, and Sergiy Yarmoluk. Cyanine dyes as intercalating agents: Kinetic and thermodynamic studies on the DNA/Cyan40 and DNA/CCyan2 systems. *Biophysical Journal*, 89(1):374–383, 2005.

[16] Kristine M. Sovenyhazy, Jason A. Bordelon, and Jeffrey T. Petty. Spectroscopic studies of the multiple binding modes of a trimethinebridged cyanine dye with DNA. *Nucleic Acids Research*, 31(10):2561–2569, 2003.

[17] Naphtali A. O'Connor, Nathan Stevens, Diana Samaroo, Marissa R. Solomon, Angel A. Marti, Joanne Dyer, Harshad Vishwasrao, Daniel L. Akins, Eric R. Kandel, and Nicholas J. Turro. A covalently linked phenanthridine-ruthenium(II) complex as a RNA probe. *Chem. Commun.*, pages 2640–2642, 2009.

Chapter 5

Ru Complexes of DPPZ Derivatives and Chrysi Analogues

Mi Hee Lim and Elizabeth Dervan synthesized ruthenium complexes bearing DPPZ derivatives. Eric Olmon performed fluorescence lifetime measurements.

5.1 Introduction

In Chapter 4, we employed a tethering strategy in an attempt to selectively amplify the luminescence of ruthenium DPPZ complexes bound to DNA mismatches through FRET. However, this strategy was limited by the binding preferences of the FRET acceptor, as well as the tendency of the ruthenium complex to bind in both grooves of DNA. In this chapter, we revisit untethered ruthenium complexes, and explore different modifications to the DPPZ ligand in an effort to improve the mismatch selectivity of the resultant complexes, while preserving their luminescence properties.

Up to date, the truly selective binders of DNA mismatches are the chrysi and phzi complexes of rhodium (see Chapter 1). Their remarkable binding affinity toward mismatched over well-matched DNA stems from the sterically expansive intercalating ligand, chrysi, or phzi. These ligands, at 11.3 Å wide, are simply too bulky to fit between well-matched DNA base pairs, which are 10.8 Å in width. However, they are able to take advantage of the thermodynamic destabilization of mismatches and bind at mismatched sites through metalloinsertion.[1] In contrast, the DPPZ ligand of ruthenium complexes is long and narrow, which facilitates intercalation at both well-matched and mismatched sites. A natural design consideration to improve the mismatch binding selectivity of the ruthenium DPPZ complexes would be to increase the width of the intercalating DPPZ ligand, such that like chrysi or phzi, it no longer fits between well-matched base pairs. In this chapter, we report several chemical modifications to the DPPZ ligand to increase its steric bulk, and discuss the luminescence properties of the resultant complexes in the presence of well-matched and defective DNA. Besides DPPZ derivatives, we also prepared chrysi complexes of ruthenium. Taken together, these efforts highlight the sensitivity of both the binding and luminescence properties of ruthenium complexes to structural perturbations. The challenge to design a true "light switch" for DNA mismatches remains.

5.2 Experimental protocols

5.2.1 Materials

All reagents and solvents were purchased from commercial suppliers and used without further purification. Phenylene diamine (**1**), 3,4-diaminobenzoic acid (**2**), 2,3-diaminonaphthalene

(**4**), and pyrene-4,5-dione (**7**) were obtained from Sigma-Aldrich. The oligonucleotides 5'-GAC CAG CTT ATC ACC CCT AGA TAA GCG-3' and 3'-CTG GTC GAA TAG TXG GGA TCT ATT CGC-5' [X = G (M), C (MM) or R (AB, R denotes a tetrahydrofuranyl abasic site)] were synthesized and purified as described in Chapters 1 and 2.

5.2.2 Synthesis of metal complexes

3,6-Diethynylbenzene-1,2-diamine (**3**). Eight equivalents of $LiAlH_4$ (in THF) were added dropwise over 10 min to a solution of 4,7-diethynylbenzo[c][1,2,5]thiadiazole[2] (200 mg, 1.1 mmol), 30 mL THF, purged with Ar for 30 min, and cooled to 0 °C). The resulting solution was stirred for 10 min at 0 °C, and the temperature was allowed to reach room temperature. The reaction was quenched by addition of water after stirring for 4 h at room temperature, and the solution was filtered. The filtrate was extracted with CH_2Cl_2 (three times). After removal of CH_2Cl_2, the crude product was purified by SiO_2 column chromatography with a solvent gradient (50%:50% Hx:CH_2Cl_2 to 100% CH_2Cl_2) to obtain the desired product (153 mg, 0.98 mmol, 89%). ^{1}H NMR ($CDCl_3$, 300 MHz, δ (ppm)): 6.82 (s, 2H), 3.98 (br, s, 2H), 3.44 (s, 2H). HREI (m/z) for M^+ calcd. 156.0687, found 156.0687.

1,4-Dibromo-2,3-diaminonaphthalene (**5**) was synthesized according to reported procedures.[3]

DPPZ derivatives. Ligands were synthesized by refluxing **1**, **2**, **3**, **4**, and **5** (0.63 mmol) with 1,10-phenanthroline-5,6-dione, or by refluxing **6** and **7** with 5,6-diamino-1,10-phenanthroline (0.63 mmol) in ethanol (10 mL) for 8 h, as shown in Figure 5.1. The yellow precipitates were collected, washed with cold ethanol (three times, 20 mL), dried under vacuum, and used for preparation of the Ru complexes without further purification.

DPPA. Yield: 86%. ESI(+)MS (m/z) for $[M+H]^+$ calcd: 327.1, found: 327.2.

DPPAE. Yield: 40%. ESI(+)MS (m/z) for $[M+H]^+$ calcd: 331.1, found: 331.2.

DPPN. Yield: 83%. ESI(+)MS (m/z) for $[M+H]^+$ calcd: 333.1, found: 333.1.

Br_2DPPN. Yield: 75%. ESI(+)MS (m/z) for $[M+H]^+$+ calcd: 490.9, found: 491.0.

Pyrene-phen. Yield: 90%. ESI(+)MS (m/z) for $[M+H]^+$ calcd: 407.1, found: 407.3.

Ru complexes. The Ru complexes, $[Ru(bpy)_2DPPZ](X)_2$ (**8**) and $[Ru(bpy)_2tactp](X)_2$ (**11**, X = PF_6 or Cl) were prepared by previously described procedures.[4,5] For the rest, ethylene glycol (7 mL) was added to a mixture of $Ru(bpy)_2Cl_2$ (0.069 mmol) and the DPPZ derivatives (0.069 mmol), and the solution was heated to 130 °C for 12 h (Figure

5.2). After cooling the reaction mixture to room temperature, the solution was diluted with water (7 mL) followed by addition of excess NH_4PF_6 (s). The orange precipitates were collected, washed with water (3 x 5 mL), and dried under vacuum. The complexes were recrystallized by addition of Et_2O into their CH_3CN solution at room temperature and afterward converted to the soluble Cl salt by an anion exchange column on Sephadex QEA. They were further purified by preparative HPLC using a gradient of H_2O (with 0.1% TFA) to CH_3CN (with 0.1% TFA) over the course of 30 min.

[Ru(bpy)$_2$(DPPA)](X)$_2$ (**9**, X = PF_6 or Cl). Yield: 63%. ^{1}H NMR (CD_3CN, 500 MHz, δ (ppm)): 9.76–9.68 (m, 2H), 9.06 (m, 1H), 8.70 (m, 1H), 8.59–8.54 (m, 4H), 8.49 (1H, m), 8.22 (s, br, 2H), 8.14 (m, 2H), 8.05 (m, 2H), 7.94 (m, 2H), 7.89 (m, 2H), 7.79 (2H, m), 7.49 (m, 2H), 7.30 (m, 2H). ESI(+)MS (m/z): $[M\text{-}2(PF_6)]^{2+}$ calcd. 370.1, found 370.0; $[M\text{-}PF_6]^+$ calcd. 885.1, found 885.2. UV-vis (in H_2O, λ (nm, ϵ (x 10^4, $M^{-1}cm^{-1}$))): 284 (10), 362 (1.9), 378 (1.9), 444 (1.6).

[Ru(bpy)$_2$(DPPAE)](X)$_2$ (**10**). The Ru complex was prepared as described above. The crude product was purified via preparative TLC (silica, 4:4.5:1, CH_3CN:water:NH_4Cl (sat, aq)) followed by preparative HPLC (a gradient of H_2O (with 0.1% TFA) to CH_3CN (with 0.1% TFA)). The Cl salt was then obtained using anion exchange chromatography on Sephadex QEA. Yield: 20%. ESI(+)MS (m/z): $[M\text{-}2Cl]^{2+}$ calcd. 372.1, found 372.0. UV-vis (in H_2O, λ (nm, ϵ (x 10^4, $M^{-1}cm^{-1}$))): 244 (4.3), 272 (sh, 4.7), 288 (6.3), 306 (4.3), 364 (1.2), 380 (1.5), 426 (1.4), 440 (1.3).

[Ru(bpy)$_2$(DPPN)](X)$_2$ (**12**). Yield: 72%. ^{1}H NMR (CD_3CN, 500 MHz, δ (ppm)): 9.71–9.681 (m, 2H), 9.17–9.16 (m, 2H), 8.57 (dd, J = 8.0 Hz, 4H), 8.41–8.39 (m, 2H), 8.18–8.14 (m, 4H), 8.10–8.05 (m, 2H), 7.94–7.88 (m, 4H), 7.82–7.78 (m, 4H), 7.52–7.49 (m, 2H), 7.34–7.31 (m, 2H). ESI(+)MS (m/z): $[M\text{-}2(PF_6)]^{2+}$ calcd. 373.1, found 373.1; $[M\text{-}PF_6]^+$ calcd. 891.1, found 891.2. UV-vis (in H_2O, λ (nm, ϵ (x 10^4, $M^{-1}cm^{-1}$))): 244 (5.3), 286 (7.0), 324 (7.4), 390 (1.6), 412 (2.2), 442 (2.0).

[Ru(bpy)$_2$(Br$_2$DPPN)](X)$_2$ (**13**). Yield: 69%. ^{1}H NMR (CD_3CN, 500 MHz, δ (ppm)): 8.43–8.41 (m, 2H), 7.49–7.46 (m, 2H), 7.43–7.39 (m, 4H), 6.96–6.94 (m, 2H), 6.87–6.84 (m, 2H), 6.79–6.76 (m, 2H), 6.66–6.55 (m, 8H), 6.23 (2H, m), 6.06 (2H, m). ESI(+)MS (m/z): $[M\text{-}2(PF_6)]^{2+}$ calcd. 451.0, found 451.0; $[M\text{-}PF_6]^+$ calcd. 1049.3, found 1049.1. UV-vis (in H_2O, λ (nm, ϵ (x 10^4, $M^{-1}cm^{-1}$))): 254 (3.7), 286 (4.5), 324 (4.3), 396 (1.0), 420 (1.4), 446 (1.4).

[Ru(bpy)$_2$(pyrene-phen)](X)$_2$ (**14**). Yield: 76%. ^{1}H NMR (CD_3CN, 500 MHz, δ (ppm)): 9.71 (d, J = 7.5 Hz, 2H), 9.47 (d, J = 7.5 Hz, 2H), 8.59 (t, J = 9.3 Hz, 4H), 8.27–8.23 (m, 4H), 8.19–8.11 (m, 4H), 8.06 (td, J = 8.0 Hz, 1.2 Hz, 2H), 8.0–7.92 (m, 4H), 7.84 (d, J = 5.1 Hz, 2H), 7.74 (s, 2H), 7.52 (m, 2H), 7.34 (m, 2H). ESI(+)MS (m/z): $[M\text{-}2(PF_6)]^{2+}$ calcd. 410.8, found 410.2; $[M\text{-}PF_6]^+$ calcd. 965.1, found 965.4. UV-vis (in H_2O, λ (nm, ϵ (x 10^4, $M^{-1}cm^{-1}$))): 236 (3.7), 288 (5.0), 348 (1.1), 452 (1.3), 476 (1.3).

The synthesis of $Ru(bpy)_2chrysi^{2+}$ was adapted from Eva Rüba's protocol (unpublished results from our laboratory).

[Ru(bpy)$_2$(NH$_3$)$_2$]Cl$_2$. $Ru(bpy)_2Cl_2$ (0.40 g, 0.83 mmol) was dissolved in methanol (5 mL), to which 10 mL of c.NH_4OH was added. The reaction mixture was heated under reflux (60 °C) for 3 h. After cooling to RT, the solvent was removed under reduced pressure. The residue was taken up in methanol to give a dark red solution. Diethyl ether was added to crash out the product as a black fine powder (0.44 g, quantitative yield). The hexafluorophosphate salt of the product was obtained by adding NH_4PF_6 to an aqueous solution of the chloride salt and collecting the red precipitate. The ppt was washed with copious amount of water to remove any excess NH_4PF_6. ^{1}H-NMR (300 MHz, CD_3OD) δ 9.20 (d, J = 5.0 Hz, 2H), 8.64 (d, J = 7.9 Hz, 2H), 8.47 (d, J = 7.8 Hz, 2H), 8.26–8.13 (m, 2H), 7.88–7.76 (m, 4H), 7.65 (d, J = 5.0 Hz, 2H), 7.25–7.14 (m, 2H), 2.93 (s, 6H).

[Ru(bpy)$_2$chrysi]Cl$_2$. This reaction was carried out under Ar and using anhydrous solvents. To a solution of $[Ru(bpy)_2(NH_3)_2](PF_6)_2$ in acetonitrile, NaH (excess) was added. After 15 min, chrysene quinone (slight excess) and ethanol was added. The reaction mixture was stirred at RT overnight, protected from light with foil. If the volume of the reaction mixture is small, it may be loaded directly to a preparative silica TLC plate. Otherwise, remove some of the solvent on the rotovap before loading onto the TLC plate. The plate was run under an Ar atmosphere in water/acetonitrile/sat. NH_4Cl (6:3:1 v/v/v) for 40 min–1h. The pink band is isolated as the PF_6 salt, washed with water, and lyophilized. The chloride salt is obtained by passing an acetonitrile/water (3:2 v/v) solution of the hexafluorophosphate salt through a sephadex QAE anion exchange column. ^{1}H-NMR (500 MHz, CD_3CN) δ 12.78 (s, 1H), 12.41 (s, 1H), 8.53 (m, 6H), 8.47 (d, J = 8.0 Hz, 1H), 8.34 (m, 1H), 8.25 (d, J = 8.7 Hz, 1H), 8.12 (m, 5H), 7.94 (d, J = 5.1 Hz, 2H), 7.82 (t, J = 7.9 Hz, 1H), 7.71–7.62 (m, 5H), 7.46 (m, 4H). ESI-MS: calc. 669.14 $(M\text{-}H)^+$, 334.57 (M^{2+}), found 335.2 (M^{2+}), 669.2 $(M\text{-}H)^+$, 814.9 $(M{+}PF_6)^+$. The concentration of the complex was roughly estimated

using ϵ_{549} = 50,000 $M^{-1}cm^{-1}$.

[Ru(bpy)$_2$(Me$_2$chrysi)]Cl$_2$. To a solution of [Ru(bpy)$_2$chrysi]TFA_2 in acetonitrile, NaH (excess) was added. After 15 min, iodomethane (excess) was added, and the reaction mixture was stirred under Ar at RT for 2 h. The solution was neutralized with dilute HCl, filtered, and the solvent evaporated to dryness under reduced pressure. The residue was redissolved in water and crashed out as the hexafluorophosphate salt with the addition of NH_4PF_6. The chloride salt was obtained by passing an acetonitrile/water (3:2 v/v) solution of the hexafluorophosphate salt through a sephadex QAE anion exchange column. ^{1}H-NMR (400 MHz, CD_3CN) δ 8.73 (d, J = 8.4 Hz, 1H), 8.66–8.55 (m, 3H), 8.53 (d, J = 8.2 Hz, 1H), 8.44 (d, J = 8.9 Hz, 1H), 8.34 (d, J = 7.7 Hz, 1H), 8.29–8.23 (m, 2H), 8.17 (dd, J = 14.2, 6.4 Hz, 1H), 8.10 (dd, J = 10.3, 6.7 Hz, 3H), 7.98 (d, J = 8.1 Hz, 1H), 7.79 (t, J = 7.7 Hz, 1H), 7.72 (dd, J = 9.1, 5.7 Hz, 2H), 7.59 (m, 2H), 7.45 (m, 3H), 7.37–7.33 (t, J = 6.7 Hz, 1H), 7.27 (d, J = 5.7 Hz, 1H), 7.24–7.17 (t, J = 8.0 Hz, 1H), 5.92 (d, J = 8.5 Hz, 1H), 3.75 (s, 3H), 3.21 (s, 3H). ESI-MS: calc. 697.17 $(M\text{-}H)^+$, 349.09 (M^{2+}), found 349.2 (M^{2+}), 684.2 $(M\text{+}H\text{-}CH_3)^+$, 697.2 $(M\text{-}H)^+$. The concentration of the complex was roughly estimated using ϵ_{532} = 30,000 $M^{-1}cm^{-1}$.

5.2.3 Steady state fluorescence

Luminescence spectra were recorded on an ISS-K2 spectrofluorometer in 5 mM Tris, 50 mM NaCl, pH 7.5 at room temperature in aerated solutions. For luminescence measurements at 77 K, complexes were dissolved in 10 M LiCl to form a clear glass.[6] The sample cuvette was immersed in a dewar sample holder filled with liquid nitrogen.

5.2.4 Fluorescence lifetimes

Samples were excited using a Nd:YAG-pumped OPO (Spectra-Physics Quanta-Ray). Laser power at 470 nm ranged from 4.0–4.5 mJ per pulse at 10 Hz. Emitted light was collected and focused onto the entrance slit of an ISA double grating (100 mm) monochromator and detected by a PMT (Hamamatsu R928). Each measurement is the average of 500 or 1000 shots. Emission decays were fit to single or biexponential functions using nonlinear least squares minimization.

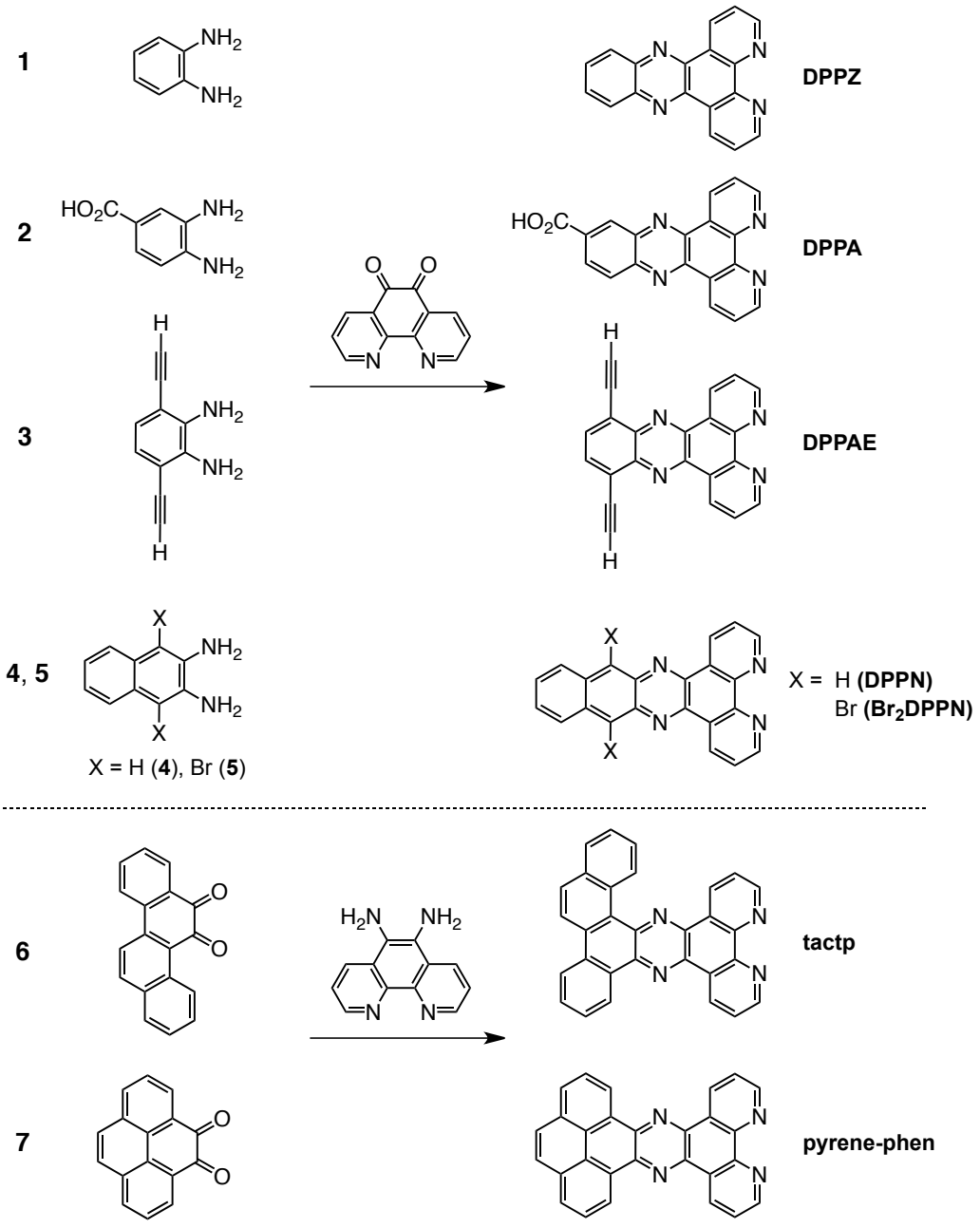

Figure 5.1. Synthesis of derivatives of the DPPZ ligand.

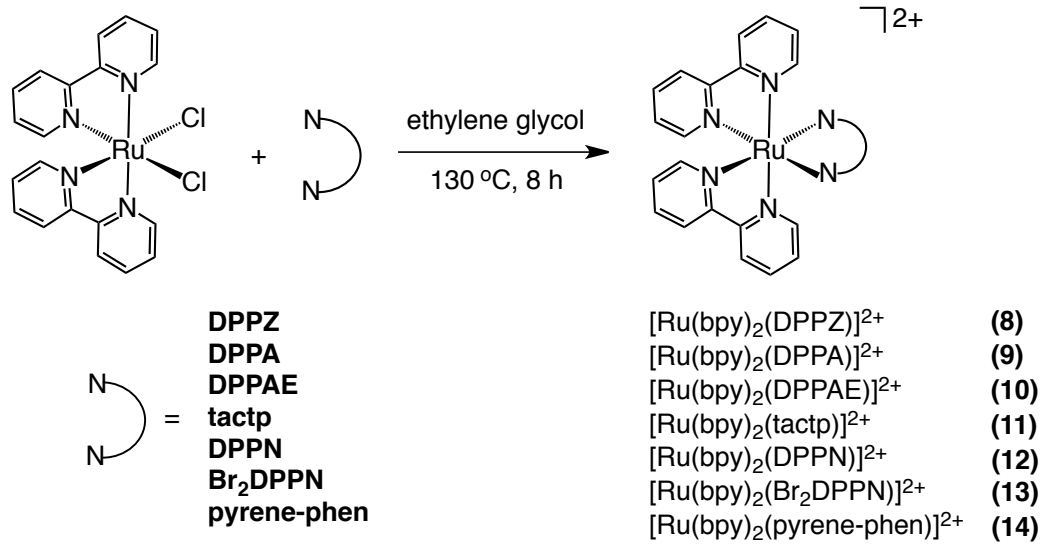

Figure 5.2. Synthesis of ruthenium complexes bearing the DPPZ or DPPZ-derivative ligand.

5.3 Results and discussion

5.3.1 Ru complexes bearing DPPZ derivatives

Design considerations. Inspired by the activity of $Rh(bpy)_2chrysi^{3+}$ and $Ru(bpy)_2DPPZ^{2+}$ toward DNA,[7,8] we aimed to develop a new framework for detecting DNA lesions based on luminescence. The key feature of the Rh(chrysi) complex that enables it to specifically recognize destabilized sites in DNA is the sterically expansive inserting chrysi ligand (see Chapter 1). Meanwhile, the luminescence-based detection for DNA by $Ru(bpy)_2DPPZ^{2+}$ (**8**) is based on the intercalation of the DPPZ ligand.[9–11] Thus, by combining characteristics of the chrysi and dppz ligands into a single ligand, it may be possible to create a Ru complex which luminesces only when specifically bound to DNA lesions. Guided by these design considerations, derivatives of the Ru(DPPZ) complex, based on the structures of both $Rh(bpy)_2chrysi^{3+}$ and $Ru(bpy)_2DPPZ^{2+}$, were prepared as candidates of luminescent reporters for DNA defects (Figures 5.1 and 5.2). Simple substituents (CO_2H, acetylene, Br, and phenyl), shown in Figure 5.1, were incorporated into the DPPZ ligand in order to increase its width, length, or both. The wider ligand framework such as in DPPAE and tactp is similar to that of the sterically bulky chrysi ligand. Lengthening DPPZ to create DPPN (Figure 5.1) might induce a significant increase in luminescence only from intercalation or insertion into destabilized sites in DNA. Since DPPN is longer than DPPZ, the nitrogen

atoms responsible for luminescence enhancement on DPPN might be less protected from water than those on DPPZ when they bind to well-matched DNA in the major groove. Furthermore, increasing both length and width (see Br_2DPPN and pyrene-phen, Figure 5.1) could combine the effects on the recognition of a DNA lesion that would be expected from DPPAE, tactp and DPPN. Lastly, the DPPZ derivatives were coordinated to the $Ru(bpy)_2$ skeleton in order to preserve the light switch behavior of **8** initiated by metal-to-ligand charge transfer (MLCT) upon excitation (Figure 5.2).

Synthesis of Ru(DPPZ) derivatives. The Ru complexes $Ru(bpy)_2DPPZ^{2+}$ (**8**) and $Ru(bpy)_2tactp^{2+}$ (**11**) were prepared by previously published methods.[4,5] For the ligands DPPA, DPPAE, DPPN, and Br_2DPPN (Figure 5.1), the amine moieties were condensed with 1,10-phenanthroline-5,6-dione in ethanol.[2,3,5] The pyrene-phen ligand was obtained by condensation of pyrene-4,5-dione (**7**) with 5,6-diamino-1,10-phenanthroline in ethanol. The complexes **9**, **10**, **12**, **13**, and **14** were obtained by refluxing a solution containing $Ru(bpy)_2Cl_2$ and 1 equivalent of the corresponding DPPZ derivatives in ethylene glycol at 130 °C over 8 h, as depicted in Figure 5.2. Addition of excess NH_4PF_6 (s) into the reaction solution of 1:1 ethylene glycol:water allows the isolation of the Ru complexes as PF_6 salts, followed by purification via recrystallization or column chromatography. All complexes show the characteristic MLCT transition absorption in the visible region at ∼440 nm.

Steady state luminescence of the Ru complexes with DNA. As shown in Figure 5.3, all Ru complexes (**8** – **14**) show "light switch" properties with matched (M), mismatched (MM) and abasic (AB) DNA. In the absence of DNA, complexes having extensively π-conjugated ligands (**11** – **14**) present noticeable intensity in luminescence. The Ru(DPPA) complex (**9**) exhibits luminescence enhancement in the presence of M, MM and AB, similar to **8**, but its binding affinity is lower than that of **8** (Figure 5.3 and Table 5.1). Introduction of the expansive DPPZ derivatives DPPAE and tactp, employing acetylene and chrysene functionalities respectively to increase the width of the ligand, does not improve luminescence response toward DNA defects (Figure 5.3). In the case of the Ru(tactp) complex (**11**), a previous study demonstrates that the luminescence increases occur not only by interaction with DNA but also by dimerization or aggregation of the complex itself with or without a DNA template.[5]

Attachment of a phenyl group to the end of the phenazine moiety increases the length of the DPPZ-type ligand (DPPN, Figure 5.1). Significantly, the Ru complex containing DPPN

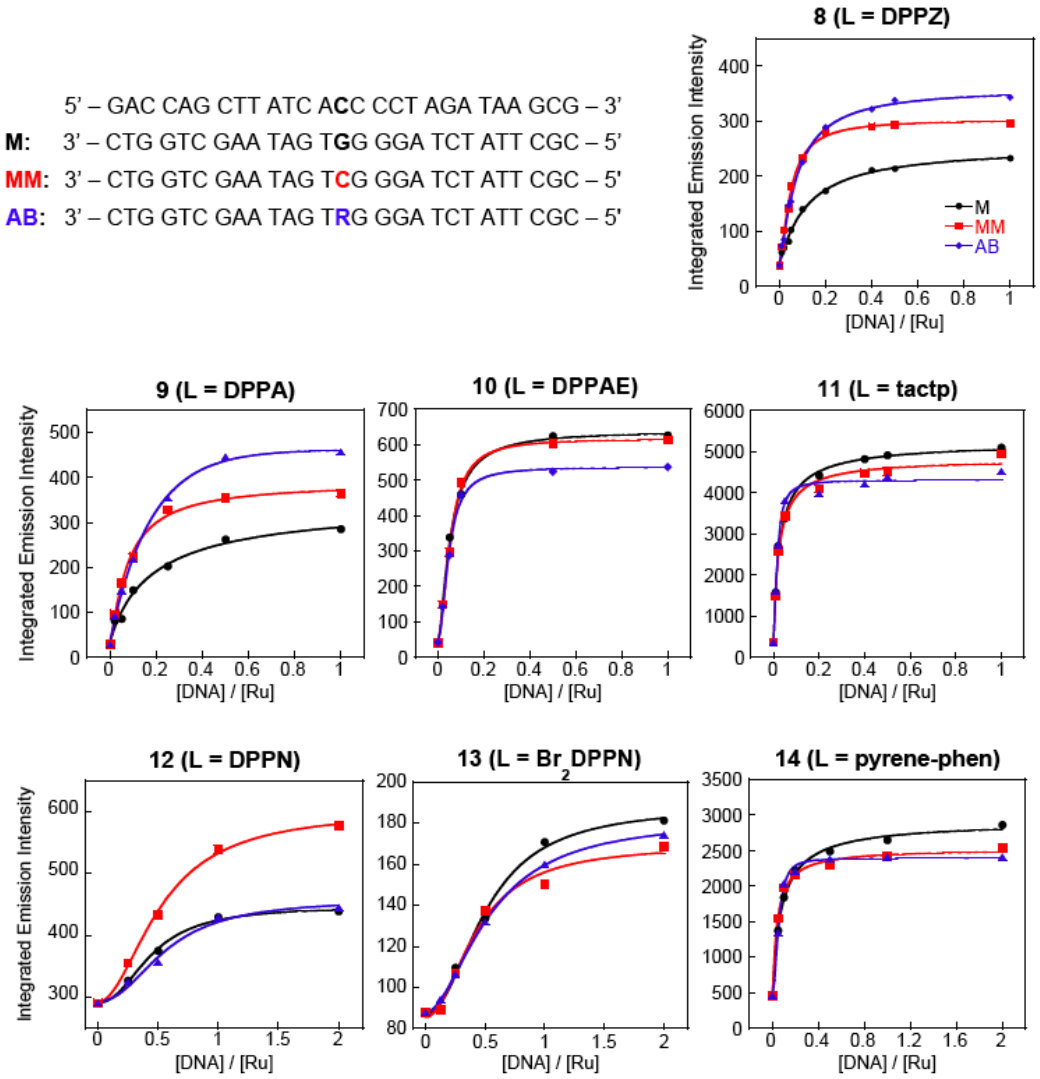

Figure 5.3. Plots of integrated emission intensity of **8** – **14** with M, MM and AB (5 mM Tris, pH 7.5, 50 mM NaCl, λ_{ex} = 440 nm). [Ru] = 0.1 μM (**8**, **11**, and **14**), 1 μM (**9** and **10**), 5 μM (**12**), and 10 μM (**13**). DNA sequences are depicted (top, left).

Table 5.1. DNA concentration at half-saturation in luminescence titrations[a]

Ru Complex	Ligand	[Ru][b] (μM)	DNA	$([DNA]/[Ru])_{1/2}$	[DNA][c] (μM)
8	DPPZ	0.1	M	0.090	0.0090
			MM	0.047	0.0047
			AB	0.065	0.0065
9	DPPA	1	M	0.12	0.12
			MM	0.070	0.070
			AB	0.11	0.11
10	DPPAE	1	M	0.050	0.050
			MM	0.050	0.050
			AB	0.043	0.043
11	tactp	0.1	M	0.023	0.0023
			MM	0.020	0.0020
			AB	0.013	0.0013
12	DPPN	5	M	0.42	2.1
			MM	0.48	2.4
			AB	0.51	2.6
13	Br_2DPPN	10	M	0.47	4.7
			MM	0.47	4.7
			AB	0.44	4.4
14	pyrene-phen	0.1	M	0.067	0.0067
			MM	0.040	0.0040
			AB	0.047	0.0047

[a]The value of (DNA/Ru) at the midpoint of the integrated emission intensity in Figure 5.3. [b]The concentration of Ru used for luminescence measurements. [c]The calculated concentration of DNA from $(DNA/Ru)_{1/2}$ and [Ru].

(**12**) exhibits an increase in luminescence with MM over M and AB (Figure 5.3). This may be because the extended DPPN ligand of **12**, when bound to well-matched DNA in the major groove, affords less protection of the phenazine nitrogens from solvent water molecules than DPPZ. But binding to mismatches presumably occurs from the minor groove, which is deep and narrow, thus allowing deeper intercalation of the ruthenium complex and consequently better protection of the ligand from solvent water. However, the luminescence of **12** upon incubation with DNA is unstable, which means that further application or modification would be limited.

Incorporation of substitutions on DPPN was also made to widen the ligand. The dervia-tives of DPPN are Br_2DPPN and phen-pyrene (Figure 5.1), which are both wider and longer than DPPZ. The Ru complexes (**13** and **14**) having Br_2DPPN and phen-pyrene do not show any differential luminescence with M, MM and AB, however (Figure 5.3). The weak luminescence of **13** was probably due to heavy-atom quenching by bromine. Increased luminescence of **14** would occur in a manner similar to that of the structurally homologous **11**.[5] In sum, the luminescence measurements of **8**–**14** suggest that structural modifications to the intercalating ligand of the Ru complex are not enough to improve detection of DNA defects.

Excited state lifetimes. Greater protection of the phenazine moiety from water via intercalation leads to longer excitation lifetimes for the two binding modes (side-on and perpendicular), a higher relative population of the longer-lived species, or both. As described in Table 5.2, **8** displays a higher relative abundance of species associated with the perpendicular mode in the presence of DNA following the order AB > MM > M. This supports the observation from steady state measurements that the luminescence intensity of **8** is present in the following order: AB > MM > M (Figure 5.3).[8] In the case of **9**, longer lifetimes corresponding to the perpendicular mode (AB > MM > M) are observed, which can explain the ordering of the steady state luminescence measurements of **9**, as shown in Figure 5.3. Furthermore, **12**, which shows differential luminescence turn-on with MM over M and AB, indicates longer lifetimes in both binding modes only with MM. In general, the excited state lifetime measurements indicate that the complexes **8**, **9**, and **12** present longer lifetimes or a higher portion of the perpendicular mode in the presence of DNA containing a lesion over well-matched DNA, indicating more protection of the phenazine nitrogens responsible for luminescence enhancement upon binding to DNA defects.

Table 5.2. Luminescence decay parameters of ruthenium complexes in the presence of M, MM and AB[a]

	– DNA		+ DNA		
Complex (Ligand)	τ (ns)[b,c]	DNA	τ_1 (ns)[c]	τ_2 (ns)[c]	τ_1:τ_2
8 (DPPZ)	180[d]	M	72	212	83:17
		MM	74	213	77:23
		AB	86	192	69:31
9 (DPPA)	192	M	32	192	95:5
		MM	32	245	96:4
		AB	26	544	93:7
10 (DPPAE)	188	M	275	3908	60:40
		MM	391	4277	67:33
		AB	503	4640	62:38
11 (tactp)	205	M	1211	–	–
		MM	1177	–	–
		AB	1121	–	–
12 (DPPN)	171	M	62	843	51:49
		MM	196	1010	49:51
		AB	35	709	58:42
13 (Br_2DPPN)	200	M	99	1056	63:37
		MM	134	876	66:34
		AB	82	801	54:46
14 (pyrene-phen)	186	M	929	–	–
		MM	879	–	–
		AB	808	–	–

[a] λ_{ex} = 470 nm, λ_{em} = 610 nm, 10 μM [Ru] and 20 μM [DNA] (5 mM Tris, pH 7.5, 50 mM NaCl). [b] [Ru] = 10 μM, CH_3CN. [c] Error is estimated to be ±10%. [d] reference 10. [e] 20 μM [Ru] and 40 μM [DNA].

The compounds **11** and **14**, which can aggregate in the presence of a DNA template, exhibit single exponential luminescent decays with DNA (Table 5.2), suggesting that their luminescence enhancement originates mainly from nonspecific binding to DNA. The compounds **10** and **13**, which have increased steric bulk on the phenazine fragment but utilize different substituents from **11** and **14**, present biexponential decays in emission. Lower abundances of long-lived species in **10** and shorter lifetimes in **13** in the presence of a DNA lesion were detected in their lifetime measurements. This is consistent with the higher steady state luminescence of **10** and **13** with well-matched DNA (Figure 5.3).

Taken together, the Ru(DPPZ) derivatives are prepared in order to specifically target DNA defects and report their presence by luminescence turn-on. The luminescent responses to DNA containing a lesion were not noticeably enhanced by the Ru complexes containing DPPZ derivatives, however. Still, the narrow ligands (DPPA and DPPN) show differential behavior in luminescence in the presence of a DNA lesion. Based on the excited state lifetime measurements, the Ru complexes **8**, **9**, and **12** display longer lifetimes or a higher portion of the perpendicular mode with MM and AB, which corresponds to their luminescence enhancement. Recent studies of **8** suggest that the perpendicular binding of Ru along the DNA dyad axis occurs at the destabilized site through the minor groove,[8] which was confirmed in an atomic-resolution crystal structure (Chapter 3). The Ru complexes with the extensively π-conjugated ligands such as tactp and pyrene-phen indicate mainly nonspecific binding to DNA. In addition, widening the DPPZ ligand using a simple functionality such as acetylene or Br does not enhance targeting of destabilized regions in DNA. In summary, the structural features of the ligand are important for intercalation or insertion into a destabilized region, but unlike the Rh(chrysi) complex, steric bulk on the DPPZ ligand of the Ru complexes does not boost specific recognition of DNA defects as reflected in their luminescent response.

5.3.2 Chrysi analogues of ruthenium

Work described in the previous section adopted a luminescence-based approach to modify the intercalating DPPZ ligand of ruthenium complexes in an attempt to improve their mismatch selectivity. In this section, we discuss a structure-based approach, starting from the mismatch-selective chrysi ligand to make $Ru(bpy)_2chrysi^{2+}$ and applying subsequent modifications to bring about enhancement in its luminescence properties.

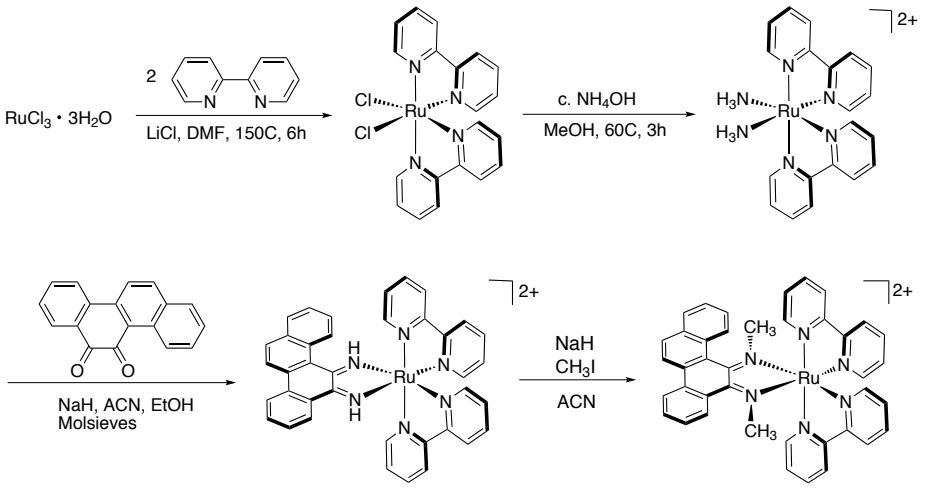

Figure 5.4. Synthesis of $Ru(bpy)_2chrysi^{2+}$ and $Ru(bpy)_2(Me_2chrysi)^{2+}$.

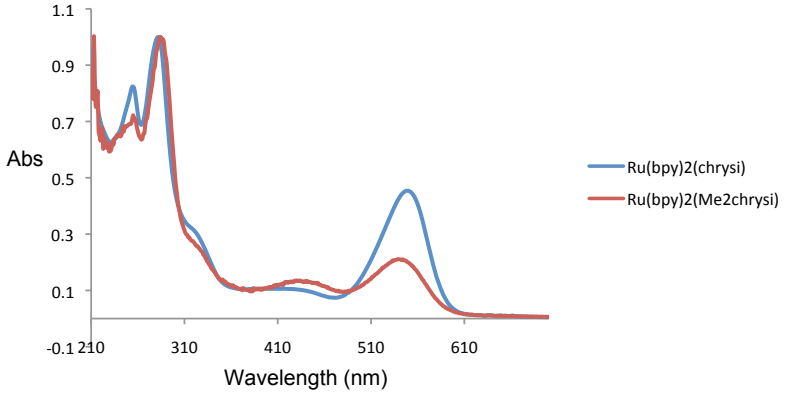

Figure 5.5. UV-vis spectra of $Ru(bpy)_2chrysi^{2+}$ and $Ru(bpy)_2(Me_2chrysi)^{2+}$ in water.

$Ru(bpy)_2chrysi^{2+}$ was synthesized in an analogous fashion to $Rh(bpy)_2chrysi^{3+}$ and methylated with iodomethane to give $Ru(bpy)_2(Me_2chrysi)^{2+}$ (Figure 5.4). The UV-vis spectrum of $Ru(bpy)_2chrysi^{2+}$ shows two excitation bands above 350 nm, with the longer-wavelength band at 549 nm blueshifted to 532 nm upon methylation (Figure 5.5). $Ru(bpy)_2chrysi^{2+}$ is nonluminescent at room temperature in water or acetonitrile (λ_{ex} = 440 or 550 nm); however, in a glass at 77 K, it becomes luminescent upon excitation at 440 nm, with an emission and excitation profile resembling those of $Ru(bpy)_3^{2+}$ (Figure 5.6). Methylation of $Ru(bpy)_2chrysi^{2+}$ restores luminescence at room temperature in both water and acetonitrile (Figure 5.7). However, when DNA is added to the dimethylated complex, mismatch discrimination in terms of luminescence output is not apparent (Figure 5.8).

The fact that $Ru(bpy)_2chrysi^{2+}$ is luminescent when it is frozen in a solid suggests

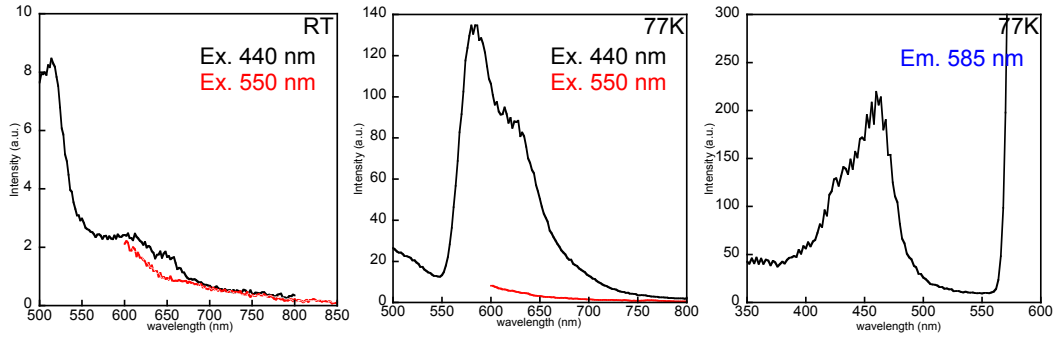

Figure 5.6. Emission (λ_{ex} = 440 and 550 nm) and excitation (λ_{em} = 585 nm) spectra of $Ru(bpy)_2chrysi^{2+}$ ($\sim$15 μM) at RT and 77 K (in 10 M LiCl).

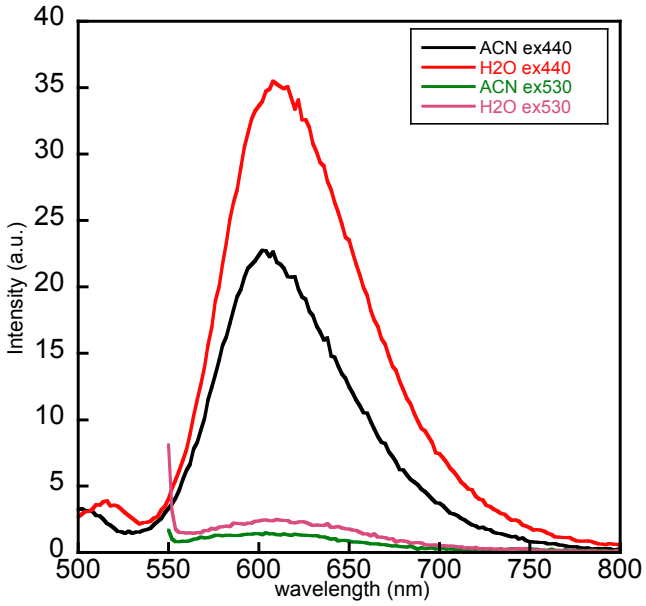

Figure 5.7. Emission spectra of $Ru(bpy)_2(Me_2chrysi)^{2+}$ ($\sim$10 μM) in water and acetonitrile (λ_{ex} = 440 and 530 nm).

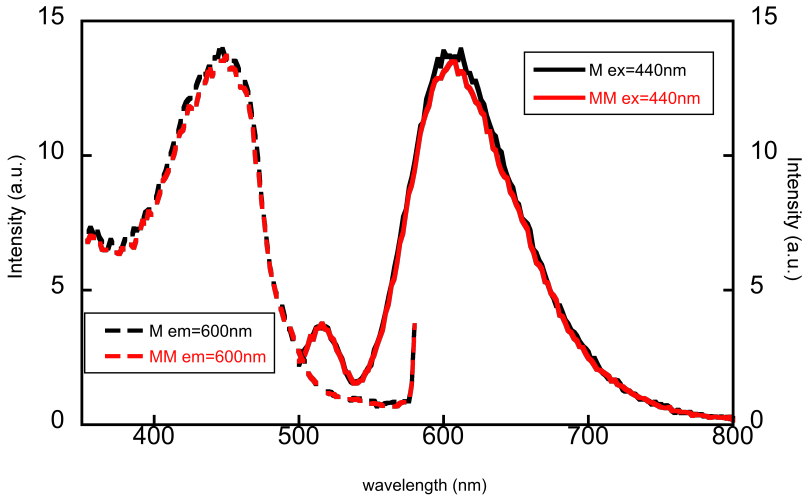

Figure 5.8. Emission (solid line) and excitation (dotted line) spectra of $Ru(bpy)_2(Me_2chrysi)^{2+}$ ($\sim$5 μM) in the presence of matched and mismatched DNA (5 μM).

that the exchangeable imino protons are responsible for quenching the luminescence at room temperature through solvent relaxation. Freezing typically improves luminescence quantum yields significantly for metal complexes by shutting off nonradiative relaxation pathways.[12] Methylation removes the imino protons and thus allows the luminescence to be restored. However, after methylation, the complex $Ru(bpy)_2(Me_2chrysi)^{2+}$ is permanently turned on, which then precludes "light switch" behavior. It is therefore not surprising that there is no mismatch discrimination in terms of luminescence when DNA is added. In fact, $Ru(bpy)_2chrysi^{2+}$ at 77 K does not show mismatch discrimination either, as it is also always "on" in a frozen state without regard to its DNA-binding status. It is unclear if $Ru(bpy)_2(Me_2chrysi)^{2+}$ binds preferentially to mismatched sites, since methylation is bound to cause strain on the chrysi ligand due to steric clashes between the methyl groups and hydrogens on the fused ring system, possibly bending the ligand and forcing it out of a planar arrangement. Further experimentation with $Ru(bpy)_2(Me_2chrysi)^{2+}$ was hindered by the decomposition of the dimethylated complex. ^{1}H-NMR of the dimethylated complex after short periods of storage showed loss of the methyl groups.

5.4 Conclusions

In this chapter, we continue our efforts in developing a luminescent ruthenium probe for DNA mismatches. We increased the steric expanse of the DPPZ ligand in order to enhance the mismatch-binding selectivity of the resultant ruthenium complexes. While some complexes show preferential binding to mismatches, none of the DPPZ derivatives achieved significant improvement in their luminescence differential between mismatched and well-matched DNA. In a separate approach, the nonluminescent chrysi complex of ruthenium was methylated to restore emission at room temperature. However, the luminescence of the dimethylated complex is no longer sensitive to changes in its environment upon DNA binding. These efforts highlight the challenge of coupling mismatch-selective binding to the luminescence properties of ruthenium complexes. The quest for a true "light switch" of DNA mismatches goes on.

Bibliography

[1] Brian M. Zeglis, Valerie C. Pierre, and Jacqueline K. Barton. Metallo-intercalators and metallo-insertors. *Chem Commun (Camb)*, (44):4565–4579, 2007.

[2] Brenno A. DaSilveira Neto, Aline Sant'Ana Lopes, Gunter Ebeling, Reinaldo S. Gonçalves, Valentim E.U. Costa, Frank H. Quina, and Jairton Dupont. Photophysical and electrochemical properties of π-extended molecular 2,1,3-benzothiadiazoles. *Tetrahedron*, 61(46):10975–10982, 2005.

[3] Jian Yang, Changyun Jiang, Yong Zhang, Renqiang Yang, Wei Yang, Qiong Hou, and Yong Cao. High-efficiency saturated red emitting polymers derived from fluorene and naphthoselenadiazole. *Macromolecules*, 37(4):1211–1218, 2004.

[4] Cindy A. Puckett and Jacqueline K. Barton. Methods to explore cellular uptake of ruthenium complexes. *Journal of the American Chemical Society*, 129(1):46–47, 2007.

[5] Eva Rüba, Jonathan R. Hart, and Jacqueline K. Barton. $[Ru(bpy)_2(L)]Cl_2$: Luminescent metal complexes that bind DNA base mismatches. *Inorganic Chemistry*, 43(15):4570–4578, 2004.

[6] Melanie A. O'Neill and Jacqueline K. Barton. DNA-mediated charge transport requires conformational motion of the DNA bases: Elimination of charge transport in rigid glasses at 77 K. *Journal of the American Chemical Society*, 126(41):13234–13235, 2004.

[7] Brian M. Zeglis and Jacqueline K. Barton. DNA base mismatch detection with bulky rhodium intercalators: Synthesis and applications. *Nature Protocol*, 2(2):357–371, 2007.

[8] Mi Hee Lim, Hang Song, Eric D. Olmon, Elizabeth E. Dervan, and Jacqueline K. Barton. Sensitivity of $Ru(bpy)_2dppz^{2+}$ luminescence to DNA defects. *Inorganic Chemistry*, 48(12):5392–5397, 2009.

[9] Alan E. Friedman, Jean Claude Chambron, Jean Pierre Sauvage, Nicholas J. Turro, and Jacqueline K. Barton. A molecular light switch for DNA: $Ru(bpy)_2(dppz)^{2+}$. *Journal of the American Chemical Society*, 112(12):4960–4962, 1990.

[10] Yonchu Jenkins, Alan E. Friedman, Nicholas J. Turro, and Jacqueline K. Barton. Characterization of dipyridophenazine complexes of ruthenium(II): The light switch effect as a function of nucleic acid sequence and conformation. *Biochemistry*, 31(44):10809–10816, 1992.

[11] Richard M. Hartshorn and Jacqueline K. Barton. Novel dipyridophenazine complexes of ruthenium(II): Exploring luminescent reporters of DNA. *Journal of the American Chemical Society*, 114(15):5919–5925, 1992.

[12] Hartmut Yersin, Werner Humbs, and Johann Strasser. Low-lying electronic states of $[Rh(bpy)_3]^{3+}$, $[Pt(bpy)_2]^{2+}$, and $[Ru(bpy)_3]^{2+}$. A comparative study based on highly resolved and time-resolved spectra. *Coordination Chemistry Reviews*, 159:325–358, 1997.

Chapter 6

RNA Mismatch Recognition by $Ru(bpy)_2dppz^{2+}$

6.1 Introduction

An early observation about the DNA "light switch" molecule, $Ru(L)_2dppz^{2+}$, is that it binds well to and luminesces strongly in the presence of B- and Z-form DNA, but does so very weakly with A-form RNA.[1,2] More recently, our laboratory has discovered that $Ru(bpy)_2dppz^{2+}$ binds more strongly to mismatched DNA, as evident in its enhanced luminescence in the presence of base mismatches;[3] the structural details of the complex bound to a mismatch have been elucidated in an atomic-resolution crystal structure (see Chapter 3). The higher affinity of $Ru(bpy)_2dppz^{2+}$ for base mismatches and the general lack of binding to well-matched A-form RNA have thus prompted us to examine the effect of a base mismatch in an RNA duplex on the luminescence response of the ruthenium complex. In this chapter, we show that $Ru(bpy)_2dppz^{2+}$ indeed binds selectively to mismatched over well-matched RNA. Correspondingly, it behaves as a "light switch" for RNA mismatches. We also explore the application of $Ru(bpy)_2dppz^{2+}$ as a luminescent sensor for RNA mismatches inside cells. Specifically, we encoded an artificial DNA sequence to be transcribed into an mRNA segment that contains several base mismatches, and imaged cells expressing this artificial sequence using confocal microscopy.

6.2 Experimental protocols

6.2.1 Materials

All commercially available materials were used as received. $[Ru(bpy)_2dppz]Cl_2$ was laboratory stocks synthesized according to previously reported procedures.[4,5] RNA was purchased from Dharmacon. DNA was synthesized and purified as described in Chapter 1. SYTO Red nucleic acid stain and cell culture supplies were purchased from Invitrogen, unless otherwise noted. Doxycycline was purchased from Sigma-Aldrich.

6.2.2 Steady state luminescence

Emission spectra were recorded on an ISS-K2 fluorimeter in 5 mM Tris, 50 mM NaCl, pH 7.5 at room temperature in aerated solutions. Experiments were performed in triplicate, and the standard deviation from the three samples was calculated.

6.2.3 Molecular cloning of artificial sequence encoding mismatched mRNA

Plasmids obtained commercially are propagated in either DH5α or XL1 Blue competent cells (Invitrogen) and stored at -80°C.

Mismatch-containing RNA is designed to be generated from the following DNA sequence: 5'- CGC **GGA TCC** TGG ACG CTG CGA CGC GGT ACG AGA TTT TTT TTC TCA TAC CAC GTC ACA GCA TCC ATA TTA TAT TGG ACG CTG CGA CGC GGT ACG AGA TTT TTT TTC TCA TAC CAC GTC ACA GCA TCC ATA TTA TAT TGG ACG CTG CGA CGC GGT ACG AGA TTT TTT TTC TCA TAC CAC GTC ACA GCA TCC A**GT CGA** CCG C -3'. *BamH*I and *Sal*I restriction sites are shown in bold.

The DNA insert (denoted by 4CAx3) was obtained from Integrated DNA Technologies as a miniGene in pIDT-SMART-Amp and PCR-amplified using PreMix G of the FailSafe PCR PreMix Selection Kit (Epicentre Biotechnologies). The insert and the tetracycline (tet)-responsive vector pTRE-Tight (Clontech) were double digested with *BamH*I and *Sal*I (New England BioLabs) and purified by agarose gel electrophoresis. The insert was then ligated into pTRE-Tight, resulting in plasmid pTRE-Tight-4CAx3. The formation of the ligated product was confirmed by sequencing (Laragen) using the following primers: 5'- GCT CGT TTA GTG AAC CGT CAG -3' (left primer) and 5'- GGG AGG TGT GGG AGG TTT T-3 (right primer). Plasmids used in subsequent transfections were isolated with QIAprep Spin Miniprep Kit (Qiagen) and the purity was confirmed by 0.9% agarose gel electrophoresis.

6.2.4 Cell culture

Tet-on HeLa cells (Clontech) were maintained in DMEM supplemented with 10% Tet-approved FBS (Clontech), 4 mM L-glutamine, 100 units/mL pennicillin, 100 μg/mL streptomycin, and 100 μg/mL Geneticin (G418). Cells were grown in tissue culture flasks (Corning Costar) and well plates (Falcon) at 37°C under 5% CO_2 and a humidified atmosphere.

6.2.5 Transfection, induction and expression of plasmids

Cells were plated and allowed to adhere overnight before transfection. Transfection was carried out with FuGENE HD Transfection Reagent (Roche) according to manufacturer's instructions, using 5:2 ratio of FuGENE:DNA. Briefly, the plasmids were diluted with OP-

TIMEM I (Invitrogen) and incubated with FuGENE for 15 min at room temperature prior to addition to cells in complete media. After 6 h the media was replaced with complete media containing 0 to 1 μg/mL doxycycline to induce the expression of Tet-on genes. pTRE-Tight-Luc (Clontech), phRL-TK (Promega) and pGEM-3Z (Promega) were cotransfected along with pTRE-Tight-4CAx3. Expression levels of pTRE-Tight-Luc and phRL-TK were measured using the Dual-Glo Luciferase Assay System (Promega).

6.2.6 Confocal microscopy

Cells used for microscopy were seeded on glass-bottom 96-well plates (Whatman) and allowed to adhere overnight. Approximately 5000 cells were seeded in 200 μL of complete media per well. After transfection and induction with doxycycline, cells were left to grow for another 12-15 h before staining with ruthenium. The cells were incubated with 150-200 μM $[Ru(bpy)_2dppz]Cl_2$ and 100 nM SYTO 61 in Hank's Balanced Salt Solution (HBSS) supplemented with 2% FBS and 10 mM HEPES for 1 h, washed with HBSS and imaged in phenol red-free complete media. For costaining with ER Tracker Green (Invitrogen), 500 nM ER Tracker Green was added along with ruthenium and SYTO 61. Live cells that exclude the dead-cell stain Trypan Blue were imaged. Images were collected on a Zeiss LSM 5 Exciter inverted laser scanning microscope using a 63x/1.4 oil immersion objective at the Caltech Biological Imaging Center. The optical slice was set to 1.1 μm. The ruthenium complexes were excited at 458 nm, with emission observed using a long-pass 560 nm filter. SYTO 61 was excited at 633 nm, with emission observed using a long-pass 650 nm filter. ER Tracker Green was excited at 488 nm, with emission observed using a 503-530 nm bandpass filter.

6.3 Results and discussion

6.3.1 Ru luminescence with a mismatched RNA hairpin

We first measured the luminescence of *rac*-$Ru(bpy)_2dppz^{2+}$ in the presence of mismatched and well-matched RNA hairpins (Figure 6.1). The melting temperature of the mismatch-containing RNA hairpin is 46°C, compared to 56°C of the well-matched counterpart (Table 6.1). The difference in the melting temperatures reflects the destabilization to the hairpin duplex caused by the base mismatch. There is very little luminescence from $Ru(bpy)_2dppz^{2+}$ added to well-matched RNA, consistent with previous observation that ruthenium lumines-

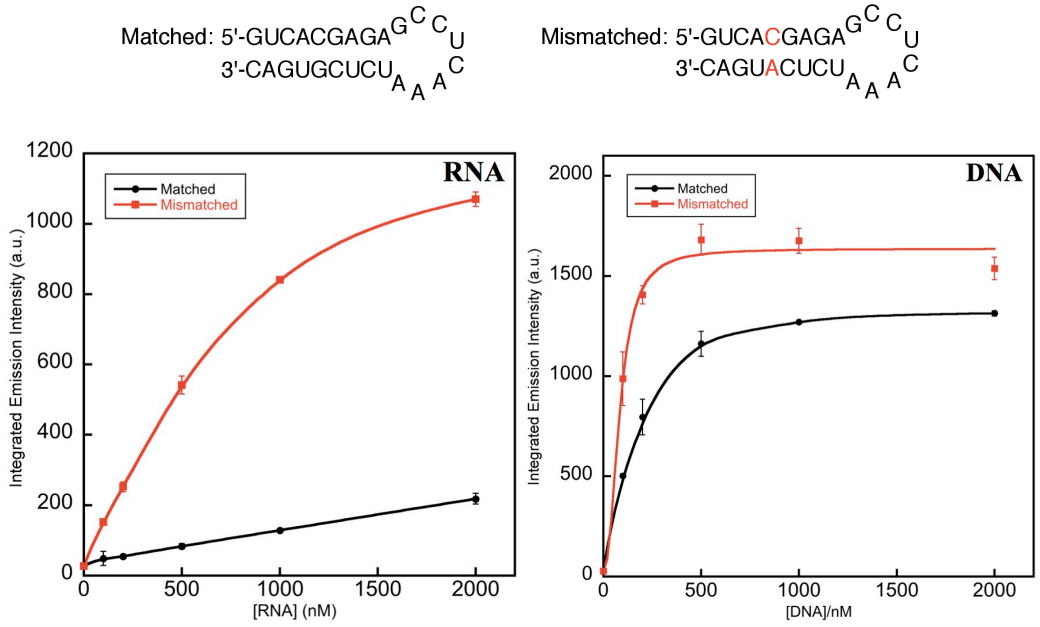

Figure 6.1. Titrations of $Ru(bpy)_2dppz^{2+}$ with RNA and DNA. Top: sequences of matched and mismatched RNA hairpins. DNA of identical sequences is used. Bottom: plots of integrated emission intensity (λ_{ex} = 440 nm) of $Ru(bpy)_2dppz^{2+}$ (500 nM) upon increasing concentrations of RNA (left) and DNA (right) in 5 mM Tris, 50 mM NaCl, pH 7.5. Error bars indicate standard deviations in the measurements.

cence is weak in the presence of A-form nucleic acids.[1,2] However, when the CA mismatch is incorporated into the hairpin, the luminescence of the ruthenium complex is significantly enhanced (Figure 6.1), up to 6-fold at 500 nM Ru and 500 nM RNA (Table 6.1).

In contrast, when $Ru(bpy)_2dppz^{2+}$ was added to DNA of identical sequences, although the overall luminescence increased for both well-matched and mismatched DNA, the differential decreased to less than 2-fold (Figure 6.1, Table 6.1). The higher luminescence intensity reflects the higher binding affinity of $Ru(bpy)_2dppz^{2+}$ for B-form DNA; the presence of a mismatch increases the luminescence only by a small amount. Consistent with its higher binding affinity to DNA, luminescence saturation was achieved at a lower DNA concentration (500 nM versus >2 μM for RNA).

The fact that ruthenium luminescence is extremely weak with well-matched RNA duplexes but significantly enhanced when a mismatch is present is consistent with the notion that $Ru(bpy)_2dppz^{2+}$ binds to well-matched nucleic acids via the major groove but inserts into mismatched sites via the minor groove. As the intercalation of dppz into the base stack is a prerequisite for luminescence turn on, with well-matched RNA, the luminescence from

Table 6.1. Melting temperatures and luminescence intensity of $Ru(bpy)_2dppz^{2+}$ with RNA and DNA

		T_m(°C)[a]	relative luminescence[b]	luminescence ratio (Mismatched/Matched)
RNA	Matched	56	1	
	Mismatched	46	6.5	6.5
DNA	Matched	52	13.9	
	Mismatched	36	20.1	1.5

[a]Uncertainties are estimated to be ±1°C. [b]Conditions are 500 nM $Ru(bpy)_2dppz^{2+}$ and 500 nM RNA or DNA in 5 mM Tris, 50 mM NaCl, pH 7.5 (λ_{ex}= 440 nm). Emission from 560 to 800 nm is integrated.

ruthenium is minimal, indicating lack of binding from either groove. The major groove of RNA, an A-form nucleic acid, is deeper and narrower, which is less accessible for ruthenium, yet ruthenium does not bind from the wider and shallower minor groove either, suggesting that binding from the minor groove is disfavored. However, the presence of an RNA base mismatch leads to a significant increase in ruthenium luminescence, consistent with intercalative binding at the mismatched site. This binding event is presumably metalloinsertion, as we have shown that metalloinsertion is the general binding mode of octahedral metal complexes at destabilized regions of nucleic acid duplexes, and that it occurs from the minor groove. In the case of DNA, ruthenium binds avidly to well-matched DNA, whose wide and shallow major groove is readily accessible. In the presence of a DNA base mismatch, the ruthenium complex can additionally bind to mismatched site from the minor groove through metalloinsertion, which leads to a small increase in luminescence compared to well-matched DNA. We note that in the case of mismatched RNA, the extrapolated luminescence intensity at saturation would be comparable to the saturation intensity with well-matched DNA, suggesting that fundamentally the ruthenium complex in an RNA base stack is as protected from solvent water as it is in a DNA base stack.

The relatively weak luminescence intensity of $Ru(bpy)_2dppz^{2+}$ bound to RNA at low concentrations can be amplified through fluorescence resonance energy transfer (FRET). We measured the emission of $Ru(bpy)_2dppz^{2+}$ in the presence of the nucleic acid stain SYTO Red series. Representative emission spectra in the absence and presence of a SYTO stain (SYTO 61) are shown in Figure 6.2. With SYTO 61 ($\lambda_{ex}/\lambda_{em}$ = 628/645 nm), upon excitation at 440 nm, the donor ruthenium emission is replaced by acceptor SYTO 61 emission,

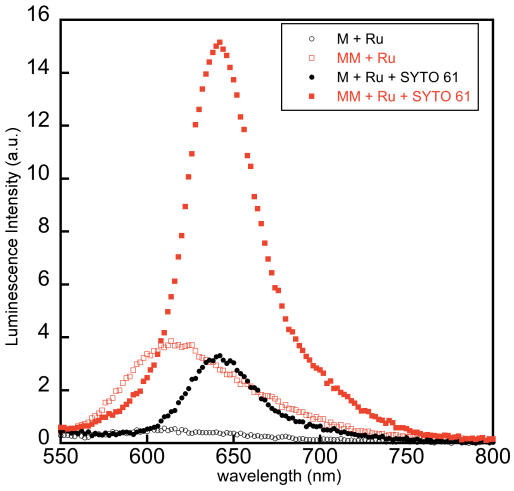

Figure 6.2. Emission spectra of $Ru(bpy)_2dppz^{2+}$ with matched (M) and mismatched (MM) RNA hairpin (sequence shown in Figure 6.1) in the absence and presence of the FRET-acceptor SYTO 61 (λ_{ex} = 440 nm). Conditions are 500 nM Ru, 500 nM RNA, 1 μM SYTO 61 in 5 mM Tris, 50 mM NaCl, pH 7.5.

as evident in the narrower profile of the emission peak and redshifted emission maximum. The emission intensity is increased more than 3-fold. The luminescence differential between mismatched and matched RNA decreased slightly from 6-fold to 4-fold, which is mostly due to residual luminescence of SYTO 61 itself when excited at 440 nm, and can be corrected by subtraction. Enhanced luminescence through FRET was also observed for SYTO 17, 59, 60, 63, 64 and TO-PRO-3. Thus, with its high mismatch selectivity and ease of signal amplification through FRET, $Ru(bpy)_2dppz^{2+}$ holds great potential as a first-generation luminescent sensor for RNA mismatches.

6.3.2 Confocal microscopy of Tet-on HeLa cells expressing mismatch-containing mRNA

The luminescence turn-on response of $Ru(bpy)_2dppz^{2+}$ to RNA mismatches immediately suggests the possibility that it may be used to image RNA mismatches inside cells. Real-time imaging of RNA, in particular mRNA, has been much sought after, as regulation of mRNA production and trafficking is believed to be an important avenue to effect the spatial and temporal control of protein expression.[6] Established mRNA imaging techniques often require fixing the cells and thus only allow determination of cellular mRNA distribution at the instance of cell fixation.[7–9] Recent developments in live-cell imaging employ tags fused to

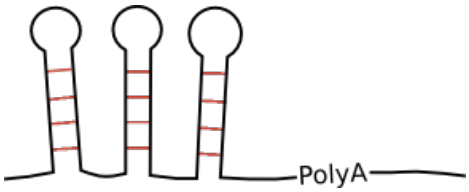

Figure 6.3. Schematic illustration of the mRNA with the mismatch (MM) tag, which consists of three hairpins, each with four CA mismatches (red).

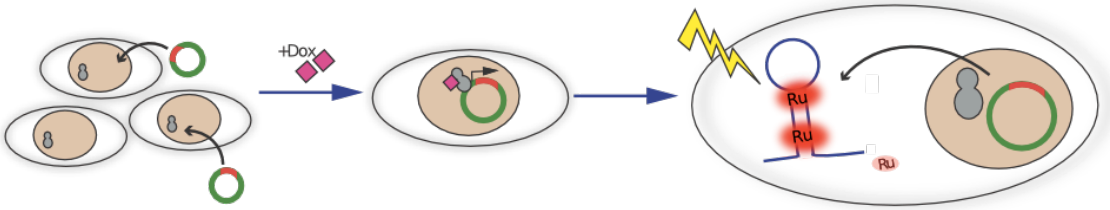

Figure 6.4. Scheme showing detection of RNA mismatches inside cells using $Ru(bpy)_2dppz^{2+}$. The tet-inducible plasmid (green) containing the DNA sequence encoding the mismatch-rich mRNA (red) is transfected into Tet-on HeLa cells. Addition of Dox induces the expression of the DNA and the mRNA transcript is detected through ruthenium luminescence.

the gene of interest and subsequent binding of the mRNA transcript by multiple fluorescent proteins fused to RNA-binding proteins that recognize the tags.[10] Single-molecule resolution is possible with this tagging strategy.[11] In an analogous fashion, the ruthenium complex may be used to recognize a special type of tag—RNA mismatches—and fluorescently track, in real time, any mRNA that displays the tag. This approach was very recently used to track RNA tagged with an aptamer for a fluorophore resembling the core of fluorescent proteins.[12] Unlike large fluorescent proteins fused to RNA-binding proteins, the ruthenium complex is a small molecule, and its binding to an mRNA transcript is expected to minimally disturb the natural fate of the mRNA. Thus, as an exploratory first step toward the development of a ruthenium probe and a suitable mismatch (MM) tag for real-time imaging of cellular mRNA, we designed a DNA sequence that will generate a mismatch-rich mRNA segment (Figure 6.3), and imaged Tet-on HeLa cells expressing this sequence after staining with $Ru(bpy)_2dppz^{2+}$ (Figure 6.4).

The DNA sequence we used to generate the mismatch-rich mRNA is 181bp long (see experimental section for full sequence), about 6% of the length of an average gene (3000 bp[13]). The mRNA transcript, if folded as designed, contains three identical RNA hairpins,

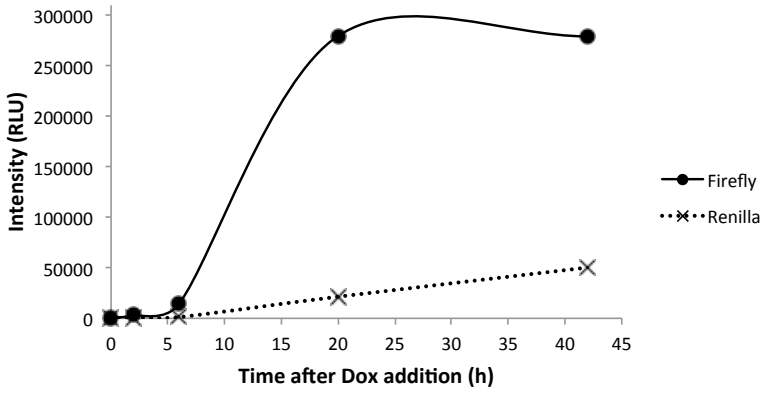

Figure 6.5. Relative luminescence intensity (in relative luminescence units, RLU) of tet-inducible firefly luciferase and constitutively expressed Renilla luciferase as a function of time after induction. The expression of Renilla luciferase increases steadily over time, but the expression of tet-inducible firefly luciferase peaks and decreases as the effect of Dox wears off.

each with four CA mismatches (Figure 6.3). Since the RNA hairpins are identical, alternative folding into different configurations will still generate the mismatches. To control the expression of this DNA sequence, we cloned it into the tet-inducible pTRE-Tight vector and transiently transfected the plasmid into Tet-on HeLa cells. To confirm that transfection and induction with doxycycline (Dox) are successful, we cotransfected the cells with pTRE-Tight-Luc and phRL-TK, which are tetracycline (tet)-inducible firefly luciferase and constitutively expressed Renilla luciferase, respectively, and measured the luminescence of the two luciferases (Figure 6.5). Luminescence is detected from the Renilla luciferase within a few hours of transfection, indicating that the cells have successfully taken up the plasmids into the nucleus. The luminescence level continues to increase over time as the cells grow and divide. In the absence of Dox, no luminescence is detected from the firefly luciferase at all times, confirming the tightness of the tet-inducible expression system. With the addition of Dox, the firefly luminescence is turned on, its intensity peaking after a day, and then declining gradually as the effect of Dox wears off. Based on the expression profile of the luciferases, we performed most imaging experiments 12-15 h post induction.

To accelerate the natural uptake of ruthenium complexes into the cells,[14] we stained the cells with $[Ru(bpy)_2dppz]Cl_2$ for 1 h in buffer with reduced serum (0%–2% FBS, see Experimental section for details). For cells expressing the MM tag, fluorescence from the ruthenium complex was observed mostly in a dense perinuclear region, likely the endoplas-

mic reticulum (ER) (Figure 6.6). Cells that were similarly transfected but did not receive Dox show less concentrated staining in the perinuclear region, with a more diffused fluorescence pattern in the cytosol, some of which is cellular autofluorescence. The proportion of cells showing prominent perinuclear staining was estimated by counting 332 cells treated with Dox (and thus expressing the MM tag), and 163 untreated cells. About 54(±5)% of treated cells show distinct perinuclear staining with very weak cytosolic fluorescence; for comparison, only 40(±8)% of untreated cells show any perinuclear accumulation of the ruthenium complex (and often with reduced fluorescence intensity). This small but significant difference in the staining pattern and intensity suggests that the more concentrated ruthenium fluorescence originated from the MM tag.

We costained the cells with SYTO 61, the nucleic acid stain that was found to be an effective FRET acceptor of ruthenium (Figure 6.2). At 1 μM in complete media, SYTO 61 stains the nucleus strongly, with very weak but uniform residual fluorescence in the cytosol. At 100 nM in reduced-serum buffer, it stains the nucleus with medium intensity, but the stringy morphology of the bright cytosolic staining indicates that it now accumulates more in the mitochondria (Figure 6.6). Merging the ruthenium and the SYTO 61 channels shows that the two did not colocalize. As a result, there was probably no FRET between ruthenium and SYTO 61 inside the cells. Thus, if we were to pursue the amplification of ruthenium fluorescence through FRET, either a different, colocalizing or a covalently tethered acceptor may be necessary.

We also costained the cells with a dye for the ER, ER Tracker Green, which confirmed that the perinuclear staining of ruthenium occurs in ER regions (Figure 6.7). This is consistent with our expectation that ruthenium is bound to folded mRNAs exported from the nucleus. In fact, when tet-inducible firefly luciferase is expressed after Dox addition, we observe more perinuclear staining compared to the Dox-free cells, as the luciferase mRNAs accumulate. Counting 148 cells expressing the firefly luciferase, 44(±8)% was found to show the ER-staining pattern. This increase in ruthenium fluorescence with nonspecific mRNA production points to the importance of having a bright signal from the MM tag. Our current design gives only a small difference between MM tag-expressing cells and control cells, and there is much room for further development through modification of the tag and also the ruthenium complex. After all, the cell is abundant with folded RNA structures and unpaired RNA bases, and the probe molecule for the mismatch-rich tag has to emerge

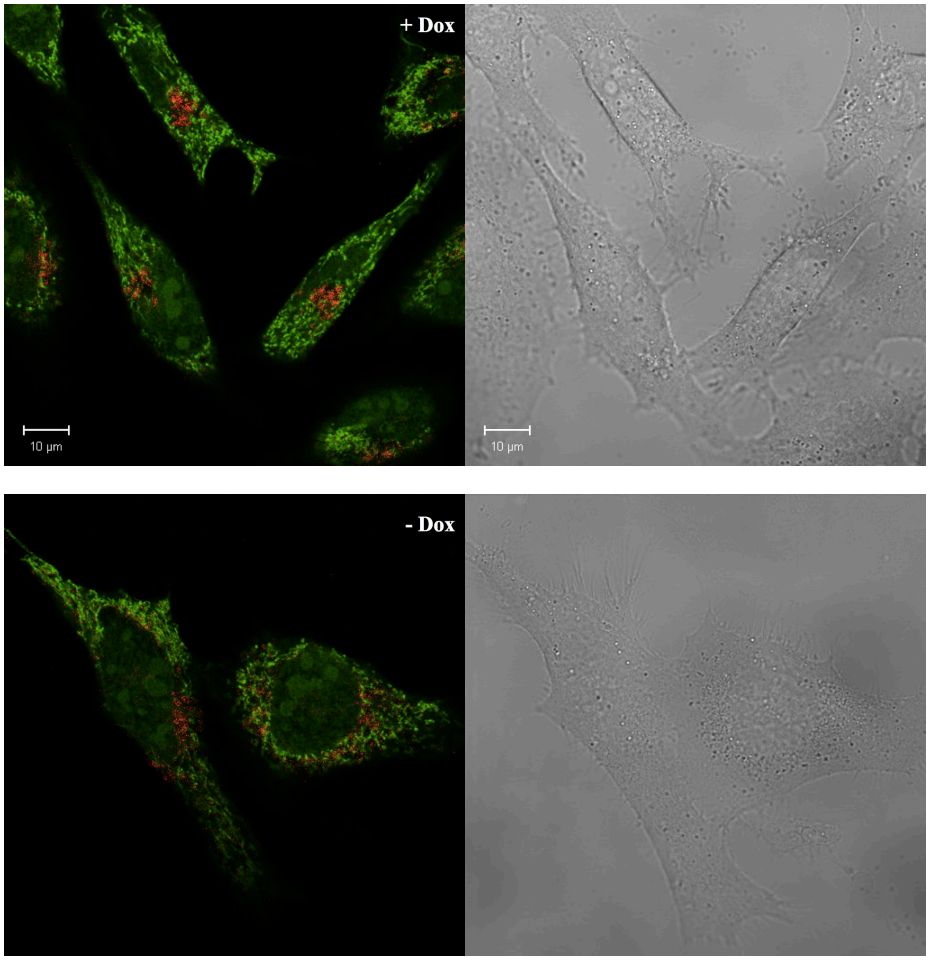

Figure 6.6. Confocal microscopy of Tet-on HeLa cells transfected with pTRE-Tight-4CAx3. Top: with the addition of Dox, $Ru(bpy)_2dppz^{2+}$ shows prominent staining in the perinuclear region (red). SYTO 61 (green) stains the nucleus and mitochondria. Bottom: in the absence of the inducer Dox, $Ru(bpy)_2dppz^{2+}$ shows a more diffused staining pattern in the cytosol, with less accumulation in the perinuclear region.

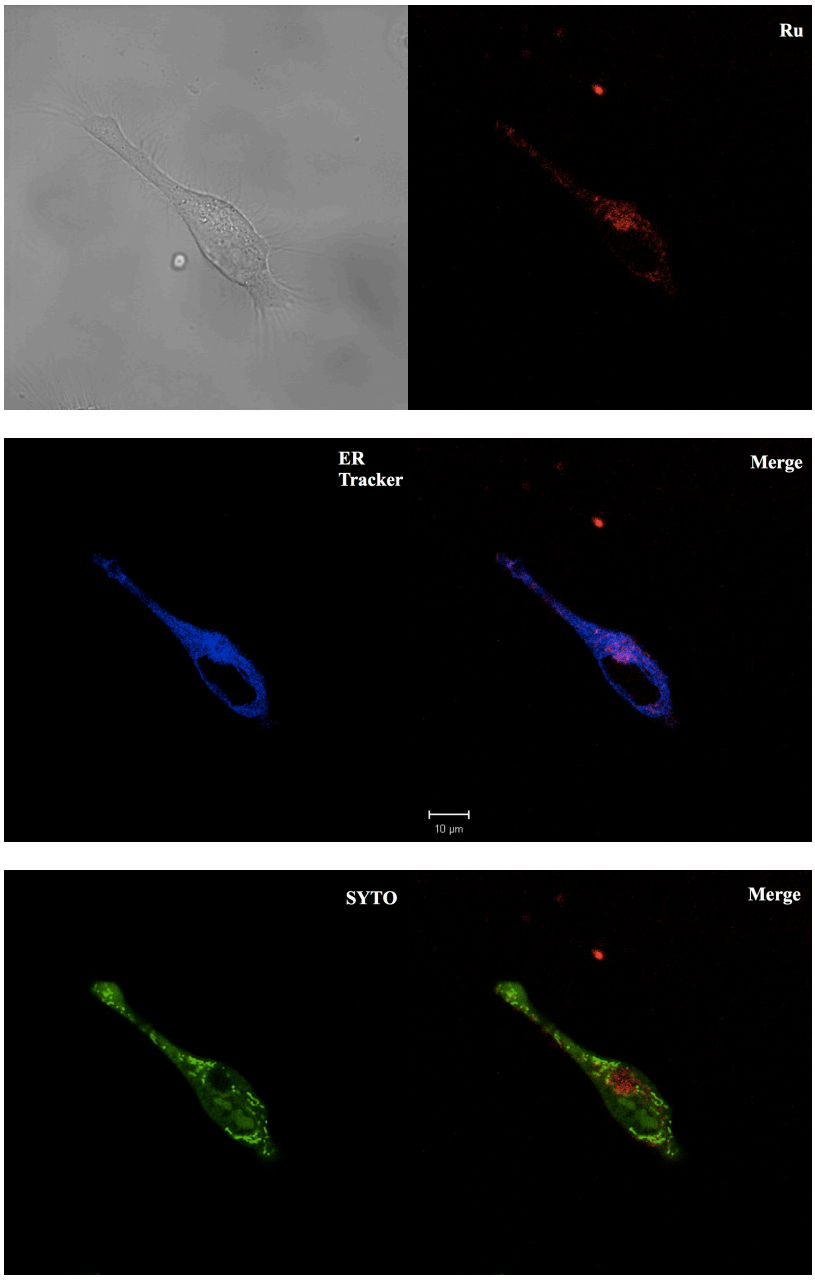

Figure 6.7. Costaining of $Ru(bpy)_2dppz^{2+}$ (red) with an ER Tracker (blue) reveals that $Ru(bpy)_2dppz^{2+}$ is localized to the ER regions in Tet-on HeLa cells expressing the MM tag. Co-staining with SYTO 61 (green) shows that the ruthenium complex is mostly excluded from the nucleus or mitochondria.

from this background. Nevertheless, the exploratory imaging experiments reported here demonstrate the proof of principle that an RNA mismatch-selective metal complex may be used to fluorescently report on cellular RNA that displays a mismatch-rich tag.

6.4 Conclusions

In this chapter, we showed that $Ru(bpy)_2dppz^{2+}$ behaves as a "light switch" for RNA mismatches. While it luminesces extremely weakly in the presence of well-matched RNA due to poor binding, its luminescence is significantly enhanced by binding to an RNA mismatch, presumably through metalloinsertion. Its luminescence intensity can be further amplified by several folds through a FRET acceptor. As a preliminary test for the biological application of this luminescent probe for RNA mismatches, we demonstrated that the ruthenium complex may be used to image RNA mismatches incorporated into an mRNA transcript in live HeLa cells. This early cell work suggests that $Ru(bpy)_2dppz^{2+}$ and future generations of complexes will be promising biological probes for real-time tracking of mismatch-tagged cellular RNAs.

Bibliography

[1] Alan E. Friedman, Jean Claude Chambron, Jean Pierre Sauvage, Nicholas J. Turro, and Jacqueline K. Barton. A molecular light switch for DNA: $Ru(bpy)_2(dppz)^{2+}$. *Journal of the American Chemical Society*, 112(12):4960–4962, 1990.

[2] Yonchu Jenkins, Alan E. Friedman, Nicholas J. Turro, and Jacqueline K. Barton. Characterization of dipyridophenazine complexes of ruthenium(II): The light switch effect as a function of nucleic acid sequence and conformation. *Biochemistry*, 31(44):10809–10816, 1992.

[3] Mi Hee Lim, Hang Song, Eric D. Olmon, Elizabeth E. Dervan, and Jacqueline K. Barton. Sensitivity of $Ru(bpy)_2dppz^{2+}$ luminescence to DNA defects. *Inorganic Chemistry*, 48(12):5392–5397, 2009.

[4] Edmond Amouyal, Abdulrazzak Homsi, Jean-Claude Chambron, and Jean-Pierre Sauvage. Synthesis and study of a mixed-ligand ruthenium(II) complex in its ground and excited states: bis(2,2'-bipyridine)(dipyrido[3,2-*a*:2',3'-*c*]phenazine-N^4N^5)ruthenium(II). *J. Chem. Soc., Dalton Trans.*, pages 1841–1845, 1990.

[5] Cindy A. Puckett. *The cellular uptake of luminescent ruthenium complexes.* PhD thesis, California Institute of Technology, 2010.

[6] Kelsey C. Martin and Anne Ephrussi. mRNA localization: Gene expression in the spatial dimension. *Cell*, 136(4):719–730, 2009.

[7] Timothy T. Weil, Richard M. Parton, and Ilan Davis. Making the message clear: Visualizing mRNA localization. *Trends in Cell Biology*, 20(7):380–390, 2010.

[8] Eric Lécuyer, Neela Parthasarathy, and Henry M. Krause. Fluorescent in situ hybridization protocols in *Drosophila* embryos and tissues. In Christian Dahmann, editor, *Drosophila*, volume 420 of *Methods in Molecular Biology*, pages 289–302. Humana Press, 2008.

[9] Arjun Raj, Patrick van den Bogaard, Scott A Rifkin, Alexander van Oudenaarden, and Sanjay Tyagi. Imaging individual mRNA molecules using multiple singly labeled probes. *Nat Meth*, 5(10):877–879, 10 2008.

[10] Susanne Lange, Yoshihiko Katayama, Maria Schmid, Ondrej Burkacky, Christoph Bräuchle, Don C. Lamb, and Ralf-Peter Jansen. Simultaneous transport of different localized mRNA species revealed by live-cell imaging. *Traffic*, 9(8):1256–1267, 2008.

[11] Mai Yamagishi, Yo Ishihama, Yoshitaka Shirasaki, Hideki Kurama, and Takashi Funatsu. Single-molecule imaging of β-actin mRNAs in the cytoplasm of a living cell. *Experimental Cell Research*, 315(7):1142–1147, 2009.

[12] Jeremy S. Paige, Karen Y. Wu, and Samie R. Jaffrey. RNA mimics of green fluorescent protein. *Science*, 333(6042):642–646, 2011.

[13] U.S. DOE human genome project, http://www.ornl.gov/hgmis/home.shtml, accessed 2011-10-15.

[14] Cindy A. Puckett and Jacqueline K. Barton. Methods to explore cellular uptake of ruthenium complexes. *Journal of the American Chemical Society*, 129(1):46–47, 2007.

Chapter 7

Conclusions

This work revolves around DNA mismatches, a precursor to mutations. Cells guard against the deleterious effects of mismatches through mismatch repair (MMR) pathways. Occasionally, MMR fails to function properly, predisposing the cell to cancerous transformations. While the cause and consequences of MMR-deficiency may take on different forms, its foremost and ultimate signature—elevated levels of base mismatches in the genome—remains a persistent target for medicinal agents. We hope that work described in this thesis contributes to the development of small molecule-based therapeutics and diagnostics in the fight against MMR-deficient cancers.

Rhodium metalloinsertors exhibit biological activity against MMR-deficient cells, which otherwise tend to be drug-resistant. Structure-activity relationship of first-generation rhodium metalloinsertors was elucidated in the opening chapter. Smaller ancillary ligands on the rhodium were found to improve both the mismatch-binding affinity *in vitro* and the preferential antiproliferative activity in MMR-deficient carcinoma cells. This correlation suggests that the rhodium complexes do act on their intended target—DNA mismatches—inside cells. The cellular uptake of rhodium metalloinsertors and possibly the subcellular localization also varied significantly with structure. The mechanism underlying the biological activity is currently under investigation in our laboratory, as we work to further enhance the efficacy of rhodium metalloinsertors for targeted therapeutics.

On the diagnostic front, luminescence-based sensing of DNA mismatches promises to be a fast and sensitive detection method for MMR-deficiency in biological samples. Chapters 2 and 3 focus on luminescent dipyridophenazine (dppz) complexes of ruthenium and examine in detail the molecular interactions between the metal complex and DNA mismatches. We found that ruthenium dppz complexes, known as a "light switch" for DNA, inherently exhibit higher luminescence in the presence of DNA mismatches, as a result of tighter binding to mismatches through metalloinsertion. This binding mode was captured (twice) in the first crystal structure of the Δ-isomer of the complex bound to mismatched oligonucleotides: just like rhodium metalloinsertors, the ruthenium complex inserts at the mismatched site from the minor groove, extrudes both mismatched bases, and effectively replaces them in the base stack with its own planar, π-conjugated dppz ligand. In the same structure, the complex is also intercalated at well-matched sites from the minor groove, which compelled us to rethink ruthenium metallointercalation in a different light.

Two more chapters were devoted to the development of ruthenium complexes for sensing DNA mismatches through luminescence output. Substantial efforts were directed toward improving the luminescence differential of the complex between mismatched and well-matched DNA through conjugation and derivatization. Concurrent with our pursuit of a luminescent sensor for DNA mismatches, we discovered that the same dppz complexes of ruthenium behave as a better luminescent reporter of RNA mismatches. Preliminary cell work suggests that the ruthenium complexes may be applied in direct imaging of cellular RNA fused to a mismatch-rich tag, as described in the last chapter.

This thesis strives to address both fundamentals and applications of mismatch-binding octahedral metal complexes. Chemical basis of the interactions between the metal complexes and DNA informs on our design of future medicinal agents; the biological effects of these agents in turn guide us to examine molecular details of the metal-DNA complex.

Our academic exercises have been carried out with every intent to spawn practical applications. In the end, we hope that the scientific insights garnered from this work will serve as lessons and inspirations for the future development of metalloinsertors as targeted therapeutic and diagnostic agents for a broad range of cancers.